1969

Activation analysis with thermal and fission neutrons

Laurene Mary Menapace
Iowa State University

ACTIVATION ANALYSIS WITH THERMAL AND FISSION NEUTRONS

by

Laurene Mary Menapace

A Dissertation Submitted to the
Graduate Faculty in Partial Fulfillment of
The Requirements for the Degree of
DOCTOR OF PHILOSOPHY

Major Subject: Analytical Chemistry

Approved:

Signature was redacted for privacy.

In Charge of Major Work

Signature was redacted for privacy.

Head of Major Department

Signature was redacted for privacy.

Dean of Graduate College

Iowa State University
Of Science and Technology
Ames, Iowa

1969

TABLE OF CONTENTS

INTRODUCTION TO ACTIVATION ANALYSIS

Many traditional methods of elemental anaylsis have been based on properties of the electron in the atom. Atomic absorption, colorimetry, X-ray spectroscopy, and electrochemical techniques are a few examples of methods commonly used which are based upon electronic behavior, whether it be transfer, rearrangement or detachment of electrons. On the contrary, newer methods, such as activation analysis, mass spectroscopy and nuclear magnetic resonance are techniques which make use of nuclear properties.

Activation analysis is a relatively new field. The technique dates back to the discovery of artificial radioactivity in 1934. One of the first analyses was done in 1936 by von Hevesy and Levi (1), who used a Ra-Be neutron source to determine europium and dysprosium in rare earth mixtures. In 1938, Seaborg and Livingood (2) bombarded iron samples with deuterons produced from the Berkeley cyclotron to detect small amounts of gallium impurity. The vast scope of activation analysis became apparent, however, with the advent of the first nuclear reactor on December 2, 1942, thereby providing for the first time a high intensity source of neutrons.

In the past two decades, advancement in electronic technology has led to the development and refinement of gamma ray detectors and spectrometers. In addition to the development of the nuclear reactor, rapid advancement in the field of activation analysis was made due to the introduction of the NaI(Tl) scintillation detector. In 1953 Kahn and Lyon (3) pointed out the usefulness of the NaI(Tl) spectrometer as an aid in the identification of radionuclides. Soon after numerous articles appeared pointing out the

potential for neutron activation analysis employing gamma ray spectrometry (4-12). However, full utilization of the scintillation counter was not made until the appearance of the multichannel analyzer in 1955 (5).

The last era has witnessed a further expansion of the activation analysis field with the development of the solid state detectors. The groups of Girardi (13), Schroeder (14), and Hollander (15) were among the first to try the lithium drifted germanium detector for activation work in 1965. In addition, the introduction of computerized programs for the handling of data has aided in efficiency, particularly for routine analysis. The area of activation analysis and its usefulness in analytical chemistry has grown rapidly. Numerous review articles and bibliographies concerning the widespread applications of activation analysis have been published (16-31).

The technique of activation analysis is based upon the fact that an isotope, when bombarded by nuclear particles, may form a radioactive nuclide which will decay emitting a characteristic radiation. Two types of electromagnetic radiation are of interest, gamma and X-rays. Most commonly used in activation analysis is gamma ray spectrometry.

Three processes may be used to explain the interaction of gamma radiation with matter: photoelectric effect, Compton scattering and pair production. The photoelectric effect is the most important process at low energies. In this process, the photon is absorbed in the atom and, as a result of energy absorption, an electron is ejected from an inner orbital with an energy whose value may be represented by the following equation.

$$E_{\text{photoelectron}} = E_{\text{absorption}} - E_{\text{binding energy of the ejected electron}} \qquad (1)$$

For photon energies greater than the K-binding energy of the absorber, the interaction will be primarily with that shell. The vacancy in an inner shell will result in electrons from higher levels filling the lower level vacancies thereby resulting in the emission of characteristic X-rays and Auger electrons. Since all of the electron and X-ray energy is absorbed in the crystal, the photoelectric process results in the transfer of the total energy of the photon to the crystal.

In a second process which occurs with greater probability with higher energy photons, only a part of the energy of the photon is transferred to an orbital electron as though it were a free electron. This process, known as Compton scattering, results in a photon which is degraded in energy and also deflected from its original path. The amount of energy transferred to the electron depends upon the angle of deflection and the energy of the incident photon. Consequently, a spectrum of scattered Compton radiation results from zero energy at $\theta = 0^{o}$ to a maximum energy at $\theta = 180^{o}$ which may be seen on a typical gamma ray spectrum as the Compton edge. The scattered photon may escape from the crystal or it may interact again either by photoelectric absorption or by a second Compton scattering. The probability of these two processes will depend on crystal size: the larger the detector, the greater the probability that the entire photon energy will be deposited in the crystal.

When the energy of the incident gamma photon is greater than 1.02 Mev, a third mechanism for the absorption of electromagnetic radiation known as pair production may occur. The incident gamma is converted in the coulombic field of the nucleus to a positron-electron pair. As two equivalent masses are formed, an energy equivalent of 1.02 Mev (2 x 0.51 Mev) is

required from the incoming photon. Above 1.02 Mev, the cross section for pair production increases with increasing energy and at approximately 4 Mev and above assumes a value proportional to the log of E_γ. The positron formed will combine with an available electron and, coincident with the annihilation of the positron, is the production of two 0.51 Mev photons. If both of these annihilation photons escape from the detector, the incident photon appears as an 'escape peak' 1.02 Mev below the actual energy. An escape peak 0.51 Mev below the actual energy will be observed if only one photon escapes. Since few of the gamma rays used in this work had energies in the proper region, the photoelectric effect was the mechanism of primary concern.

As can be readily seen from the above discussion, the three mechanisms of electromagnetic radiation absorption are energy dependent. For energies up to 0.5 Mev the photoelectric process is the most dominant; in the region between 0.5 and approximately 2 Mev the Compton process predominates and above this pair production occurs.

In activation analysis, the spectrum obtained from a radioactive sample will indicate photopeaks which are representative of distinct gamma energies characteristic of a particular radionuclide. The full energy or photopeak areas are usually used to measure and identify the nuclide of interest.

Elemental determinations using activation analysis techniques require a consideration of the laws governing the rate of growth and decay. Upon irradiation of a sample, the rate of growth of a particular radioactive species may be represented by the following equation:

$$R_{Growth} = \varphi \sigma N^{*} \tag{2}$$

$$\text{where } N^{*} = \frac{m I N_o}{at.wt.} \tag{3}$$

$$\text{therefore } R_{Growth} = \frac{\varphi \sigma m I N_o}{at.wt.} \quad . \tag{4}$$

In these and subsequent equations, the following defined terms will be used.

φ = thermal neutron flux

σ = thermal neutron cross section

N^{*} = number of atoms of target element

m = weight of sample

I = per cent abundance of the parent isotope

N_o = Avogadros number, 6.023×10^{23}

λ = decay constant characteristic for each species

$t_{\frac{1}{2}}$ = half-life of radioactive species produced

t = length of irradiation

T = time following irradiation

In addition to the rate of formation of a particular species, the rate of its decay must also be taken into consideration. The rate of decay may be represented by the following:

$$R_{Decay} = \frac{-dN}{dt} = \lambda N \quad . \tag{5}$$

Therefore in considering the overall rate of formation of a given nuclide, its rate of formation during irradiation and also its decay must be taken into consideration and may be represented as:

$$\frac{dN}{dT} = \text{Rate of growth - Rate of decay} \tag{6}$$

$$= \sigma \varphi N^{*} - \lambda N \tag{7}$$

which upon integration yields

$$\frac{dN}{dT} = \sigma \varphi N^{*} (1 - e^{-\lambda t}) \cdot \tag{8}$$

At any given time, T, after irradiation the activity, A, may be found from equation (9).

$$A = \sigma \varphi N^{*} (1 - e^{-\lambda t}) (e^{-\lambda T}) \tag{9}$$

As may be seen from the above equations, the weight of an element under consideration may be determined from the measured disintegration rate, if the neutron flux and the neutron cross section are known. Thermal neutron cross sections have been determined but the accuracy with which many of them are known is quite poor. Because of this, and the fairly unconstant nature of the flux in a reactor, the absolute method of activation analysis as described is seldom used. Therefore, a relative method of activation is usually applied which makes use of an external standard.

In using an external standard, a sample is prepared which contains the element to be determined in a non-interfering matrix. Homogeneity in the standards is of the utmost importance. Then standards and samples are irradiated simultaneously, and the weight of the unknown element is accurately determined by means of the following relationship:

$$\frac{\text{weight of standard}}{\text{A of standard}} = \frac{\text{weight of sample}}{\text{A of sample}} \cdot \tag{10}$$

Equation (10) may be used if the same flux is received by the

standards and samples. Frequently, however, this is not a valid assumption because of factors which may cause variations in flux. The problem of self-shielding, or flux attentuation due to self absorption in the sample is the most difficult. If an element of high neutron cross section is present in the sample to be irradiated, a reduction in neutron flux within the sample occurs due to absorption of neutrons by those atoms closer to the surface. This absorption results in a flux gradient which reaches a minimum value at the center of the sample (32). The self-shielding problem has been treated in some detail and may be evaluated on a semi-empirical basis (33-34). Problems associated with self-shielding may be avoided or considerably reduced by dilution with an inert material, reducing the sample size, or use of an internal standard method of analysis.

The internal standard method of analysis involves the preparation of a mixture of a known quantity of the element to be determined and a quantity of the sample which is to be measured. The mixture serves as a reference standard and is irradiated together with the samples to be determined. Using an internal standard has tremendous advantages because there is no need to know the irradiation flux, the neutron cross section, the sample weight, or the reaction yield. Also maintaining strictly uniform irradiation times and irradiation and counting geometry is a severe limitation to the precision of activation analysis. All these difficulties are obviated through the use of an internal standard method. However, there is one requisite of the utmost importance and upon which the validity of the technique rests and that is the homogeneity of the mixtures. The ability of the technique to be flux independent rests upon this prerequisite. It is also essential, of course, that standards and

samples be measured under the same conditions.

The advantage of an internal standard method of analysis can be readily seen from the following equations. The terms have been previously defined with the exception of ϵ which shall here be defined as the photopeak efficiency. Because the internal standard method is based on the comparison of photopeak areas within a standard sample to the same photopeak areas in an unknown, the following subscript notation will be used:

A_{1s} = area under photopeak 1 in the standard

A_{2s} = area under photopeak 2 in the standard

A_{1u} = area under photopeak 1 in the unknown

A_{2u} = area under photopeak 2 in the unknown

The ratio of the two photopeak areas in the standard may be written as:

$$\frac{A_{1s}}{A_{2s}} = \frac{\epsilon_1 \varphi_{1s} \sigma_1 N_{1s} (1-e^{-\lambda_1 t_s})\, e^{-\lambda_1 T_{1s}}}{\epsilon_2 \varphi_{2s} \sigma_2 N_{2s} (1-e^{-\lambda_2 t_s})\, e^{-\lambda_2 T_{2s}}} \cdot \qquad (11)$$

The ratio of the same two photopeak areas in the unknown may be written as:

$$\frac{A_{1u}}{A_{2u}} = \frac{\epsilon_1 \varphi_{1u} \sigma_1 N_{1u} (1-e^{-\lambda_1 t_u})\, e^{-\lambda_1 T_{1u}}}{\epsilon_2 \varphi_{2u} \sigma_2 N_{2u} (1-e^{-\lambda_2 t_u})\, e^{-\lambda_2 T_{2u}}} \cdot \qquad (12)$$

The ratio of photopeak areas in the standard to the ratio of photopeak areas in the unknown yields the following:

$$\frac{A_{1s}/A_{2s}}{A_{1u}/A_{2u}} = \frac{\dfrac{\varepsilon_1 \varphi_{1s} \sigma_1 N_{1s}(1-e^{-\lambda_1 t_s}) e^{-\lambda_1 T_{1s}}}{\varepsilon_2 \varphi_{2s} \sigma_2 N_{2s}(1-e^{-\lambda_2 t_s}) e^{-\lambda_2 T_{2s}}}}{\dfrac{\varepsilon_1 \varphi_{1u} \sigma_1 N_{1u}(1-e^{-\lambda_1 t_u}) e^{-\lambda_1 T_{1u}}}{\varepsilon_2 \varphi_{2u} \sigma_2 N_{2u}(1-e^{-\lambda_2 t_u}) e^{-\lambda_2 T_{2u}}}} \quad . \quad (13)$$

Since the irradiation times for the standard and the unknown are the same, t_s is equal to t_u. All activities are corrected to T = 0 also, so equation (13) may be rewritten as the following:

$$\frac{A_{1s}/A_{2s}}{A_{1u}/A_{2u}} = \frac{\varphi_{1s}}{\varphi_{1u}} \times \frac{\varphi_{2u}}{\varphi_{2s}} \times \frac{N_{1s}/N_{2s}}{N_{1u}/N_{2u}} \quad . \quad (14)$$

Since the fluxes received by both the standard and the unknown are identical, $\varphi_{1s}/\varphi_{1u}$ and $\varphi_{2u}/\varphi_{2s}$ are equal to unity, and equation (14) becomes:

$$\frac{A_{1s}/A_{2s}}{A_{1u}/A_{2u}} = \frac{N_{1s}/N_{2s}}{N_{1u}/N_{2u}} = \frac{(W_1/W_2)\text{std.}}{(W_1/W_2)\text{unk.}} \quad . \quad (15)$$

THERMAL NEUTRON ACTIVATION OF TUNGSTEN BRONZES

Introduction

A method was developed for the nondestructive thermal neutron activation analysis of potassium, holmium and lanthanum tungsten bronzes. Holmium and lanthanum bronzes had previously been determined nondestructively by neutron activation analysis using scintillation spectroscopy and an external standard technique (35). The potassium bronzes had previously been determined by high energy photon activation using scintillation spectroscopy and an external standard method of analysis (36).

The present work had as its purpose two aspects of particular interest: (1) determining if an internal standard method of analysis would be feasible and useful for those tungsten bronzes which had been previously analyzed by using an external standard and (2) comparing the usefulness, advantages and disadvantages, of the scintillation detector and the solid state detector in the particular case of the metal-tungsten bronzes.

The primary advantage of the solid state detector over all other forms of gamma ray detection is a 10-50 fold increase in resolution for gamma rays; however, associated with this is about a 100 fold decrease in sensitivity. It would appear that for some systems the greater resolution and consequently less interference from neighboring gamma rays, would far outweigh the loss of efficiency particularly at energies greater than 1 Mev.

The actual analysis of the bronzes consisted in determining the 'x' value or metal to tungsten ratio, for the potassium, holmium and lanthanum tungsten bronzes. The nuclear properties (37) of these bronzes are

summarized in Table 1.

As may be noted from the data in Table 1, ^{186}W has a considerably larger thermal neutron activation cross section, and therefore care must be taken in choosing the photopeaks of interest for the metal ions to avoid interference from ^{187}W gamma rays. Figure A-1 in Appendix A represents a spectrum of ^{187}W taken using the solid state detector. All subsequent spectra were also taken on the solid state detector. As can be noted from the spectrum, the photopeaks of interest for ^{187}W are well resolved. For the following analyses, the 0.479 Mev and/or the 0.686 Mev photopeaks were chosen for comparison.

For the analysis of K_xWO_3, the 1.52 Mev photopeak of ^{41}K was used for the analysis of potassium. Figures A-2, A-3 and A-4 in Appendix A represent gamma ray spectra of ^{41}K, a potassium tungsten standard, and a potassium tungsten bronze with $x = 0.298$. As can be seen from the spectra, the 1.52 Mev photopeak of ^{41}K is isolated from the ^{187}W photopeaks. However, as also will be noticed, the intensity of the 1.52 peak is low; this in part may be attributed to the lower efficiency of the solid state detector as compared to the scintillation detector in the region beyond 1 Mev. The potassium bronzes were also analyzed using scintillation spectroscopy and, although the spectra are not here included, the greater resolution of the ^{41}K peak using the solid state system would appear to compensate for the disadvantage of the lower efficiency.

Holmium-166 was used for the analysis of holmium in the Ho_xWO_3 bronzes. Figures A-5, A-6 and A-7 in Appendix A are the gamma spectra obtained for holmium, a 1:1 atom ratio Ho/W standard, and a holmium bronze with $x = 0.100$ respectively. Here again, the ^{166}Ho photopeaks at 1.38,

Table 1. Nuclear properties of tungsten bronze constituents subject to thermal neutron activation

Target Nuclide	Abundance (%)	Cross Section (Barns)	(n,γ) Product	Product Half-life	Principal Gamma-rays (Mev)
^{39}K	93.22	2.0	^{40}K	Stable	
^{40}K	0.118	70.	^{41}K	Stable	
^{41}K	6.77	1.2	^{42}K	12.36h	0.31(0.2%), 1.524(18%)
^{165}Ho	100.0	64.	^{166}Ho	26.9 h	0.081(5.4%), 1.380(0.9%), 1.582(0.20%) 1.663(0.16%)
^{138}La	0.089	---	^{139}La	Stable	
^{139}La	99.911	8.9	^{140}La	40.22h	0.329(20%), 0.487(40%), 0.815(19%), 0.923(10%), 1.596(96%), 2.53(3%)
^{180}W	0.135	< 20.	^{181}W	140 d	0.006(1%), 0.136(0.1%), 0.152(0.1%)
^{182}W	26.4	20.	^{183}W	Stable	
		0.5	^{183m}W	5.5 sec	0.046(8%), 0.053(11%), 0.099(9%), 0.102(4%), 0.108(19%), 0.160(6%)
^{183}W	14.4	11.	^{184}W	Stable	
^{184}W	30.6	2.1	^{185}W	75 d	No γ
^{186}W	28.4	40.	^{187}W	23.9h	0.072(11%), 0.134(9%), 0.479(23%), 0.552(5%), 0.618(6%), 0.686(27%), 0.773(4%)
^{16}O	99.759	1.8×10^{-4}	^{17}O	Stable	
^{17}O	0.037	---	^{18}O	Stable	
^{18}O	0.204	2.1×10^{-4}	^{19}O	29.1 sec	0.197(97%), 1.37(59%)

1.58 and 1.66 Mev are free from tungsten interference.

For the lanthanum bronzes, the photopeak of interest was the 1.60 Mev gamma ray from ^{140}La produced from the (n,γ) reaction of ^{139}La. Figures A-8, A-9 and A-10 in Appendix A represent gamma ray spectra of La_2O_3, a 1:1 atom mixture of La/W standard, and a lanthanum bronze with x = 0.15. As can be seen from the spectra, the ^{187}W peaks do not interfere with the 1.60 Mev photopeaks of ^{140}La.

All bronzes used for analysis were obtained from H. Shanks of the Ames Laboratory, Ames, Iowa. The technique used in all cases was an internal standard method of analysis. A standard, of known metal to tungsten ratio, was irradiated simultaneously with samples of unknown metal to tungsten ratios. Following irradiation, the ratio of the area under the photopeak associated with the metal ion to the area under the 0.479 and/or 0.686 Mev ^{187}W peaks in the standards was compared to the ratio of the same two peaks in the unknown and from this the 'x' value, or metal to tungsten ratio, was determined as is indicated by the following:

$$x_{bronze} = \frac{x_{std}\,(W/M)_{std}}{(W/M)_{bronze}} \cdot \qquad (16)$$

Prior to attempting the determination of the actual 'x' value in the bronzes of interest, it was desired to test the reproducibility and establish the method of analysis. For this purpose, powdered dried samples of K_2WO_4 varying in weight from 9 to 166 mg were enclosed in polyethylene ampoules for irradiation. Samples were irradiated for ten seconds at a flux of 1×10^{13} n/cm^2 sec. Immediately following irradiation, samples were counted for varying time periods using both the solid state detector and

the scintillation detector. The areas under the 0.479 Mev ^{187}W peak and the 1.52 Mev ^{41}K photopeaks were calculated, corrected for decay and the counting rate ratio, W/K, was determined for each sample. Samples counted using the solid state detector were placed 1 cm from the face of the detector; samples counted using the scintillation detector were placed 6 cm above the well and counted in some instances with 2.5 cm of lead to depress the lower energy ^{187}W peaks. Table 2 indicates the results obtained. The W/K peak area ratios determined by using the scintillation crystal with lead is approximately 1/3 the ratio for samples counted without additional lead shielding. Reproducible results were obtained as can be seen from the table.

The areas under the photopeaks of interest for the previously discussed samples were determined by two different methods. Photopeak areas for samples counted using the scintillation detector were determined using classical methods in which the area of a spectral peak is computed so as to exclude the Compton continuum upon which it rests.

Halfhill, in 1958, anticipated the need for reading out pulse height data in a form which would be computer compatible, magnetic tape (38). Soon after, methods of computation for pulse height spectra accumulated with multichannel analyzers began to appear in the literature. By 1960, computer coupled activiation analysis was described by Kuykendall (39) and associates.

In the present work, all data taken using the solid state detection system were transferred to IBM cards and submitted for analysis with a computer program called ICPEAX written in FORTRAN for use with the IBM

Table 2. W/K counting rate ratios for K_2WO_4

Crystal	Weight (mg)	Counting Time (minutes)		$\frac{W}{K}$
	NaI(Tl) Detected Samples			
NaI(Tl)	13.9	5		38.2
NaI(Tl)	32.5	5		39.4
NaI(Tl)	166.0	5		37.9
NaI(Tl)	166.0	10		38.7
			Avg.	38.6 ± 0.3
	NaI(Tl) Detected Samples - 2.5 cm Lead			
NaI(Tl)	50.4	4		11.1
NaI(Tl)	10.6	4		11.3
NaI(Tl)	10.6	12		10.1
NaI(Tl)	50.4	12		9.4
NaI(Tl)	9.0	4		10.8
NaI(Tl)	9.0	12		11.0
NaI(Tl)	27.3	4		10.5
NaI(Tl)	27.3	8		10.7
NaI(Tl)	45.0	4		11.1
NaI(Tl)	10.6	8		9.9
NaI(Tl)	27.3	12		10.7
NaI(Tl)	45.0	12		10.9
			Avg.	10.6 ± 0.5
	Ge(Li) Detected Samples			
Ge(Li)	50.4	4		252.6
Ge(Li)	50.4	8		234.8
Ge(Li)	10.6	4		239.7
Ge(Li)	10.6	8		260.4
Ge(Li)	9.0	4		246.4
Ge(Li)	9.0	8		250.4
Ge(Li)	9.0	12		252.4
Ge(Li)	27.3	4		235.1
Ge(Li)	27.3	8		232.4
Ge(Li)	45.0	4		250.8
Ge(Li)	45.0	8		251.4
Ge(Li)	45.0	12		230.7
Ge(Li)	13.9	5		234.6
Ge(Li)	13.9	10		245.1
Ge(Li)	32.5	5		238.6
Ge(Li)	32.5	10		225.6
Ge(Li)	135.4	5		246.6
Ge(Li)	79.6	5		259.2
Ge(Li)	166.0	5		261.0
			Avg.	244.6 ± 9.4

360-50 computer.[1]

The ICPEAX program is designed to automatically detect photopeaks in Ge(Li) spectra and determine the peak parameters. This is done by an analysis of the smoothed second derivative of the spectrum. A Gaussian fit is attempted on all peaks found in a preliminary search. In addition to the three basic peak parameters found, width, location, and height, the area is also determined, and the energies of the photopeaks of interest.

Tungsten Bronzes

The tungsten bronzes are nonstoichiometric compounds represented by the general formula M_xWO_3 where x may be any value from 0 to 1 and M may be any of several elements. The more commonly known tungsten bronzes are those of the alkali metals (40-45) and rare earths (46), but bronzes have also been reported for barium (47), uranium,[2] copper (48), silver (49) and thallium (50).

As a class of compounds the tungsten bronzes may be termed chemically inert. They can be oxidized with oxygen in the presence of base to tungstates, and in basic solution, they will reduce silver nitrate to silver; however, they are resistant to all acids and water. Some of the bronzes have been analyzed by classical chemical methods (51-54); however, procedures used require a considerable length of time and the sample in each case is destroyed.

---

[1]Korthoven, P. J and P. Haustein, Ames, Iowa. Use of a computer program to resolve gamma ray spectra. Private communication. 1967.

[2]Ostertag, W., Wright-Patterson A.F.B., Ohio. Information on the uranium tungsten bronzes. Private communication. 1966.

The first nondestructive analysis of tungsten bronzes was done in 1963 by Reuland and Voigt (55) who analyzed the sodium content in the sodium tungsten bronzes by thermal neutron activation. Since that time, potassium, rubidium and barium have been determined nondestructively (36) in their tungsten bronzes by neutron and high energy photon activation. The determination of lanthanum, holmium and uranium tungsten bronzes has also been accomplished nondestructively by thermal neutron activation (35).

Irradiation Facilities and Detection Equipment

All bronze samples were irradiated in the Ames Laboratory Research Reactor. The ALRR is a heavy water moderated and cooled steady state reactor operated at five megawatts thermal power output.

Pneumatic transfer systems are used for rapid access to high neutron fluxes. For all irradiation, the systems used were either 'R-6' or 'R-4'. The R-6 system accommodates a "rabbit" two inches in diameter. Its irradiation position is at the edge of and 14 inches below the core, and at full power the thermal neutron flux available is 8×10^{12} n/cm^2 sec. The R-4 system, accommodating a rabbit the same size as that used in R-6, is located directly across from R-6 and also terminates below the core. The thermal neutron flux available at full power in the R-4 position is 1×10^{13} n/cm^2 sec.

The detection system consisted of a lead shielded Ge(Li) solid state detector having a trapezoidal active area of 11 cm^2 and drifted depth of 1.1 cm. The relative peak efficiency at 1.33 Mev is 3.5 percent. The system resolution at 1.33 Mev FWHM is 3.48 Kev.

For purposes of comparison, some counting was also done using a lead

shielded four inch by four inch thallium activated sodium-iodide well type scintillation crystal coupled to a photomultiplier tube which in turn is coupled to a pulse height analyzer.

The solid state detector is coupled to a preamplifier and an amplifier which, in turn, is coupled to a pulse height analyzer. In this work all counting was done on a RIDL 1600 channel analyzer, Model 24-3, which stores and sorts the output pulses in one of a series of storage units called channels, each channel representing a preset energy range.

Analysis of K_xWO_3

The determination of potassium in K_xWO_3 was accomplished nondestructively by means of an internal standard method of analysis using K_2WO_4 as the comparison standard. Powdered samples of dried K_2WO_4 were sealed in polyethylene ampoules for irradiation. Bronze samples, previously analyzed by beta counting, were also sealed in polyethylene ampoules. Each irradiation consisted of two samples and three K_2WO_4 standards irradiated for 30 seconds at a flux of 8×10^{12} n/cm^2 sec. Samples were counted immediately after their removal from the reactor. Samples counted using the solid state detector were 3 cm from the detector face while for scintillation counting the samples were 4 cm away with 1.6 cm of lead to suppress the lower ^{187}W peaks. Data taken using the solid state detector were analyzed using the ICPEAX peak-finding program to determine the energy of the photopeak and the area under the peak. For data taken using the scintillation detector the areas under the photopeaks of interest were determined by hand calculation.

For each sample the ratio of the area under the 1.52 Mev ^{41}K peak to

each of five ^{187}W peaks at 0.480, 0.552, 0.619, 0.686 and 0.773 Mev was made, and an 'x' value calculated from each comparison. The 'x' values were calculated from the ratio of the counting rate ratio of W/K for the standard to that for the unknown. These 'x' values were then averaged for a single determination.

The results obtained are indicated in Table 3. As can be seen from the table, the data obtained using the Ge(Li) detector are much more precise than those results obtained using the scintillation detector. Also, it may be noted that the discrepancy between the Ge(Li) data and the data obtained from beta counting is considerably less than the difference between the solid state and the scintillation detector.

The potassium bronze was one example of a system in which one might have expected to obtain a better analysis using the scintillation detector because of the poor efficiency of the solid state detector for gamma energies greater than 1 Mev. However, the greater resolution of the solid state detector appeared to outweigh its lower efficiency even for as small an amount of potassium relative to the amount of tungsten present in the bronzes.

One possible source of error in the analysis of K_xWO_3 lies in the assumption that the ratio of K to W in the standards is exactly 2.0. For this reason standard samples of a 1:1 atom ratio of K:W were prepared by taking appropriate aliquots of potassium and tungsten from stock solutions of potassium hydroxide and tungsten oxide (WO_3) dissolved in ammonium hydroxide. For the standard analysis five standards were irradiated for one minute at full power and counted approximately one hour after removal

Table 3. Analysis for K in K_xWO_3

Sample Number	X value Ge(Li)	X value NaI(Tl)	X value β
K9H -1	0.326	0.213	
2	0.333	0.234	
3	0.304	0.202	
4	0.332	0.472	
5	0.327	0.416	
6	---	0.401	
Avg.	0.324 ± 0.012	0.323 ± 0.120	0.276
K14K-1	0.293	0.413	
2	0.296	0.441	
3	0.298	0.398	
4	0.298	0.406	
5	---	0.421	
Avg.	0.296 ± 0.002	0.416 ± 0.015	0.312
K1B -1	0.308	0.403	
2	0.307	0.386	
3	0.304	0.398	
4	0.307	0.423	
5	0.321	---	
Avg.	0.309 ± 0.007	0.402 ± 0.015	0.284
K15H-1	0.280	0.321	
2	0.277	0.334	
3	0.289	0.298	
4	0.281	0.340	
5	0.285	---	
Avg.	0.282 ± 0.005	0.323 ± 0.019	0.302
K10A-1	0.298	0.341	
2	0.296	0.322	
3	0.301	0.414	
4	0.295	0.297	
5	0.298	---	
Avg.	0.298 ± 0.002	0.344 ± 0.035	0.304

from the reactor. Table 4 indicates the results obtained. Within the precision obtained, the K/W ratio in the standard, a 1:1 mixture of K:W, was found to be 1.

Table 4. Analysis for K in a 1:1 standard mixture of K:W

Sample	'x' Values
Std-1	0.9912
Std-2	0.9987
Std-3	1.029
Std-4	0.9964
Std-5	0.9959
	$x = 1.002 \pm 0.015$
	nominal x value = 1.000

Since the standards appeared to be reproducible, five samples of bronze unknown, K1B, were analyzed using an internal standard method. Samples and standards were irradiated for one minute at full power and counted approximately one hour after irradiation. Table 5 indicates the results obtained and also the results from the previous analysis. In both cases, the results indicate excellent agreement and precision.

Table 5. Comparison of K 'x' values determined using two different standards

	K_2WO_4 Standard	1:1 Mixture of K:W Standard
	'x' value	'x' value
1	0.308	0.306
2	0.307	0.308
3	0.304	0.308
4	0.307	0.307
5	0.321	0.310
	$x = 0.309 \pm 0.007$	$x = 0.308 \pm 0.002$

Analysis of Ho_xWO_3

The determination of holmium in Ho_xWO_3 was also accomplished by means of a nondestructive method of analysis. Standard samples of a 1:1 atom ratio of holmium to tungsten were prepared by dissolving Ho_2O_3 in HNO_3 to a concentration of 10.000 mg/ml. The source of tungsten was tungsten oxide (WO_3) which had been dried, weighed and dissolved in ammonium hydroxide to a concentration of 10.000 mg/ml. Aliquots (200 lambda) of each were withdrawn, pipetted into small polyethylene irradiation vials, evaporated and sealed for irradiation. Two sets of standards, each consisting of eight samples, were irradiated. The first set of standards was irradiated for five minutes at five megawatts and counted approximately seven hours after irradiation. The second set was irradiated for one minute

at full power and counted approximately an hour following removal from the reactor. In each case, the sample was counted six centimeters from the face of the crystal. Each sample was counted for a thirty minute live time period. Data was processed using the ICPEAX peak-finding program and the respective activities corrected for decay.

For the first set of standards direct comparison of the 0.479 Mev, 0.686 Mev, and 0.773 Mev ^{187}W peaks was made to each of three ^{166}Ho peaks at 1.38, 1.58 and 1.66 Mev. Three peaks were chosen for comparison because, although the cross section for the production of ^{166}Ho from ^{165}Ho by means of an (n,γ) reaction is relatively large, 64 barns, the intensity of the gamma rays emitted by ^{166}Ho are fairly low as can be seen from Table 1. Also the respective energies of the three photopeaks of interest lie above 1 Mev in energy and, as has been pointed out previously, the efficiency of the solid state detector tends to drop considerably in the region beyond 1 Mev.

Results obtained are indicated in Table 6. As was done for previous bronzes, the first sample in each case was arbitrarily assigned an 'x' value (Ho/W ratio) of 1.000 and the remaining 'x' values determined using this as a comparison. As is apparent from the table, the most intense ^{166}Ho peak at 1.38 Mev indicated results that were most reproducible.

For the second set of standards irradiated only the 1.38 Mev ^{166}Ho photopeak was chosen for comparison purposes as is indicated in Table 7. Also, the 0.680 Mev ^{187}W was the only tungsten peak chosen for comparison because, as will be noticed from the spectrum in Fig. 1, the 0.480 Mev tungsten peak is not as well resolved as is the 0.680 Mev photopeak

Table 6. Analysis for Ho in a 1:1 standard mixture of Ho:W

Sample	Counting Rate Ratio		Counting Rate Ratio		Counting Rate Ratio	
	$\frac{W-.479}{Ho-1.38}$	Ho/W	$\frac{W-.479}{Ho-1.58}$	Ho/W	$\frac{W-.479}{Ho-1.66}$	Ho/W
Std-1	25.93	1.000	149.6	1.000	256.4	1.000
2	25.94	0.9996	150.7	0.9927	247.3	1.037
3	24.59	1.054	153.2	0.9765	235.4	1.089
4	25.71	1.008	151.4	0.9881	251.3	1.020
5	25.88	1.002	150.5	0.9940	255.7	1.003
6	25.97	0.9984	152.7	0.9797	249.8	1.026
7	24.79	1.046	152.0	0.9842	238.3	1.076
8	25.80	1.005	151.1	0.9901	250.7	1.023
	Avg.	1.014 ± 0.022	Avg.	0.9882 ± 0.0070	Avg.	1.034 ± 0.032
	$\frac{W-.686}{Ho-1.38}$	Ho/W	$\frac{W-.686}{Ho-1.58}$	Ho/W	$\frac{W-.686}{Ho-1.66}$	Ho/W
Std-1	18.58	1.000	107.2	1.000	183.7	1.000
2	18.67	0.9952	108.5	0.9980	178.0	1.032
3	18.39	1.010	114.6	0.9354	176.1	1.043
4	18.46	1.006	109.8	0.9763	179.7	1.022
5	18.51	1.004	111.7	0.9597	175.2	1.048
6	18.63	0.9973	110.4	0.9710	176.9	1.038
7	18.57	1.001	109.9	0.9754	178.7	1.027
8	18.49	1.005	107.8	0.9944	180.5	1.018
	Avg.	1.002 ± 0.005	Avg.	0.9763 ± 0.022	Avg.	1.028 ± 0.015
	$\frac{W-.773}{Ho-1.38}$	Ho/W	$\frac{W-.773}{Ho-1.58}$	Ho/W	$\frac{W-.773}{Ho-1.66}$	Ho/W
Std-1	2.357	1.000	13.60	1.000	23.31	1.000
2	2.412	0.9722	14.02	0.9700	22.99	1.014
3	2.346	1.005	14.62	0.9302	22.46	1.038
4	2.351	1.002	14.11	0.9638	22.72	1.026
5	2.349	1.003	14.70	0.9252	22.23	1.049
6	2.352	1.002	14.67	0.9271	25.54	0.9127
7	2.400	0.9821	14.35	0.9477	22.96	1.015
8	2.356	1.000	13.92	0.9770	23.02	1.013
	Avg.	0.9958 ± 0.012	Avg.	0.9551 ± 0.027	Avg.	1.008 ± 0.042

although the 0.480 peak is the more intense. The 0.773 Mev photopeak was not used because of its lower intensity.

Table 7. Analysis for Ho in a 1:1 standard mixture of Ho:W using the 1.38 Mev photopeak of ^{166}Ho for comparison

Sample	Counting Rate Ratio $\frac{W\ .686}{Ho\ 1.38}$	Ho/W
Std-1	15.82	1.000
-2	15.76	1.004
-3	15.93	0.9931
-4	15.79	1.002
-5	15.75	1.004
-6	15.66	1.010
-7	15.81	1.001
-8	15.70	1.008
		Avg. = 1.003 ± 0.005

Since the standards were reproducible, a series of holmium bronzes having a nominal 'x' value (Ho/W ratio) of 0.100 was analyzed using an internal standard method. For the first irradiation, four standards and three unknowns were irradiated in the same rabbit capsule for five minutes at five megawatts. Counting was done approximately eight hours after removal from the reactor. The sample in each case was six centimeters from the crystal face and data was accumulated for thirty minutes. Data was processed in the same manner as for the standards. Results are indicated in Table 8.

For the second irradiation, five standards and six samples were

Table 8. Analysis for Ho in Ho_xWO_3

Sample		Counting Rate Ratio $\frac{W\ .479}{Ho\ 1.38}$	Counting Rate Ratio $\frac{W\ .686}{Ho\ 1.38}$	$(Ho/W)_{.479}$	$(Ho/W)_{.686}$
IRRADIATION 1					
Std-1		25.78	18.83		
Std-2		25.49	18.54		
Std-3		25.25	18.32		
Std-4		25.55	18.62		
	Avg.	25.52	18.58		
S-1		308.9	229.5	0.0826	0.0810
S-2		308.0	228.4	0.0828	0.0813
S-3		308.8	230.1	0.0826	0.0807
				Avg. 0.0827 ± 0.0004	0.0810 ± 0.0003
IRRADIATION 2					
Std-1		39.23	30.08		
Std-2		39.41	29.96		
Std-3		39.31	30.22		
Std-4		39.66	30.18		
Std-5		39.40	30.03		
	Avg.	39.40	30.09		
S-1		481.7	372.9	0.0818	0.0807
S-2		473.6	376.1	0.0832	0.0800
S-3		478.2	365.2	0.0824	0.0824
S-4		479.9	348.3	0.0821	0.0864
S-5		487.6	369.7	0.0808	0.0814
S-6		479.3	366.1	0.0822	0.0822
				Avg. 0.0821 ± 0.0009	0.0822 ± 0.0022

irradiated simultaneously for five minutes at full power. Counting intervals, geometry and data processing were identical to the first irradiation. Table 8 also indicates the results obtained.

Analysis of La_xWO_3

The determination of lanthanum in La_xWO_3 was accomplished nondestructively by an internal standard method of analysis. To ensure homogeneity in samples to be used as standards, all standards were made in solution, dried, and the dried samples irradiated. Therefore, an appropriate amount of WO_3 was dried, weighed and dissolved in NH_4OH to make a solution of concentration 10.000 mg/ml. Likewise an appropriate amount of La_2O_3 was dried, weighed, and dissolved in HNO_3 to a concentration of 10.000 mg/ml. From these stock solutions, aliquots were withdrawn (200 lambda) and pipetted into small polyethylene irradiation capsules and evaporated. The polyethylene capsules were previously washed in HNO_3 and vacuum dried.

To determine the reproducibility of the standards, two series of 8-10 samples, with a 1:1 atom ratio of La:W were irradiated for five minutes at five megawatts and counted about six hours after removal from the reactor. Samples in each case were 4 centimeters from the detector face and data accumulated for 10 minute live time periods. Data obtained was processed using the ICPEAX peak-finding program, and the respective activities corrected for decay. Direct comparison of the 1.60 Mev photopeak of ^{140}La was made with the 0.686 Mev photopeak of ^{187}W and an 'x' value for the lanthanum in tungsten in each bronze calculated by comparing the W/La ratio in the standard to the ratio in the unknown. The 1.60 Mev

^{140}La photopeak was chosen for comparison because of its intensity (Table 1) and also because the energy of the gamma rays produced from the (n,γ) reaction of ^{139}La lie in the area 0.329 to 0.923 Mev and would be subject to interference from ^{187}W. The 'x' values obtained are indicated in Table 9. The counting rate ratio of the first sample was arbitrarily taken to be a standard and assigned an 'x' value of 1.000. The 'x' values for the other samples were determined using the first samples as a standard. As can be seen from the table, the results indicated reproducibility.

A second series of standards prepared in the same manner was also irradiated for five minutes at full power and counted about six hours after removal from the reactor. All values were calculated in the same manner as they were for the first set of standards. Table 9 indicates the results obtained. Sample results again indicated reproducibility.

For the analysis of the bronzes, the same procedure was used as for the standards. For each irradiation, five standards and three samples were irradiated simultaneously for five minutes at five megawatts at a flux of 8×10^{12} neutrons/cm^2 sec. Standards and samples were counted approximately six hours after removal from the reactor. Data was processed using the ICPEAX program of analysis, and the activities obtained for a given photopeak corrected for decay. The counting rate ratio, W/La, for the standards was averaged for each irradiation, and this average was then used to determine the 'x' value for the bronze. Table 10 indicates the results obtained for the analysis of two bronzes with nominal 'x' values of 0.015 and 0.15.

Table 9. Analysis for La in a 1:1 standard mixture of La:W

Sample	Counting Rate Ratio W/La	La/W
Std-1	1.985	1.00
Std-2	2.01	0.985
Std-3	1.96	1.01
Std-4	2.00	0.990
Std-5	1.89	1.05
Std-6	1.96	1.01
Std-7	1.97	1.01
Std-8	1.98	1.00
Std-9	2.00	0.990
Std-10	1.98	1.00
		$\bar{x}$ = 1.007 ± 0.006
		Nominal 'x' value = 1.000
Std-1	2.009	1.00
Std-2	2.12	0.991
Std-3	2.08	1.01
Std-4	2.07	1.01
Std-5	2.11	0.995
Std-6	2.10	1.00
Std-7	--	--
Std-8	--	--
Std-9	2.09	1.00
Std-10	2.10	1.00
		$\bar{x}$ = 1.007 ± 0.006
		Nominal 'x' value = 1.000

Table 10. Analysis for La in La_xWO_3

Sample	Counting Rate Ratio W/La	La/W
IRRADIATION 1		
Std-1	1.90	
Std-2	1.86	
Std-3	1.88	
Std-4	1.88	
	Avg. = 1.88	
S-1	39.73	0.0473
S-2	36.56	0.0514
S-3	41.08	0.0458
S-4	40.44	0.0465
S-5	38.39	0.0490
		x = 0.0480 ± 0.0024
	Nominal 'x' value	= 0.015
IRRADIATION 2		
Std-1	1.20	
Std-2	1.24	
Std-3	1.24	
Std-4	1.24	
Std-5	1.24	
	Avg. = 1.23	
S-1	9.26	0.133
S-2	8.82	0.139
S-3	8.67	0.142
S-4	8.93	0.138
S-5	8.80	0.139
S-6	9.06	0.136
		x = 0.138 ± 0.004
	Nominal 'x' value	= 0.150

Table 10. (Continued)

Sample	Counting Rate Ratio W/La	La/W
IRRADIATION 3		
Std-1	1.78	
Std-2	1.75	
Std-3	1.82	
Std-4	1.81	
Std-5	1.78	
	Avg. = 1.79	
S-1	13.0	0.137
S-2	12.7	0.141
S-3	12.9	0.139
		x = 0.139 ± 0.003
	Nominal 'x' value = 0.150	
IRRADIATION 4		
Std-1	2.04	
Std-2	2.11	
Std-3	2.01	
Std-4	2.08	
Std-5	2.07	
	Avg. = 2.06	
S-1	--	--
S-2	14.8	0.139
S-3	15.3	0.135
		x = 0.137 ± 0.004
	Nominal 'x' value = 0.150	

ACTIVATION WITH FISSION NEUTRONS

Introduction

The process of nuclear fission was first observed in 1939 when O. Hahn and F. Strassman (56) discovered that the uranium nucleus, upon bombardment with neutrons, could split into two large fragments each possessing extremely high kinetic energies. The process they observed differed from previous nuclear reactions studied in which particles of low mass, protons or alpha particles, were emitted with comparatively moderate energies.

In the fission process the weights and charges of the fission products are roughly half that of the target nucleus and the energy released in the fission process approximately 200 Mev. Fission into two equal fragments is not the most likely or even the most probable mode of fragmentation. Maximum fission product yields occur at A = 95 and A = 138. Figure 1 indicates the yields of fission product chains as a function of mass number for the slow neutron fission of ^{235}U. From the curve, it may be seen that symmetrical fission, which would produce two fission products of equal mass about 117, is rather rare.

For heavy elements the ratio of neutrons to protons is greater than for the light elements. Consequently, the fission products formed contain more neutrons than the stable isotopes of the same element. For example, we can consider the typical fission products ^{148}La and ^{88}Br, heavily neutron rich, as compared to stable ^{139}La and ^{81}Br. Because the neutron excess is so large, some neutrons are emitted instantaneously before the fission products have completely separated. These neutrons are known as

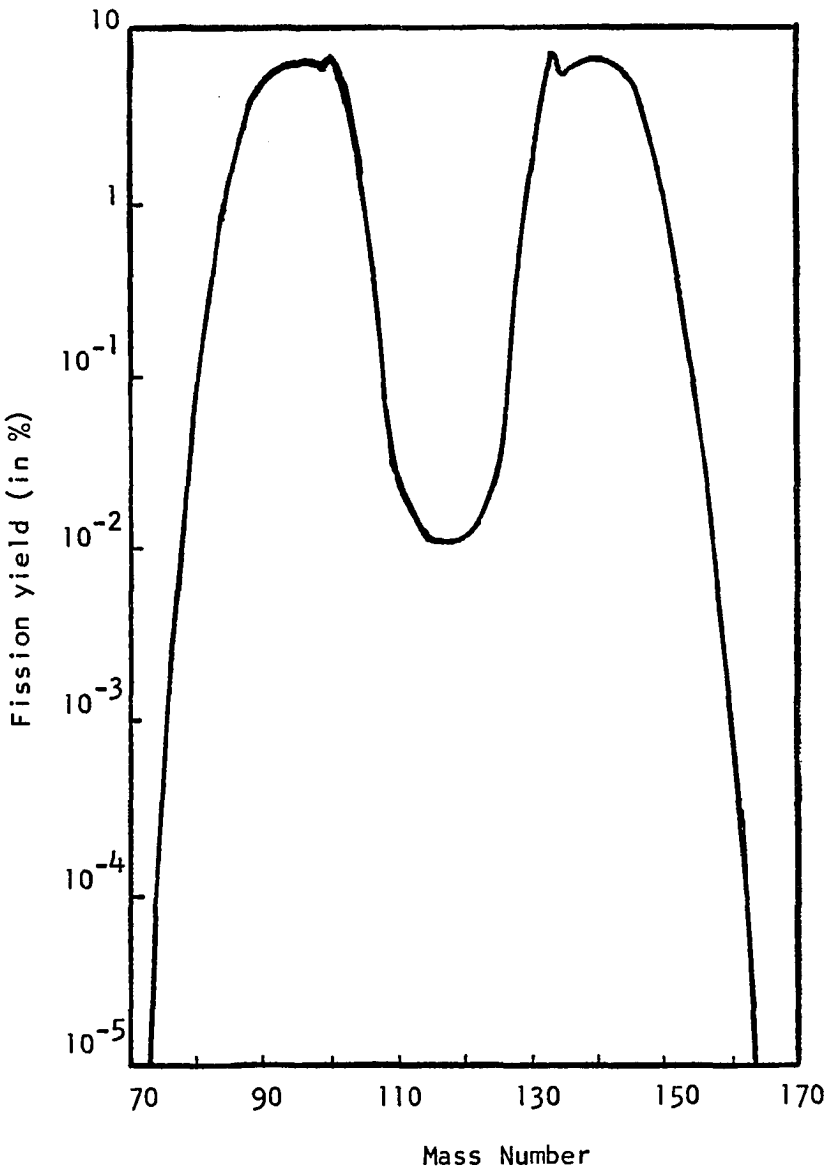

Figure 1. Yields of fission-product chains as a function of mass number for the slow neutron fission of ^{235}U (57)

'fission' or 'prompt' neutrons so as to distinguish them from the delayed neutrons. On an average 2.5 fission or prompt neutrons are emitted per ^{235}U fission. Fission products, even after emission of fission neutrons, are still far from stable and consequently undergo beta decay. Some fission products, particularly those of low neutron binding energy, will emit neutrons following beta decay. These are known as 'delayed' neutrons.

A nuclear reactor, being the most prolific source of neutrons, is an assembly of fissionable materials such as uranium enriched in ^{235}U and arranged in such a manner as to maintain a self-sustaining chain reaction. For each ^{235}U nucleus that fissions, an average of 2.44 neutrons are emitted. The only requirement for a self-sustaining reaction is that at least one of these neutrons be available to continue the fission process. Therefore, for any given reactor there is a minimum or critical size necessary to maintain a self-sustaining chain reaction. Most reactors, including the ALRR, because they use thermal neutrons for the propagation of the chain reaction, contain a moderator such as heavy water whose purpose it is to slow down the fast neutrons emitted at the time of fission to thermal energies.

In considering the neutrons that are produced in a nuclear reactor, it is customary to divide them into three main categories based on the energy of the neutron: fast, resonance or epi-cadmium, and thermal. Before any type of moderation, fission neutrons show extremely wide energy ranges, from zero to 15 Mev, as can be seen from the 'fission spectrum' illustrated in Figure 2.

Despite the energy classification, the title of the categories refers

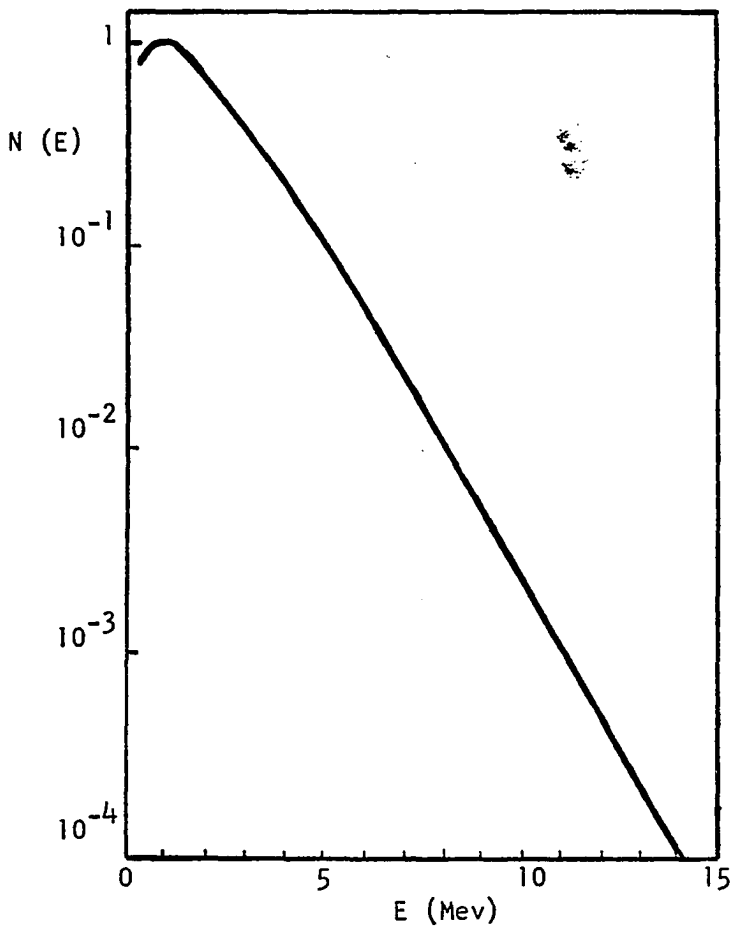

Figure 2. Typical fission spectrum indicating the number of neutrons per unit energy N(E) as a function of neutron energy (58)

to the manner in which the neutrons are obtained and not the nuclear reaction produced by them. The term 'fast' neutron refers to those neutrons produced in fission that have not been moderated by collision. The fast neutrons comprise an energy range from 15 to 1 Mev. Resonance or epicadmium neutrons are those neutrons which range from 1 Mev down to 1 ev. Thermal neutrons are those neutrons which have lost their excess energy in collisions with the moderator nuclei and therefore have an energy corresponding to the temperature of the ambient matter. They show a Maxwell-Boltzmann energy distribution and have at room temperature a mean energy of 0.025 ev.

The flux of fast neutrons near a uranium fuel rod will be on the same order of magnitude as the thermal neutron flux at that point. However, the intensity of fast neutrons of a given energy will drop rapidly with increasing distance from the fuel rod because of moderation. Therefore, although a high flux of fast neutrons is available, its usefulness for research may be complicated by the wide energy range of the fast neutrons represented (Figure 2) and also by the presence of an intense resonance flux. Fast neutrons can be obtained at high intensities and accompanied by a great reduction in thermal flux by means of a neutron converter.

A neutron converter assembly was designed and built for use in the ALRR and installed in the V-3 position of the ALRR. Prior to installation, the thermal flux in the side thimbles was approximately 1.6×10^{12} n/cm^2 sec. The converter assembly, Figure 3, is composed of three concentric fuel tubes containing an aluminum-uranium fuel section enriched in ^{235}U. This assembly has a total mass of 170 grams of ^{235}U distributed in the three

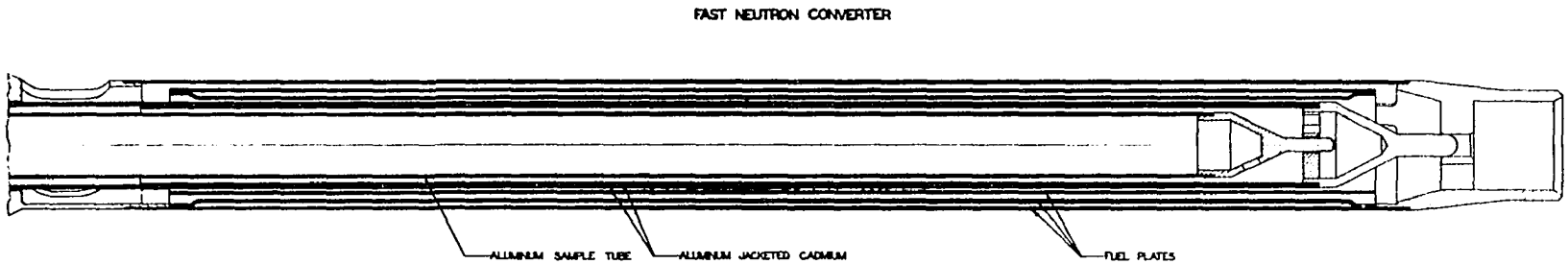

Figure 3. Neutron converter assembly

tubes. The design of the converter is such that it provides a hollow fuel array cooled by a forced flow of heavy water. After the flux converter was installed, the fast neutron flux was measured at various positions using nickel foil monitors at the reactor ambient temperatures (50°C). A neutron flux of 2.7×10^{12} n/cm^2 sec for E > 1 Mev was recorded over a 10-inch section starting three inches from the bottom.

Metastable Isomers

Strictly speaking, any excited state of a nucleus is a metastable state, but by custom, the term is usually reserved for those excited states with $t_{\frac{1}{2}}$ equal to 10^{-9} seconds or greater. Metastable isomers of stable isotopes may be formed in a nuclear reactor by any of four different methods:

(1) radiative neutron capture of a neighboring isotope,

$$^{A-1}Z(n,\gamma)^{Am}Z$$

(2) photoexcitation of the stable isotope

$$^{A}Z(\gamma)^{Am}Z$$

(3) n,2n reactions on neighboring stable isotopes

$$^{A+1}Z(n,2n)^{Am}Z \qquad \text{and}$$

(4) by inelastic neutron scattering on the stable isotope

$$^{A}Z(n,n')^{Am}Z \ .$$

The purpose of the present investigation was (1) to determine the

relative importance of the (n,γ) and the (n,n') reactions and the contribution of each to the production of the metastable isomer, and (2) to evaluate the usefulness of the metastable isomers as sensitive indicators in activation analysis.

The inelastic scattering process (n,n') is usually considered relatively unimportant when compared to the (n,γ) reaction because of the low cross sections and also the low flux of higher energy neutrons available in most reactor irradiation facilities. However, with the installation of the neutron converter assembly in the ALRR, a high intensity fast flux source became available.

In the inelastic scattering process, the fast neutron is captured by a target nucleus to form an excited state of the compound nucleus. A neutron of lower kinetic energy is then emitted, leaving the target nucleus in an excited state. Therefore, in an inelastic scattering collision, some or all of the kinetic energy of the neutron is converted into excitation energy of the target nucleus. The excess energy is subsequently emitted as one or more photons of gamma radiation. If E_A equals the total kinetic energy of the neutron and target nucleus before collision, and E_B equals the kinetic energy after collision, then E_γ, the energy of the emitted gamma radiation, may be represented by:

$$E_A - E_B = E_\gamma \quad . \tag{17}$$

What is important here is to note that E_A must be at least equal to E_γ for the reaction to occur.

Since the kinetic energy of the target nucleus is generally considered

negligible compared to that of the incident neutron, the initial energy of the neutron must exceed the threshold energy of the target nucleus for the reaction. The minimum excitation energy of elements of moderate to high mass number is usually from 0.1 to 1 Mev. With decreasing mass number of the target nucleus, there is a tendency for the threshold energy to increase so that neutrons of higher energy are necessary for inelastic scattering to occur.

Therefore, the probability of (n,n') reactions occurring as opposed to (n,γ) or other reactions following neutron absorption, increases with increasing neutron energy. This is because the separation of the possible excited levels a nucleus might occupy is smaller at high excitation energies and consequently there are more excitation levels a nucleus can occupy within a given energy interval after expulsion of a neutron.

The problem of determining the cross sections for neutron reactions is complex because the cross section depends not only upon the energy of the incident neutron, but also varies with each isotope of the same element and also with the nature of the reaction. For many elements, particularly heavy elements with a mass number greater than 100, the variation of absorptive cross section with neutron energy reveals three separate regions. A low energy region exists in which the absorption cross section, σ_a, varies inversely as the square root of the neutron energy. Since the energy of the neutron is kinetic energy, σ_a is inversely porportional to the neutron velocity. This region, therefore, is called the 1/v region and the neutrons obey the 1/v law.

Following the 1/v region, a resonance region for a given element

occurs for neutrons of about 0.1 to 1000 ev in energy. This region is characterized by the occurrence of peaks where the absorption cross section rises quite sharply to high values for certain neutron energies and then falls again.

At energies greater than 10 Kev, a fast neutron region occurs. The cross sections in this region are extremely low, on the order of less than 10 barns, and becoming smaller for energies greater than 0.1 Mev. Some resonance behavior does occur in this fast neutron region.

At high neutron energies, generally in excess of 1 Mev, the cross section both for absorption plus inelastic scattering, and also for elastic scattering, approaches the cross section of the nucleus. Therefore, the total cross section tends toward πR^2 where R is the nuclear radius. The total cross section of the nucleus, σ_t, with a high energy neutron approaches a limit of $\sigma_t = 2\pi R^2$.

Hauser and Feshbach (59) in 1952 pointed out that just above threshold energy, the cross section for the production of an excited state of a target nucleus by inelastic scattering is sensitive to the spins of the ground and excited states and to a lesser extent to the parities of these states. The statistical theory of nuclear reactions proposed by Hauser and Feshbach, which was used for estimating inelastic scattering cross sections, was modified somewhat by Moldauer in 1961 (60).

Recent work that has been done on the determination of neutron fluxes shows the need to obtain better cross section data through the use of reactions sensitive to neutrons in the energy region 10 Kev to 2 Mev. The upper part of this energy interval is covered by (n,n') reactions which

form metastable isomers. Excitation cross sections have been measured for many isotopes with monoenergetic neutrons (61, 62).

Cross sections for the reaction, $^{111}Cd(n,n')^{111m}Cd$ and $^{87}Sr(n,n')^{87m}Sr$, have been measured in the energy region 2.2 to 3.5 Mev and 13.7 to 14.8 Mev (63). The results obtained indicated the usefulness of these isotopes as neutron flux monitors. The application of metastable isomers formed by inelastic neutron scattering for the determination of fast neutron flux densities and the average (n,n') cross sections have been cited by Kohler and Knopf (64) for several elements. Kramer and Wahl (65) determined the cross section for fission neutrons, σ_f, for ^{77m}Se, ^{87m}Sr, ^{111m}Cd, and ^{137m}Ba and indicated the usefulness of these metastable isomers in activation analysis. In recent years, many publications have appeared dealing with inelastic scattering collisions in the production of metastable isomers and their usefulness in determining cross sections and flux densities (66-75).

In the present work, consideration was given to the production of the metastable isomers from radiative neutron capture and the inelastic scattering process. To determine the yield of the two different processes, the contribution of each was determined by calculating the cross section ratio, $\sigma_{(n,n')}/\sigma_{(n,\gamma)}$, for the production of each isomer. The metastable isomers investigated, together with their characteristic properties, are listed in Table II.

Irradiation Facilities and Detection Equipment

All samples were irradiated using two reactor locations for purposes of comparison. Samples irradiated using the thermal flux facility were

Table II. Nuclear properties of isotopes used and isomers produced

Target Nuclide	Thermal σ (Barns)[a]	Fission σ (Barns)	Excitation Energy (Mev)	Product Nuclide (from n,n' or n,γ reaction)	$t_{\frac{1}{2}}$	Transition (Mev)	Intensity (%)
^{86}Sr	1.3						
^{87}Sr		0.12[b]	0.388	^{87m}Sr	2.83h	0.388	80
		0.091[c]					
^{110}Cd	0.1						
^{111}Cd		0.14[b]	0.396	^{111m}Cd	48.6m	0.150	30
						0.247	94
		0.289[c]					

[a]Values taken from Table of Isotopes (37)

[b]Values taken from Kramer and Wahl (65)

[c]Values taken from Kohler and Knopf (64)

Table 11. (Continued)

Target Nuclide	Thermal σ (Barns)	Fission σ (Barns)	Excitation Energy (Mev)	Product Nuclide (from n,n' or n,γ reaction)	$t_{\frac{1}{2}}$	Transition (Mev)	Intensity (%)
^{136}Ba	0.010						
^{137}Ba	4	0.22[d]	0.662	^{137m}Ba	2.55m	0.662	89
		0.189[e]					
^{179}Hf	0.2						
^{180}Hf	10		1.142	^{180m}Hf	5.5h	0.093	16
						0.215	82
						0.333	93
						0.444	80
						0.501	17

[d]Values taken from Kramer and Wahl (65)

[e]Values taken from Kohler and Knopf (64)

Table 11. (Continued)

Target Nuclide	Thermal σ (Barns)	Fission σ (Barns)	Excitation Energy (Mev)	Product Nuclide (from n,n' or n,γ reaction)	$t_{\frac{1}{2}}$	Transition (Mev)	Intensity (%)
^{189}Os	0.008						
^{190}Os	3.9		1.706	^{190m}Os	9.9m	0.187 0.361 0.502 0.616	70 94 98 99
^{194}Pt	0.09						
^{195}Pt	27		0.259	^{195m}Pt	4.1d	0.099 0.129	11 1
^{198}Hg	0.02						
^{199}Hg	2000		0.533	^{199m}Hg	43 m	0.158 0.375	53 15

subject to an avilable flux of 1 x 10^{13} n/cm^2 sec. A fast neutron flux was also provided by a neutron flux converter assembly which was installed in the V-3 position of the ALRR. Prior to installation, the thermal flux in the side thimbles was approximately 1.6 x 10^{12} n/cm^2 sec. With the installation of the converter assembly, a neutron fast flux of 2.7 x 10^{12} n/cm^2 sec with E > 1 Mev was recorded. For all irradiations using the converter assembly, a spacer was used so as to maintain constant sample position in the converter.

The detection system used for all samples consisted of a Ge(Li) solid state detector coupled to a 1600 channel analyzer as described previously. Data were analyzed using the ICPEAX peak-finding program unless otherwise indicated.

Procedure for Determining the Yield of (n,n'/n,γ) Reactions

In the elements studied, the metastable isomers of stable isotopes could be produced by the (n,γ) reaction from the neighboring isotope as well as by the (n,n') excitation of the stable isomer. In order to determine the yield of the latter reaction, it was necessary to estimate the contribution of the two reactions. This was done by determining the cross section ratio, $\sigma_{(n,n')}/\sigma_{(n,\gamma)}$, through the use of isotopically enriched samples of the elements. The enriched materials were purchased from Oak Ridge National Laboratory in the form of metal, oxide or nitrate, thus avoiding interfering activities from other elements.

The procedure used to determine the ratio of (n,n') yield to (n,γ) was that as described in a previous work (76), but for clarity shall be restated in terms of the data appropriate for mercury. From the activities,

calculated from the photopeak areas and corrected for decay, and the weights of the samples involved, the following two equations could be solved:

HgO, normal abundance: $$(\sigma\varphi)_{198}N_{198} + (\sigma\varphi)_{199}N_{199} = Z \quad (18)$$

HgO, isotopically enriched: $$(\sigma\varphi)_{198}N'_{198} + (\sigma\varphi)_{199}N'_{199} = Z' \quad (19)$$

where σ = neutron cross section

φ = neutron flux

N = number of atoms of each isotope

Z, Z' = respective activities.

Since the enriched and the normally abundant samples were irradiated simultaneously, the following substitution can be made:

$$X = (\sigma\varphi)_{198} \quad (20)$$

$$Y = (\sigma\varphi)_{199} \quad (21)$$

therefore, substitution into equations (18) and (19) yields:

$$X_{198}N_{198} + Y_{199}N_{199} = Z \quad (22)$$

$$X_{198}N'_{198} + Y_{199}N'_{199} = Z' \quad (23)$$

Upon rearrangement, the above equations, (22) and (23) yield:

$$\frac{Y}{X} = \frac{(N'_{198})(Z) - (N_{198})(Z')}{(N_{199})(Z') - (N'_{199})(Z)} \quad . \quad (24)$$

The ratio Y/X represents the product of cross section and neutron flux for the two reactions. Since both cross section and flux are

functions of energy, X and Y are integrals of these products over all neutron energies. Not much can be done to obtain such products over a narrow range of neutron energies, but a fission flux facility was used as well as the usual thermal flux location to obtain two sets of yield ratios for each element under consideration.

Strontium

Powdered samples of $Sr(NO_3)_2$, of normal isotopic abundance and 93% enriched in ^{87}Sr, were weighed and sealed in polyethylene tubing. Table 12 indicates the percent abundance of the normal and enriched isotopes under consideration for strontium and for all other isotopes used in this investigation. For each irradiation, a sample of the normal and the enriched $Sr(NO_3)_2$ was enclosed in small polyethylene vials and irradiated for five minutes in the fast flux facility. Following irradiation, samples were counted for five minutes live time and the data processed using the ICPEAX peak-finding program. The area under the 0.388 Mev photopeak of ^{87m}Sr was chosen for comparison, corrected for decay, and from these areas and the weight of the sample, the $n,n'/n,\gamma$ ratio was determined as described in the preceding discussion. Table B-1 indicates the results obtained for the determination of the $n,n'/n,\gamma$ ratios. Figures E-1 and E-2 are representative of the spectra obtained for the irradiation of enriched and normally abundant strontium in the fast flux facility.

Samples of the enriched and the normally abundant isotope of $Sr(NO_3)_2$ were also irradiated in the thermal flux facility. Irradiation and counting time periods were identical to those used for irradiations in the fast flux facility; however, as can be seen from the ratios obtained and

Table 12. Isotopic abundance of target nuclide

Nuclide	Atomic Percent Normal	Atomic Percent Enriched
^{86}Sr	9.86	0.72 ± 0.05
^{87}Sr	7.02	93.29 ± 0.10
^{110}Cd	12.39	0.63 ± 0.05
^{111}Cd	12.75	96.5 ± 0.1
^{136}Ba	7.81	0.58 ± 0.05
^{137}Ba	11.32	89.6 ± 0.1
^{179}Hf	13.75	2.66
^{180}Hf	35.24	93.89
^{189}Os	16.1	1.41 ± 0.05
^{190}Os	26.4	95.46 ± 0.05
^{194}Pt	32.9	27.87 ± 0.1
^{195}Pt	33.8	59.86 ± 0.1
^{198}Hg	10.02	2.3 ± 0.05
^{199}Hg	16.84	83.45 ± 0.1

presented in Table B-2, the error is exceedingly large. Also, the range of values is considerable.

A number of samples which varied in weight, irradiation time, and counting time were run in an attempt to improve the precision. A possible source of error might be self-shielding although sample sizes were chosen to be deliberately small. The cross section for the n,γ reaction is large which also might be a factor influencing the low yield of the excitation reaction and consequently the large error in the ratio determinations. Figures E-3 and E-4 are representative of enriched and normally abundant samples irradiated in the thermal flux facility. The area under the 0.388 Mev photopeak from ^{87m}Sr was determined by using the ICPEAX peak-finding program. The area was also summed by hand to see if a possible source of error might be in the area determinations. The results agreed to within 1% so this possibility was eliminated. As can be seen from the spectra, the photopeaks are well resolved and should present no problem in determining the area under the peak by either method.

Cadmium

Powdered samples of CdO of natural abundance and 96.5% enriched in ^{111}Cd were weighed and sealed in polyethylene tubing. For each irradiation, a sample of the enriched and the naturally abundant oxides were enclosed in a small polyethylene vial, sealed and irradiated for five minutes at full power in the fast flux facility. Immediately following removal from the reactor, samples were counted for live time periods five minutes in length, and the data processed using the ICPEAX peak-finding program.

Of interest in this case was the area under the 0.150 and the 0.247 Mev photopeaks from ^{111m}Cd, and from these corrected areas and the sample weights, the n,n'/n,γ ratio was determined as previously described. Table B-3 in Appendix B indicates the results that were obtained.

Samples of the enriched and normally abundant isotopes were also irradiated for a five-minute period in the thermal flux facility and each sample counted for five minutes. Data were obtained and the n,n'/n,γ ratio calculated as previously described. Table B-4 indicates the results obtained.

As can be seen from Tables B-3 and B-4, there is good agreement between the n,n'/n,γ ratios obtained using the 0.150 Mev photopeak and the ratio obtained using the 0.247 Mev photopeak. The agreement is good for samples irradiated in both the fast and the thermal facilities. A possible source of error in determining the n,n'/n/γ ratio might be in the self shielding in the CdO. However, small sample sizes were deliberately chosen so as to minimize this effect as much as possible. Representative spectra using both irradiation facilities may be found in Figures E-5 through E-8 in Appendix E.

Barium

Powdered samples of normally abundant $Ba(NO_3)_2$ and 90% enriched in ^{137}Ba were weighed and enclosed in polyethylene tubing. As in previous cases, samples of each were irradiated simultaneously. All barium samples were irradiated for one minute at full power in the fast flux facility. Immediately upon removal from the reactor, samples were counted for one minute live time periods. The area under the 0.662 Mev photopeak of

^{137m}Ba was chosen for comparison. The areas were determined by classical methods, corrected for decay, and these areas together with the sample weights were used to calculate the n,n'/n,γ ratios. The results obtained are listed in Table B-5 and the respective spectra are Figures E-9 and E-10 in Appendix E.

Barium samples were also irradiated for one minute exposures in the thermal flux facility and counted immediately following removal from the rabbit system for one minute live time periods. The n,n'/n,γ ratios obtained are to be found listed in Table B-6. As in the previous case, the photopeak areas were determined by classical methods and not through use of the computer program. Figures E-11 and E-12 are representative of the spectra obtained.

The results for the n,n'/n,γ ratio determined using the fast flux facility show considerably greater precision than those ratios determined using the thermal flux facility. Very little activity was observed for the enriched barium samples irradiated in the thermal facility, as will be noted from the data in Table B-6. However, longer counting intervals were not practical because of the short half life of the isomer, 2.6 min, and the elapsed time between the end of the irradiation and the start of the counting period.

Hafnium

Powdered samples of normally abundant HfO_2 and 94% enriched in ^{180}Hf were weighed and enclosed in polyethylene tubing. For each irradiation, a sample of each was enclosed in a small polyethylene irradiation vial and irradiated for ten minutes at full power in the fast flux facility.

Samples were counted immediately following irradiation for ten minutes live time. The areas under three photopeaks, 0.215, 0.333 and 0.444 Mev, were used for comparison purposes. The $n,n'/n,\gamma$ ratios for each photopeak are listed in Table B-7. The agreement between the three photopeaks used is good.

Samples of the normally abundant and enriched hafnium were also irradiated for ten minutes using the thermal flux facility. Samples were counted immediately following removal from the reactor for periods of ten minutes, live time, in length. The same three photopeaks were used for comparison purposes as were used for irradiations in the fast flux facility. Table B-8 contains the results obtained. Figures E-13 through E-16 represent spectra of the normally abundant and the enriched isotopes irradiated using both the thermal and the fast flux facility.

Osmium

Powdered samples of osmium metal, normally abundant, and 95% enriched in ^{190}Os were weighed and encapsulated in polyethylene tubing for irradiation. Samples of each were irradiated simultaneously for five minutes in the fast flux facility. Samples were counted immediately following removal from the reactor for five minutes live time periods. The 0.361 Mev photopeak was chosen for comparison because it appeared to be the most well resolved. The spectra may be seen in Figures E-17 and E-18. Table B-9 lists the data obtained.

Osmium samples were also irradiated in the thermal flux facility. Irradiation and counting time periods and geometry were identical to those used for the fast flux irradiations. Table B-10 lists the $n,n'/n,\gamma$ ratios

obtained. Figures E-19 and E-20 are representative spectra of the normally abundant and the enriched isotope irradiated using thermal neutrons.

Platinum

Powdered samples of platinum metal, 60% enriched in ^{195}Pt, were weighed and sealed in polyethylene tubing for irradiation. Fine pieces of normal platinum wire were cut, weighed, and also sealed in tubing for irradiation. Each irradiation consisted of a sample of the enriched metal and the normal metal irradiated simultaneously for fifteen minutes in the fast flux facility. Samples were counted approximately 48 hours after removal from the reactor. Each sample was counted for a fifteen minute live time period and the area under the 0.099 Mev photopeak of ^{195m}Pt determined using the ICPEAX peak-finding program. The n,n'/n,Y ratios are listed in Table B-11.

Platinum samples were also irradiated for fifteen minute exposure periods at full power in the thermal flux facility. These samples were also counted for 15 minutes, approximately 48 hours after removal from the reactor and the data processed in like manner as the above. Table B-12 lists the results obtained for the n,n'/n,Y ratios.

For the platinum irradiations the precision obtained for those samples irradiated in the thermal flux facility is much greater than for those samples irradiated using fission neutrons. Figures E-21 through E-24 are spectra of the samples irradiated using both facilities. The spectra of the irradiated platinum samples show the most noticeable difference, of isotopes studied thus far, between the normally abundant and the enriched isotopic samples irradiated in either facility.

Mercury

Powdered samples of HgO, of normal isotopic abundance and 83.5% in ^{199}Hg were weighed on the Cahn electrobalance and sealed in polyethylene tubing. For each irradiation, samples of the normal and enriched oxides were enclosed in small polyethylene vials, sealed, and irradiated for five minutes at full power in the fast flux facility. Samples were counted for five minutes live time immediately following irradiation and the data processed using the ICPEAX peak-finding computer program. The areas under the 0.158 and the 0.375 Mev photopeaks of ^{199m}Hg were determined, corrected for decay, and from these areas and the weight of each sample the n,n'/n,γ ratio was determined as in the preceding discussions.

After a reasonable time had elapsed for decay of the induced radioactivity, these samples were again irradiated for five minutes in the thermal flux facility. As in the previous case, samples were counted for five minutes live time immediately following removal of the sample from the reactor; n,n'/n,γ ratios were determined. The data obtained for irradiation in both the fast and thermal flux facilities are indicated in Tables B-13 and B-14 in Appendix B.

From Table B-13, it will be noted that there is a slight discrepancy in the values obtained for the n,n'/n,γ ratio using the 0.158 Mev photopeak, n,n'/n,γ equals 2.14 $\pm$ 0.06, and the 0.375 Mev photopeak in which the n,n'/n,γ ratio equals 1.77 $\pm$ 0.0/. This discrepancy may be accounted for in several ways. Samples were counted for live-time periods not exceeding five minutes, and longer counting periods could sufficiently improve counting statistics and possibly result in greater agreement between the two

sets of values. Another possible source of discrepancy might be the fact that the photopeak area determination for the 0.158 Mev peak was determined by using the ICPEAX peak finding program which attempts a Gaussian fit on all preliminary photopeaks found and the lower energy 0.158 Mev photopeak is not as ideally Gaussian shaped as one would like.

Another source of discrepancy is the fact that the 0.375 Mev photopeak has a very low intensity; this could be improved with longer irradiation times and longer counting periods. From the data presented in Table B-14, it will be noted that for irradiations using the thermal flux facility, the 0.375 Mev photopeak was not intense enough to be detected. The spectra obtained, for both the enriched and normally abundant isotopes irradiated in both facilities are represented by Figures E-25 through E-28 in Appendix E.

A summary of the results obtained for the above described experiments may be found in Table 13. The average value from each table in Appendix B was used in compiling Table 13.

The contribution of these two processes, the n,n' and the n,γ, is important because if the yield of the isomer produced from the n,n' reaction is high, the problem of self-shielding of thermal neutrons may be greatly reduced. It would be reasonable to assume that a large cross section for the n,γ reaction would result in an appreciably small n,n' yield. The possibility of thermal neutron activation in the present work was larger than what was hoped for due to the design of the converter assembly. In the facility used, the cadmium liner did not extend across the bottom of the converter assembly, thus enabling a small percentage of

Table 13. Summary of the average n,n'/n,Y yield ratios

Isotope	Y-ray Energy (Mev)	$\frac{n,n'}{n,Y}$ Yield Ratios		
		Thermal Flux Facility	Epi-cadmium	Fission Flux Facility
^{87m}Sr	0.388	0.00148		0.461
^{111m}Cd	0.150	0.0134		1.09
	0.247	0.0143	0.228	1.06
^{137m}Ba	0.662	0.0573		3.84
^{180m}Hf	0.215	0.0157		0.0192
	0.333	0.0147		0.0198
	0.444	0.0164		0.0195
^{190m}Os	0.361	0.0926		1.90
^{195m}Pt	0.099	0.101		0.837
^{199m}Hg	0.158	0.0182	0.172	2.14
	0.375	---		1.77

thermal neutron activation.

The percentage of the n,n' reaction contributing to the production of the metastable isomer may be calculated from the n,n'/n,γ yield ratios summarized and presented in Table 13, and the percent abundance of the isotope (Table 12) according to Equation (25).

$$\% = \frac{\text{Isotopic Abundance of A}}{\frac{1}{\text{Yield Ratio}}[\text{Isotopic Abundance of (A-1)}] + \text{Isotopic Abundance of A}} \qquad (25)$$

The percent contribution of the n,n' reaction to the total yield of the isomeric state was calculated for the naturally abundant isotope irradiated in both the fast and the thermal flux facility. The results are listed in Table 14. The epi-cadmium results indicated in both Table 13 and Table 14 were taken from a previous work (76) in which samples were enclosed in cadmium containers before insertion into the rabbit capsule for irradiation in the thermal flux facility.

Analysis of Barium and Strontium Mixtures

Solutions containing 10.00 mg/ml of $Ba(NO_3)_2$ and $Sr(NO_3)_2$ were prepared. Mixtures of barium and strontium were prepared by taking 500, 250, 50 and 5 microliter samples of one solution and adding to these 500 microliters of the other component so that mixtures resulted with Ba/Sr weight ratios from 1:100 and 100:1. The samples, prepared in small polyethylene vials which had been cleaned in HNO_3, were subsequently evaporated and sealed for irradiation.

Several samples of each composition were irradiated in both the

Table 14. Percent contribution of the n,n' process to the total yield of metastable isomer

Isomer	E γ Ray (Mev)	Thermal Facility	Epi-cadmium	Fast Facility
^{87m}Sr	0.388	0.105		24.7
^{111m}Cd	0.150	1.36		52.9
	0.247	1.45	19.0	52.2
^{137m}Ba	0.662	7.67		84.8
^{180m}Hf	0.215	3.87		4.69
	0.333	3.63		4.83
	0.444	4.03		4.76
^{190m}Os	0.361	13.2		75.7
^{195m}Pt	0.099	9.40		46.2
^{199m}Hg	0.158	2.97	22.4	78.2
	0.375	--		74.8

thermal flux facility and the fast flux facility for purposes of comparison. Each irradiation consisted of a one minute exposure at full operating power. Samples were counted immediately upon removal from the reactor for one minute live time periods.

For all samples, the area under the photopeaks of interest, 0.388 Mev ^{87m}Sr and 0.662 Mev for ^{137m}Ba, was determined by classical methods. This method was chosen in preference to using the computer and the ICPEAX peak-finding program for area determinations because of a time differential on the order of six minutes for printing out the data depending upon which system is used. Due to the short half life of ^{137m}Ba the quickest method of printout was used.

The results obtained, for the irradiation of each mixture of barium and strontium in both the thermal and the fission flux facilities, may be found in Appendix C, Tables C-1 through C-14. From four to six samples were irradiated in most cases; for results in which precision was obviously poor, more samples were irradiated.

From the data presented in Tables C-1 and C-2, a 1:1 weight ratio of Ba:Sr irradiated with fission and thermal neutrons respectively, a large difference in the area under the 0.662 Mev photopeak of ^{137}Ba will be noticed. Irradiation in the fast facility provides more neutrons with an energy greater than 0.025 ev, average thermal energy, thereby enhancing the possibility of n,n' reactions.

The 1:2 mixture of Ba:Sr irradiated using the thermal facility has a much larger error associated with it, 6.3%, than the same composition irradiated using fission neutrons, 0.16%. This may in part be due to the

lower count rate of ^{137m}Ba irradiated using thermal neutrons. For the 2:1 mixture, however, the greater error was found for those samples irradiated using thermal neutrons 0.6%. A fairly low count rate for the ^{87m}Sr irradiated with fission neutrons was also observed.

Because this analysis of barium and strontium is based on peak area ratios, it is reasonable to expect that the analysis will be most accurate if the peak areas are comparable. For irradiations with fission neutrons, the peak area ratio is 13.8 for the 1:1 mixture of Ba:Sr. Using the 1:1 mixture as a standard from which to calculate the expected values of the various weight compositions, it may be seen that for a range of from 10 to 1% barium in strontium the expected peak area ratios would be from 1.38 to 0.138 and the two photopeaks will be of comparable size for measurement.

However, for large amounts of barium relative to strontium, the area ratio approaches 138 and 1380, and the photopeaks associated with ^{87m}Sr are so small compared to the 0.662 Mev peak associated with ^{137m}Ba that very poor precision and accuracy results. For the 1:1 mixture of Ba:Sr irradiated with thermal neutrons, the ratio of the ^{137m}Ba:^{87m}Sr photopeaks is 0.18. Therefore, for mixtures that are high in barium, photopeak areas of comparable size are observed, and results are good even for those samples with 1% strontium content. Quite obviously then, a careful selection of the reference mixtures of known composition will give reproducible and accurate results for Ba/Sr mixtures much greater or less than 1.0.

The spectra of a 1:1, 1:2, and 2:1 mixture of Ba:Sr, irradiated in both the fast and the thermal facilities, are included in Appendix F,

Figures F-1 through F-6. The 0.388 Mev photopeak of ^{87m}Sr and the 0.662 Mev photopeak of ^{137m}Ba were chosen for comparison. The photopeaks of interest in the spectra of the mixtures irradiated and not here included, increased or decreased in intensity in accordance with an increase or decrease in composition.

Table 15 indicates the average ^{137m}Ba:^{87m}Sr ratio obtained for each composition using both the thermal and the fission flux facilities, the calculated ratios as determined using the 1:1 ratio as a standard, and the standard deviation for the irradiations made of each mixture. The standard deviations ranged from 0.1 to 2% error with an average error of 0.8% for fission neutrons and 5.7% for thermal neutrons. These values were determined excluding the 100:1 Ba/Sr mixture for fission neutrons, because of the large range of values involved, and excluding the 1:100 Ba/Sr ratio for thermal neutron irradiations because of the relatively large standard deviation. The deviation between the calculated and experimental results ranged from 0.7% to 9% for fission neutron irradiations and from 1.1 to 12% for thermal neutron irradiations.

For irradiations using the fast flux facility, a very definite limit is set in determining strontium and barium mixtures of varying compositions. For samples ranging in 1-10% strontium in barium the photopeak area for the amount of strontium present is so small compared to the area for the amount of barium, that an accurate analysis was not possible for the 100:1 mixtures of barium and strontium.

The 100:1 mixture analyzed in the thermal flux facility showed some improvement; the average experimental results deviated slightly from that

Table 15. Summary of Ba/Sr ratios

Ba/Sr	Fission Neutrons		Thermal Neutrons	
	Calculated	Experimental	Calculated	Experimental
1:1	---	13.8 ± 0.1	---	0.182 ± 0.002
1:2	6.9	6.26 ± 0.01	0.091	0.090 ± 0.006
2:1	27.6	28.0 ± 0.5	0.364	0.344 ± 0.002
1:10	1.38	1.37 ± 0.01	0.0182	0.0203 ± 0.0011
10:1	138.	140. ± 1.	1.82	1.80 ± 0.04
1:100	0.138	0.127 ± 0.001	0.00182	0.0158 ± 0.0029
100:1	1380.	142 - 940 (range)	18.2	18.5 ± 2.8

calculated; however, the individual values obtained per irradiation showed a fairly large range (Table C-14).

Analysis of Cadmium and Mercury Mixtures

Solutions of cadmium and mercury were prepared by dissolving CdO and HgO in HNO_3 and diluting to volume chosen to prepare solutions of concentrations 10.00 mg/ml. Mixtures of cadmium and mercury were prepared by taking 500, 250, 50 and 5 microliter samples of one solution and adding to it 500 microliters of the other solution resulting in mixtures which varied in Cd to Hg weight ratios from 1:100 to 100:1. The samples were prepared in small polyethylene irradiation vials, previously cleaned in HNO_3, evaporated and sealed for irradiation.

Several samples of each composition were irradiated in both the thermal and the fast flux facility for comparison purposes. Irradiation time in all cases was five minutes and samples were counted for five minute live time periods following removal from the reactor.

The data obtained was processed using the ICPEAX peak-finding program for area determinations. The areas under the photopeaks of interest, 0.150 and 0.247 Mev for ^{111m}Cd and 0.158 and 0.375 Mev for ^{199m}Hg, were chosen for comparison. Appendix D, Tables D-1 through D-14 indicate the results obtained. Representative spectra of Cd/Hg mixtures of composition 1:1, 1:2, and 2:1 irradiated in both facilities are included in Appendix G, Figures G-1 through G-6. The photopeaks of interest in mixtures analyzed whose spectra are not here included decreased or increased in accordance with a decrease or increase in composition.

The average ratio obtained for each composition irradiated in both reactor facilities used is listed in Tables 16 and 17. Table 16 lists the average experimental values obtained, the calculated values which were determined by using the 1:1 mixture as a standard reference, and the standard deviation obtained for each irradiation, for the mixtures irradiated using the fission flux facility. Table 17 lists the same type data for samples irradiated using the thermal flux facility.

For the fission neutron irradiations, ratios obtained using the 0.247/0.375 Mev photopeaks for comparison are considerably better than those ratios obtained using any of the other compared photopeaks. Most probably this is due to the fact that these two photopeaks show much better resolution than the 0.150 and the 0.158 Mev photopeaks for cadmium and mercury respectively, although the latter are the more intense. The resolution factor may readily be seen from the spectra in Figures G-1 through G-6. For those mixtures in which the amount of one component dropped to 10% or less, the photopeak was barely discernable. For the 100:1 and the 1:100 compositions the 0.158 and the 0.150 Mev photopeaks respectively were not determined to be real peaks using the ICPEAX peak-finding program. Using the 0.247 and the 0.375 Mev photopeaks for comparison, the average deviations of the experimental values from the calculated values is 2.9%.

For those mixtures irradiated using the thermal flux facility, the same four photopeaks were used for comparison. The standard deviations, as will be noted in Table 17, are considerably larger than they are for samples irradiated using the fast flux facility. Also, as will be noted from the table, the deviation from the calculated value is considerably

Table 16. Determination of Cd/Hg ratio using fission neutrons

Cd/Hg	(150/158) Mev Calc.	(150/158) Mev Exp.	(150/375) Mev Calc.	(150/375) Mev Exp.	(247/158) Mev Calc.	(247/158) Mev Exp.	(247/375) Mev Calc.	(247/375) Mev Exp.
1:1	---	0.856 ± 0.029	---	10.4 ± 0.5	---	1.39 ± 0.04	---	16.9 ± 0.2
1:2	0.428	0.451 ± 0.016	5.2	5.52 ± 0.18	0.695	0.727 ± 0.013	8.45	8.89 ± 0.18
2:1	1.71	1.61 ± 0.60	20.8	19.9 ± 0.3	3.78	2.48 ± 0.52	33.8	34.2 ± 0.3
1:10	0.0856	0.107 ± 0.011	1.04	1.26 ± 0.15	0.139	0.149 ± 0.002	1.69	1.76 ± 0.06
10:1	8.56	49.9 ± 4.6	104.	120. ± 1.	13.9	75.5 ± 6.8	169.	182. ± 2.
1:100	0.00856	---	0.104	---	0.0139	0.0142 ± 0.0008	0.169	0.171 ± 0.002
100:1	85.6	---	1040.	137. ± 18.	139.	---	1690.	241. ± 25.

Table 17. Determination of Cd/Hg ratio using thermal neutrons

Cd/Hg	(150/158) Mev Calc.	(150/158) Mev Exp.	(150/375) Mev Calc.	(150/375) Mev Exp.	(247/158) Mev Calc.	(247/158) Mev Exp.	(247/375) Mev Calc.	(247/375) Mev Exp.
1:1	---	2.17 ± 0.33	---	34.7 ± 1.8	---	3.39 ± 0.42	---	54.3 ± 3.4
1:2	1.09	1.79 ± 0.32	17.4	11.0 ± 1.1	1.70	4.40 ± 1.10	27.2	27.2 ± 0.5
2:1	4.34	3.62 ± 0.77	69.4	70.3 ± 14.3	6.78	6.22 ± 0.91	109.	122. ± 25.
1:10	0.217	0.226 ± 0.076	3.47	2.68 ± 0.99	0.339	0.470 ± 0.010	5.43	5.55 ± 0.26
10:1	21.7	5.70 ± 3.09	347.	395.	33.9	9.01 ± 4.91	543.	620.
1:100	0.0217	---	0.347	---	0.0339	0.0467 ± 0.0038	0.543	0.503 ± 0.044
100:1	217.	---	3470.	131. ± 4.	339.	---	5430.	236. ± 6.

larger than for those samples irradiated in the fast flux facility.

One very possible source of error here might be the large absorption cross section of cadmium and consequently the possibility of self-shielding. This is particularly true for those samples with large percentages of cadmium present relative to the amount of mercury: 2:1, 10:1, and 100:1 Cd/Hg ratios. In these cases the standard deviations are extremely large, and the experimental ratio in some cases does not even approach the calculated Cd/Hg ratio. Results for these same compositions using fission neutrons are considerably better (Table 16).

SUMMARY

An internal standard method of analysis was used for the thermal neutron activation of three tungsten bronzes. The 'x' values, or metal/tungsten ratios, were determined for potassium, holmium and lanthanum tungsten bronzes.

The 'x' values in each case were determined by activation with thermal neutrons followed by detection of the photopeaks using a Ge(Li) semiconductor detector and a FORTRAN peak-finding program called ICPEAX. The photopeak area ratios of metal/tungsten were compared for standards of known composition and for unknown bronzes and the 'x' values were determined from the comparison ratios.

Potassium, in K_xWO_3, was determined by comparing the area under the 1.52 Mev photopeak of ^{41}K to either or both of the ^{187}W activities at 0.479 and 0.686 Mev. Holmium was determined in Ho_xWO_3 by comparing the activity under the 1.38 Mev photopeak of ^{166}Ho to the photopeaks from ^{187}W. Lanthanum was also determined by thermal neutron activation using the 1.60 Mev ^{140}La photopeak for comparison. In all cases the photopeak chosen for the metal to be determined was selected to be the least subject to interference from ^{187}W. The accuracy of all bronze determinations was based on the accuracy of determining the M/W ratio in the standards which were prepared and treated in an identical manner to the unknowns. Results indicated that, with the improved resolution afforded by using the solid state detectors, many tungsten bronzes could be analyzed nondestructively and accurately using an internal standard method of analysis.

A fission flux facility, provided by the installation of a neutron converter assembly in the ALRR, was used on samples of normally abundant and enriched isotopes to determine the n,n'/n,γ yield ratios of metastable isomers. Pairs of nuclides were chosen which would yield metastable isomers by the following reactions: $^{A-1}_{Z}(n,\gamma)^{Am}_{Z}$ and $^{A}_{Z}(n,n')^{Am}_{Z}$. Both the fast and thermal flux facilities were used for comparison purposes. The percent of the total yield from the n,n' reactions in the normally abundant isotopes was calculated for ^{87m}Sr, ^{111m}Cd, ^{137m}Ba, ^{180m}Hf, ^{190m}Os, ^{195m}Pt, and ^{199m}Hg. The use of metastable isomers as analytical indicators in activation analysis was also investigated. Mixtures of barium and strontium were analyzed using the ^{137m}Ba and the ^{87m}Sr activities for analysis. Mixtures of cadmium and mercury were also analyzed using the ^{111m}Cd and the ^{199m}Hg activities for comparison.

Results indicated that the activities from the metastable isomers may be used to great advantage in activation analysis. Fission spectrum neutrons may be used in place of thermal neutrons and may produce a large change in the relative yield of the product, thus enabling greater accuracy and precision.

LITERATURE CITED

1. von Hevesy, G. and Levi, H., Danske Videnskab. Selskab. Math.-fys. Medd., 14, No. 5, 1 (1936).

2. Seaborg, G. T. and Livingood, J. J., J. Am. Chem. Soc., 60, 1784 (1938).

3. Kahn, B. and Lyon, W. S., Nucleonics, 11, No. 11, 61 (1953).

4. Connally, R. E. and Leboeuf, M. B., Anal. Chem., 25, 1095 (1953).

5. Lyon, W. S. and Reynolds, S. A., Nucleonics, 13, No. 10, 61 (1955).

6. Morrison, G. H. and Cosgrove, J. F., Anal. Chem., 27, 811 (1955).

7. Upson, U. L., Connally, R. E. and Leboeuf, M. B., Nucleonics, 13, No. 4, 39 (1955).

8. Breitenberger, E., Progr. in Nuclear Phys., 4, 56 (1955).

9. Connally, R. E., Anal. Chem., 28, 1847 (1956).

10. Putnam, J. L. and Taylor, W. H., Intern. J. Appl. Radiation and Isotopes, 1, 315 (1957).

11. Cook, C. S., American Scientist, 45, 245 (1957).

12. Cosgrove, J. F. and Morrison, G. H., Anal. Chem., 29, 1017 (1957).

13. Girardi, F., Guzzi, G. and Pauly, L., Radiochim. Acta, 4 (2), 109 (1965).

14. Schroeder, G. L., Kraner, H. W., Evans, R. G. and Brydges, T., Science, 151, 815 (1966).

15. Hollander, J. M., Prussian, S. G., Harris, J. A. and Lamb, J. F., Anal. Chem., 38, 813 (1966).

16. Beamish, F. E., Chung, K. S. and Chow, A., Talanta, 14, 1 (1967).

17. Taylor, T. I. and Havens, W. W., Jr., Nucleonics, 6, No. 4, 54 (1950).

18. Leddicotte, G. W., Anal. Chem., 36, No. 5, 419R (1964).

19. Leddicotte, G. W. and Reynolds, S. A., U. S. Atomic Energy Commission Report CF-52-12-155 [Oak Ridge National Laboratory], (1952).

20. Brooksbank, W. A., Leddicotte, G. W. and Mahlman, H. A., J. Phys. Chem., 57, 815 (1953).

21. Gordon, C. L., Anal. Chem., 26, No. 1, 176 (1954).

22. Meinke, W. W., Anal. Chem., 28, 736 (1956).

23. Meinke, W. W., Anal. Chem., 30, No. 5, 686 (1958).

24. Meinke, W. W., Anal. Chem., 32, No. 5, 104R (1960).

25. Leddicotte, G. W., Anal. Chem., 34, 143R (1962).

26. Lyon, W. S., Ricci, E. and Ross, H. H., Anal. Chem., 38, 521R (1966).

27. Koch, R. C. Activation Analysis Handbook. New York, N. Y., Academic Press, Inc. 1960.

28. Lyon, W. S., Jr., ed. Guide to Activation Analysis. Princeton, N. J., D. Van Nostrand Co., Inc. 1964.

29. Crouthamel, C. E. Applied Gamma-Ray Spectrometry. New York, N. Y., Pergamon Press, Inc. 1960.

30. Jenkins, E. N. and Smales, A. A., Quart. Revs. (London) 10, 83 (1956).

31. Atkins, D. H. F. and Smales, A. A., Advances in Inorganic Chemistry and Radiochemistry, 1, 315 (1959).

32. Lewis, W. B., Nucleonics, 13, No. 10, 82 (1955).

33. Reynolds, S. A. and Mullins, W. T., Intern. J. Appl. Radiation and Isotopes, 14, 421 (1963).

34. Zweifel, P. F., Nucleonics, 18, No. 11, 174 (1960).

35. Wechter, M. and Voigt, A. F., Anal. Chem. Acta, 41, 181 (1968).

36. Wechter, M. and Voigt, A. F., Anal. Chem., 38, 1681 (1966).

37. Lederer, C. M., Hollander, J. M. and Perlman, I. Table of Isotopes Sixth Ed., New York, N. Y., John Wiley and Sons, Inc. 1967.

38. Halfhill, D. W., Nucleonics, 16, No. 12, 55 (1958).

39. Kuykendall, W. E. and Wainerdi, R. E., Proceedings, IAEA Conf., "The Uses of Radioisotopes in Physical Science and Industry", Copenhagen, Denmark. 1960.

40. Hallpoeau, L. A., Ann. chim. phys., 19, 117 (1900).

41. Brunner, O. Beitrage zur Kenntnis der Wolframbronzen. Unpublished Ph.D. Thesis. Zurich, Switzerland, Library, University of Zurich. (1903).

42. Magneli, A., Acta Chem. Scand., 1, 315 (1953).

43. Laurent, A., Ann. chim. phys., 67, No. 2, 215 (1838).

44. Schaefer, E., Z. Anorg. u. Allgem. Chem., 38, 158 (1904).

45. Brimm, E. O., Brantley, J. C., Lorenz, J. H. and Jellinek, M. H., J. Am. Chem. Soc., 73, 5427 (1951).

46. Ostertag, W., Inorg. Chem., 5, 758 (1966).

47. Conroy, L E. and Yokokawa, T., Inorg. Chem., 4, 994 (1950).

48. Conroy, L. E. and Sienko, M. J., J. Am. Chem. Soc., 79, 4048 (1957).

49. Sienko, M. J. and Mazumder, B. R., J. Am. Chem. Soc., 82, 3508 (1960).

50. Sienko, M. J., J. Am. Chem. Soc., 81, 5556 (1959).

51. Spitzin, V. and Kaschtanoff, L., Z. Anorg. u. Allgem. Chem., 157, 141 (1926).

52. Spitzin, V. and Kaschtanoff, L., Z. Anal. Chem., 75, 440 (1928).

53. Raby, B. A. and Banks, C. V., Anal. Chem., 36, 1106 (1964).

54. Sienko, M. J. and Morehouse, S. M., Inorg. Chem., 2, 485 (1963).

55. Reuland, R. J. and Voigt, A. F., Anal. Chem., 35, 1263 (1963).

56. Hahn, O. and Strassmann, F., Naturwiss, 27, 11 (1939).

57. Friedlander, G., Kennedy, J. W. and Miller, J. M. Nuclear and Radiochemistry. 2nd ed. New York, N. Y., John Wiley and Sons, Inc. 1949.

58. Hughes, D. J. Pile Neutron Research. Cambridge, Mass., Addison-Wesley Publ. Co., Inc. 1953.

59. Hauser, W. and Feshbach, H., Phys. Rev., 87, 366 (1952).

60. Moldauer, P. A., Phys. Rev., 123, 968 (1961).

61. Tucker, A. B., Wells, J. T. and Mayerhof, W. E., Phys. Rev., 137, 1181 (1965).

62. Abramov, A. I., Atomnaya Energ., 12, 62 (1962).

63. Temperley, J. K., Nuclear Science and Engineering, 32, 195 (1968).

64. Kohler, W. and Knopf, K., Nukleonik, 10, 181 (1967).

65. Kramer, Henry H. and Wahl, H., Nuclear Science and Engineering, 22, 373 (1965).

66. Hole, N., Arkiv Mat. Astron. Fysik, 34, No. 19 (1947).

67. Goldhaber, M. and Hill, R. D., Revs. Modern Phys., 24, 179 (1952).

68. Margolis, B., Phys. Rev. 93, 204 (1954).

69. Bormann, M., Fretwurst, E., Schehka, P., Wrege, G., Buttner, H., Lindner, A. and Meldner, H., Nucl. Phys., 63, 438 (1965).

70. Francis, A. E., McCue, J. J. G. and Goodman, C., Phys. Rev., 89, 1232 (1953).

71. Swann, C. P. and Metzger, F. R., Phys. Rev., 100, 1329 (1955).

72. Morgan, I. L., Phys. Rev., 103, 1031 (1956).

73. Rothman, M. A. and Mandeville, C. E., Phys. Rev., 93, 796 (1954).

74. Kiehn, R. M. and Goodman, C., Phys. Rev., 92, 652 (1953).

75. Van Loef, J. J. and Lind, D. A., Phys. Rev., 101, 103 (1956).

76. Menapace, L. M. Use of Metastable States in Activation Analysis. Unpublished M.S. Thesis. Ames, Iowa, Library, Iowa State University. (1967).

ACKNOWLEDGEMENTS

The author wishes to express her sincere gratitude to Dr. Adolf Voigt for his guidance throughout the course of this investigation. She is also grateful for his assistance and encouragement throughout her years at Iowa State University.

The author would also like to acknowledge and personally thank the many wonderful people, too numerous to mention, who by their assistance, moral support and encouragement, and friendliness have helped so much in the completion of this work.

APPENDIX A. TUNGSTEN BRONZE SPECTRA

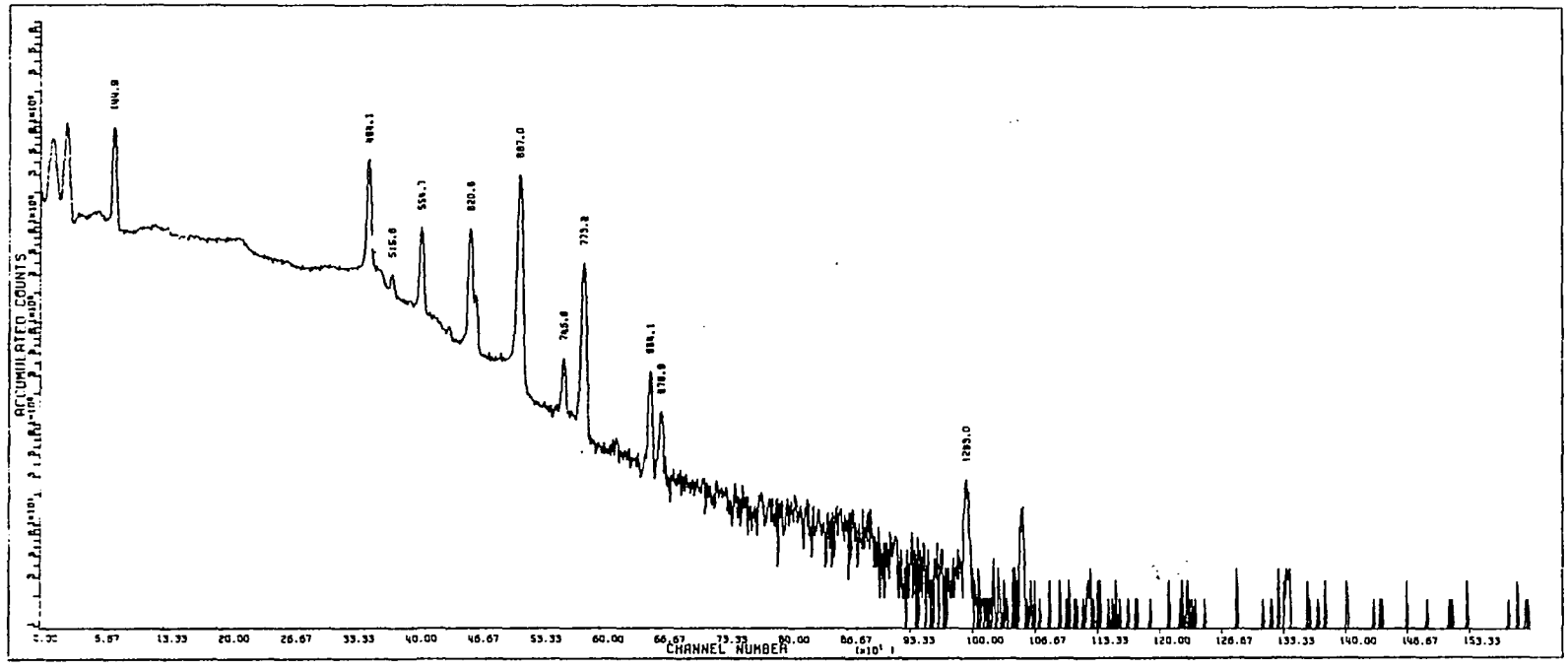

Figure A-1. Gamma-ray spectrum of ^{187}W

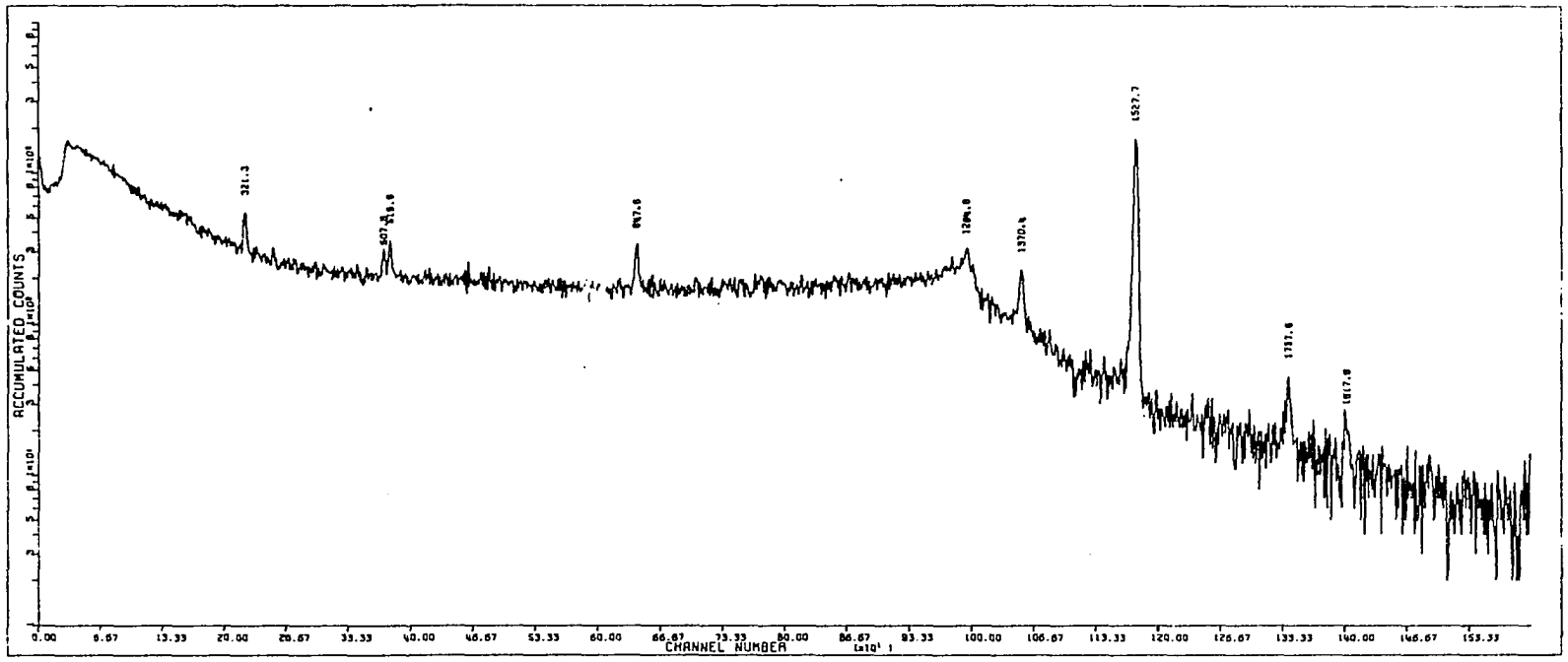

Figure A-2. Gamma-ray spectrum of ^{41}K

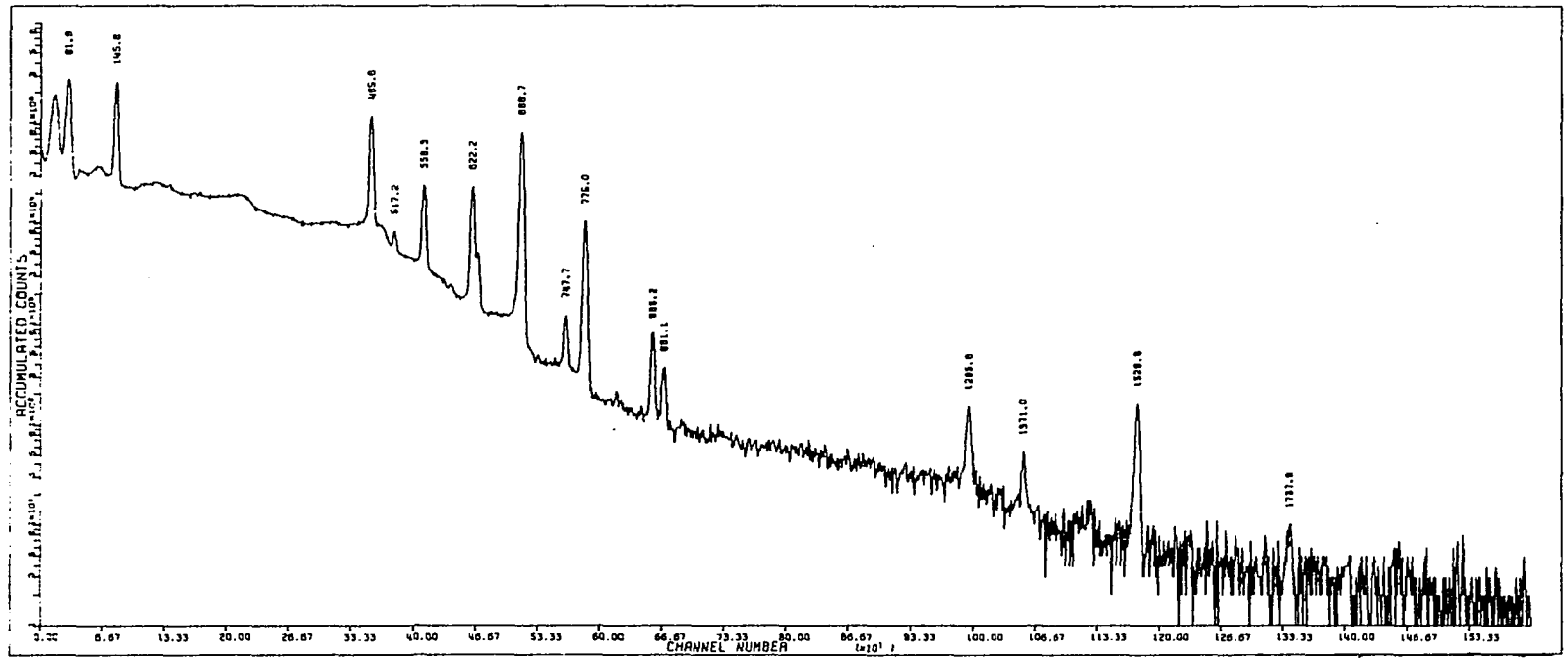

Figure A-3. Gamma-ray spectrum of K:W standard

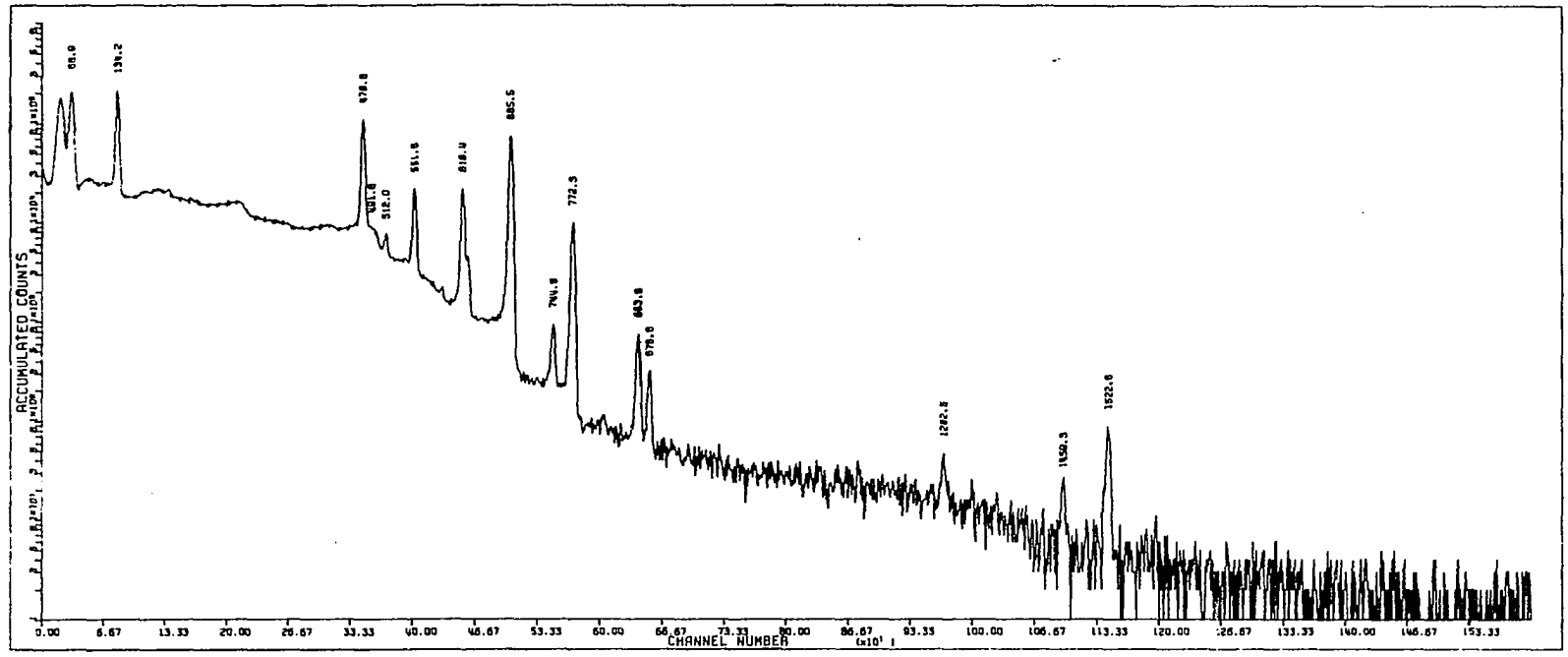

Figure A-4. Gamma-ray spectrum of K_xWO_3

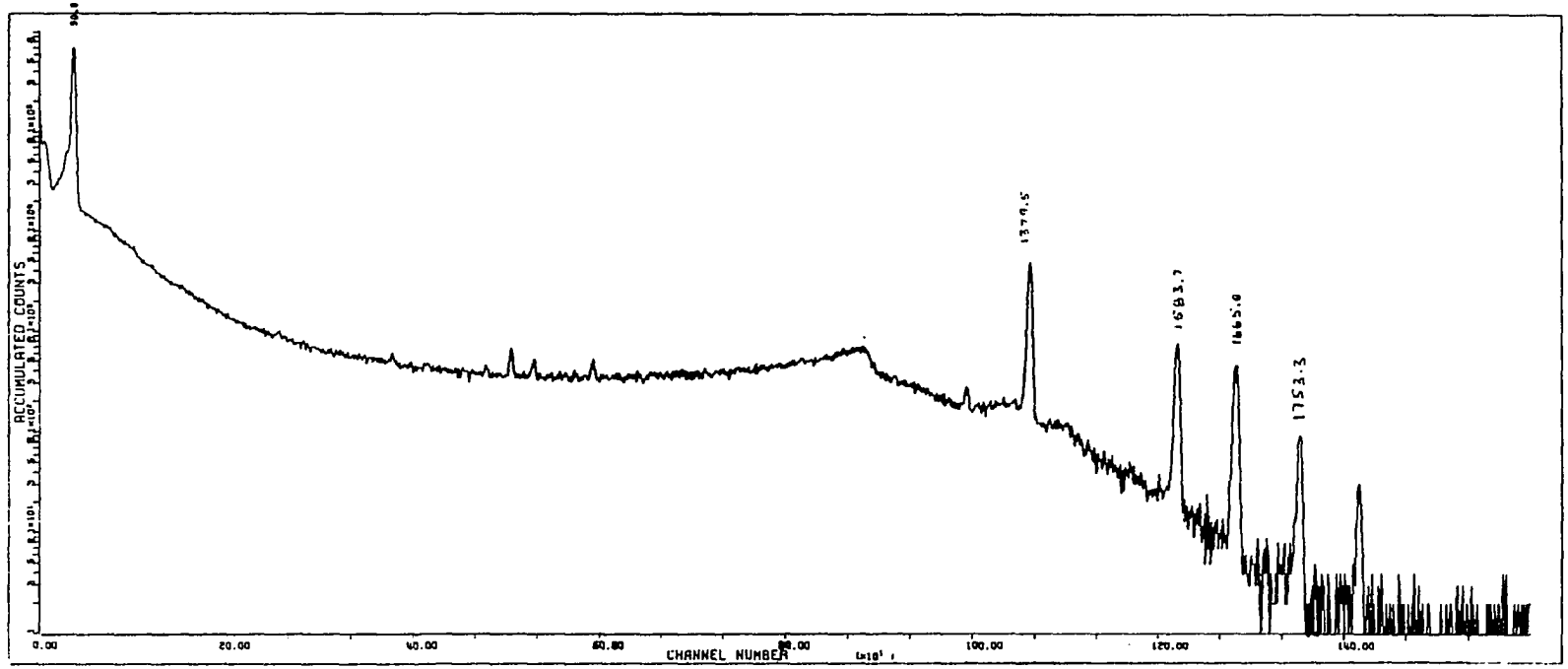

Figure A-5. Gamma-ray spectrum of ^{166}Ho

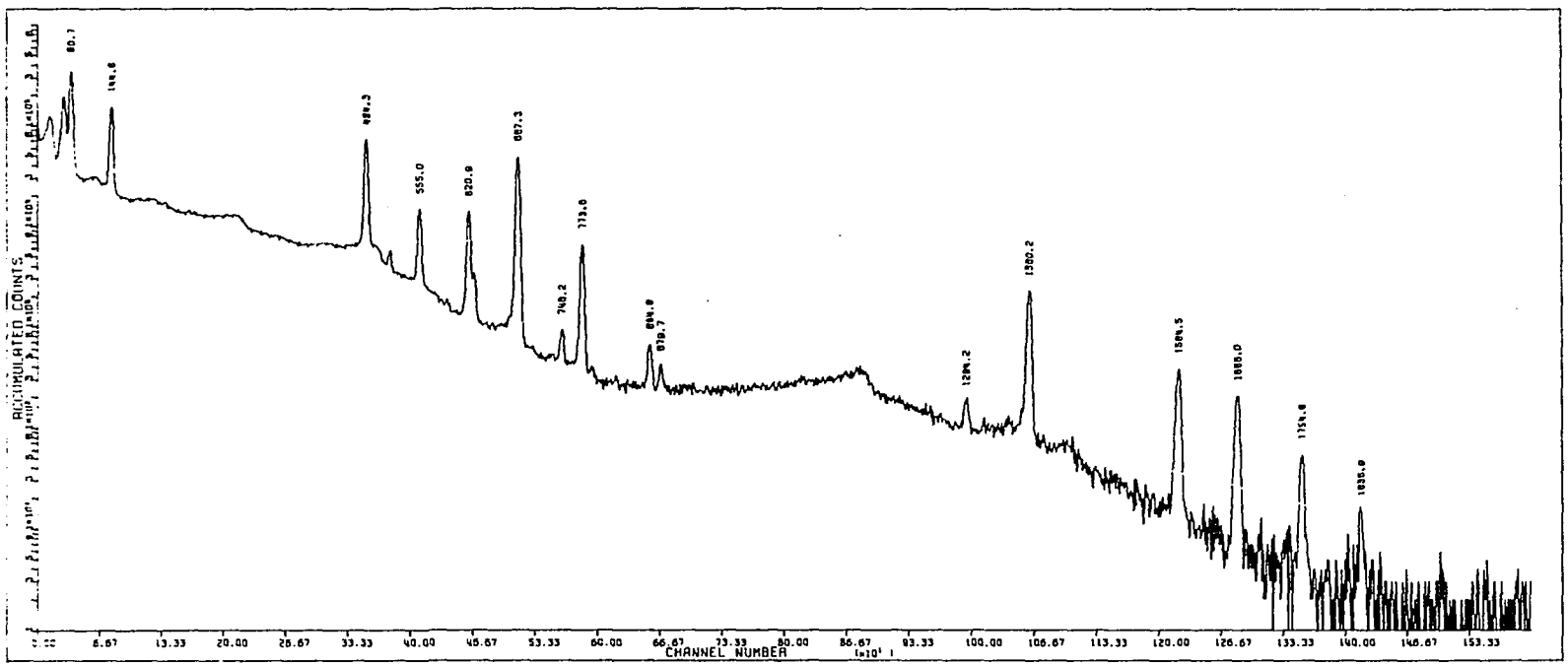

Figure A-6. Gamma-ray spectrum of Ho:W standard

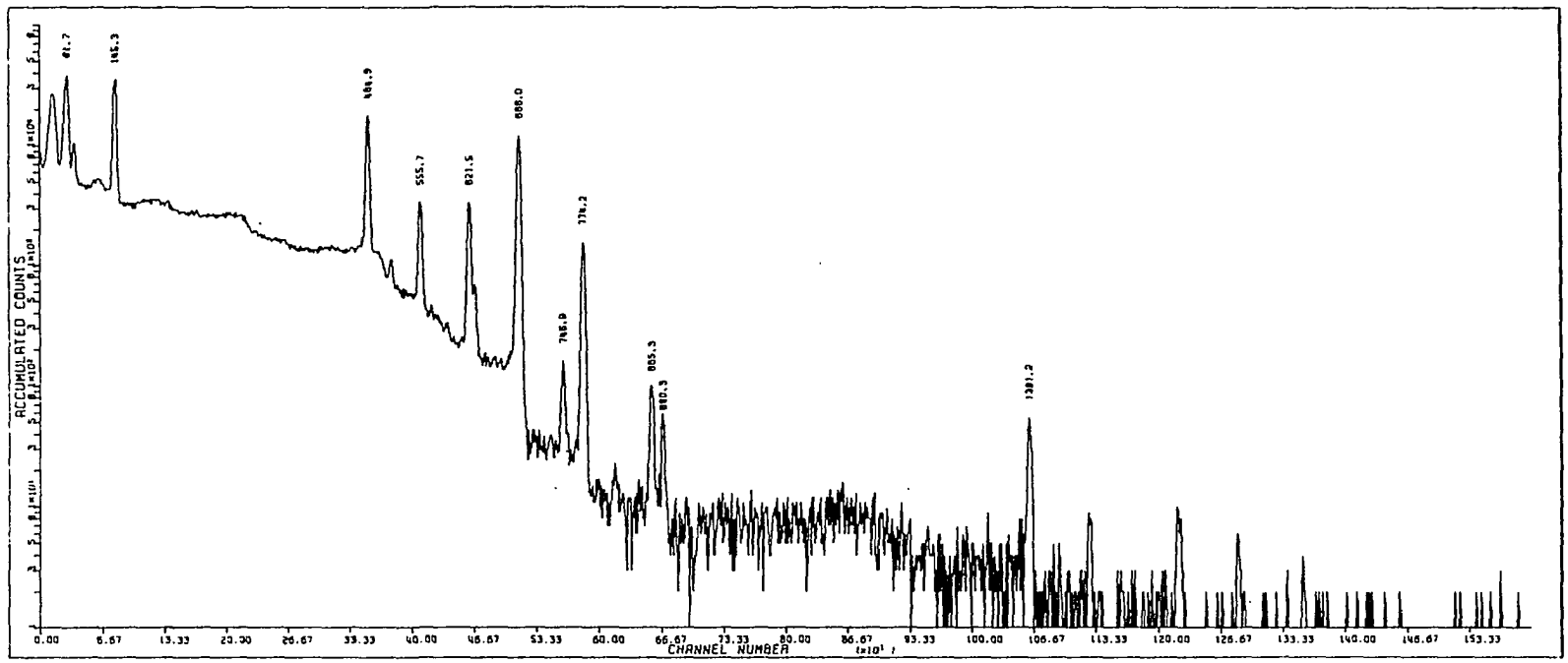

Figure A-7. Gamma-ray spectrum of Ho_xWO_3

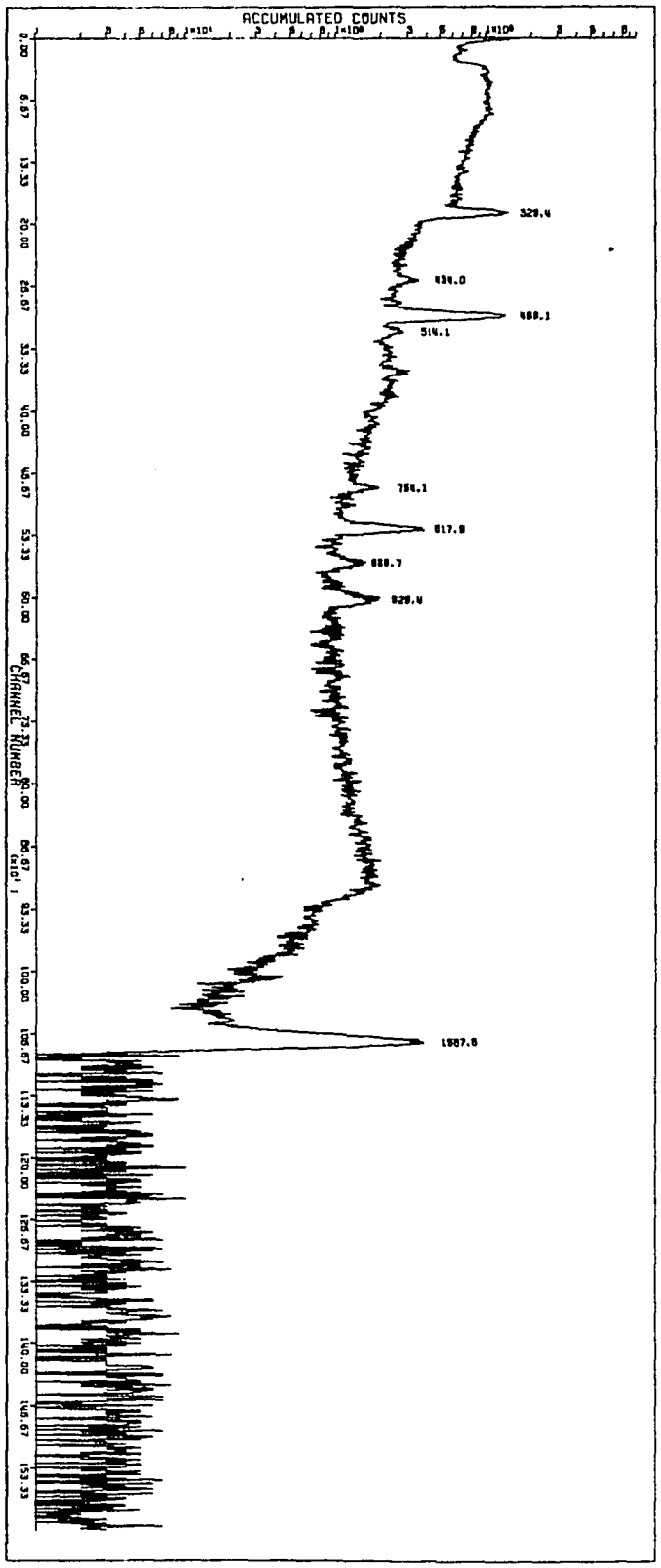

Figure A-8. Gamma-ray spectrum of ^{140}La

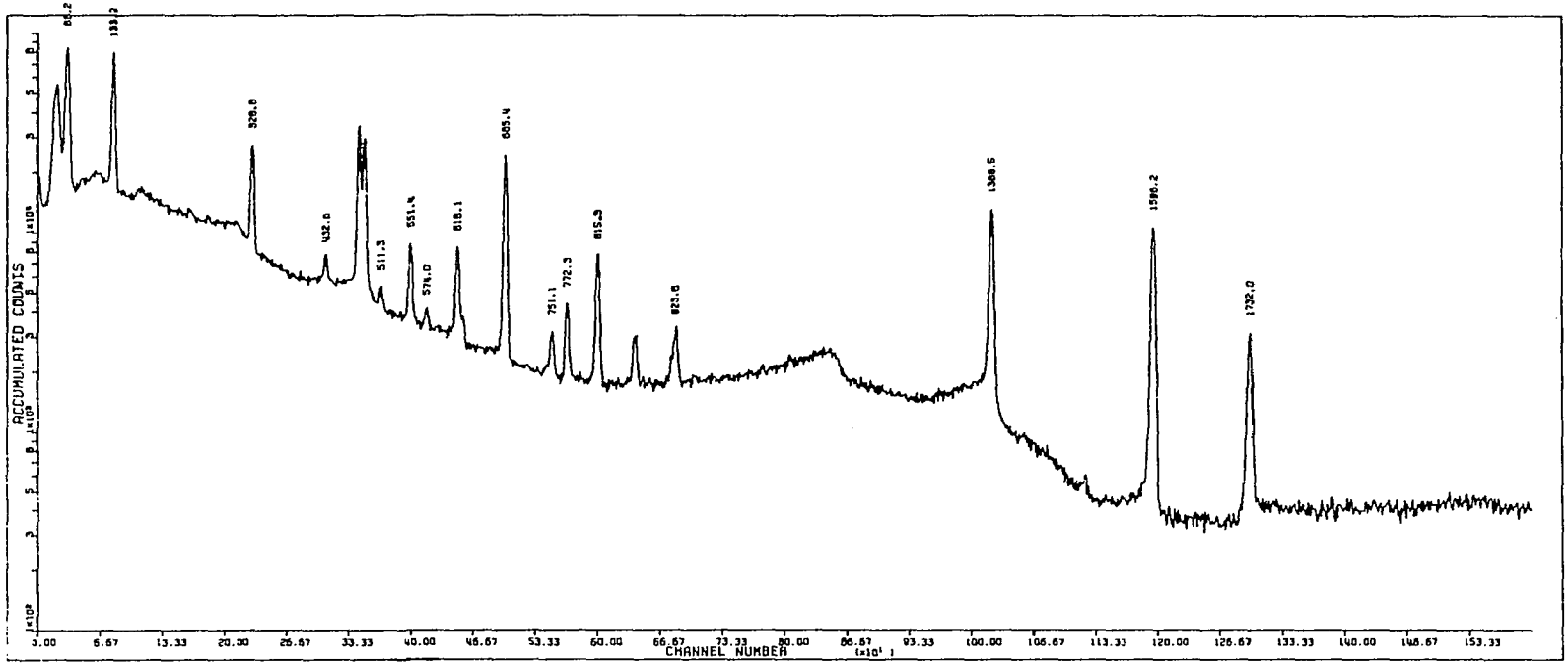

Figure A-9. Gamma-ray spectrum of La:W standard

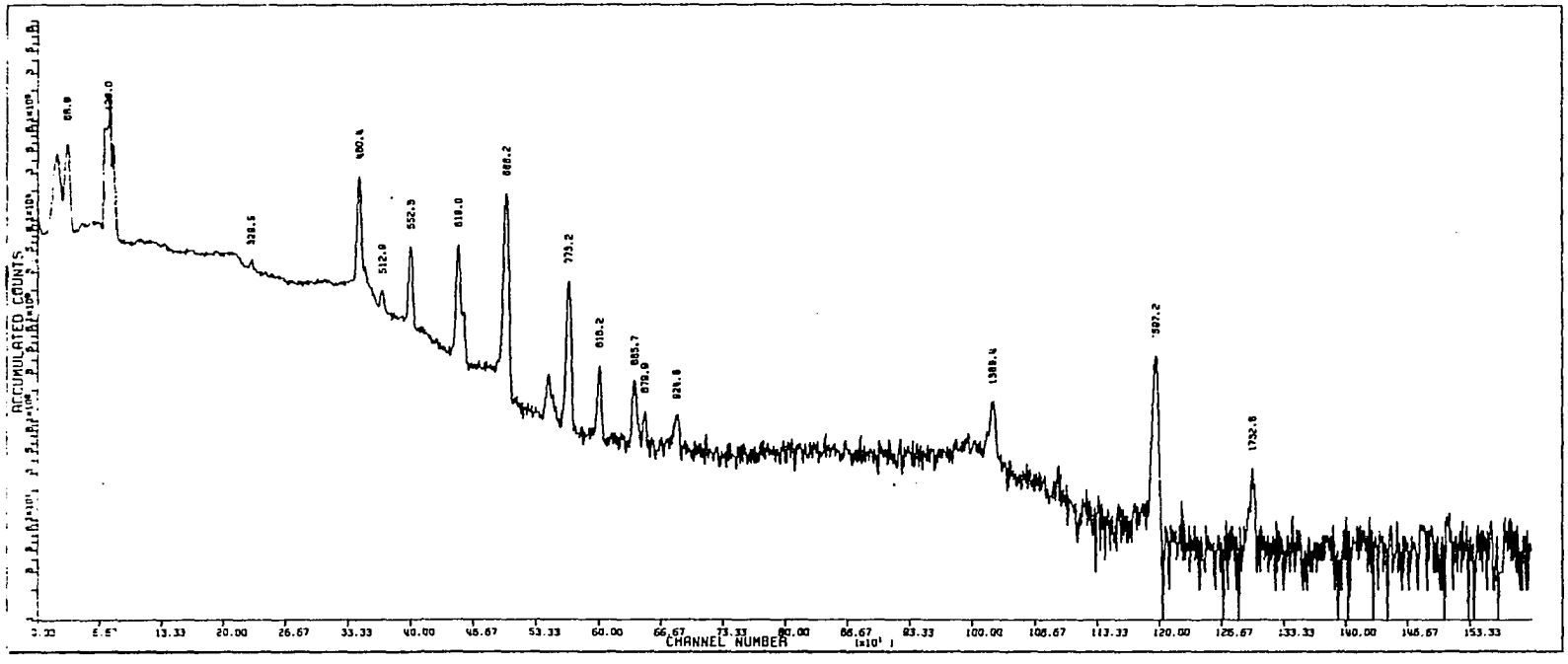

Figure A-10. Gamma-ray spectrum of La_xWO_3

APPENDIX B. TABLES OF n,n'/n,γ RATIOS FOR FISSION AND THERMAL NEUTRON IRRADIATIONS

Table B-1. $Sr(NO_3)_2$ irradiated using fission neutrons

Sample Number	Weight (mg)	Atoms 86 $\times 10^{-17}$	Atoms 87 $\times 10^{-17}$	A $\times 10^{-4}$ (.388 Mev)	$\frac{n,n'}{n,\gamma}$ (.388 Mev)
1-E	2.00	0.41108	53.262	3.971	0.485
2-N	3.85	10.803	7.6914	2.198	
3-E	1.11	0.22815	29.561	2.440	0.513
4-N	4.88	13.6932	9.7491	2.961	
5-E	0.942	0.19362	25.087	2.042	0.455
6-N	1.32	3.7039	2.6371	0.8638	
7-E	1.04	0.21376	27.696	2.092	0.437
8-N	3.29	9.2317	6.5727	2.054	
9-E	2.00	0.41108	53.262	4.343	0.427
10-N	3.85	10.803	7.6914	2.638	
11-E	1.11	0.22815	29.561	2.591	0.461
12-N	4.88	13.693	9.7491	3.400	
13-E	0.942	0.19362	25.087	2.218	0.452
14-N	1.32	3.7039	2.6371	0.9398	
				Avg.	0.461 ± 0.029

Table B-2. $Sr(NO_3)_2$ irradiated using thermal neutrons

Sample Number	Weight (mg)	Atoms 86 $\times 10^{-17}$	Atoms 87 $\times 10^{-17}$	A $\times 10^{-4}$ (.388 Mev)	$\frac{n,n'}{n,\gamma}$ (.388 Mev)
1-E	1.038	0.21335	27.643	0.2272	0.00109
2-N	3.286	9.2205	6.5647	8.610	
3-E	1.106	0.22733	29.454	0.2591	0.00171
4-N	4.878	13.688	9.7451	12.79	
5-E	2.002	0.41149	53.316	0.4492	0.00147
6-N	3.848	10.797	7.6874	9.914	
7-E	0.824	0.16936	21.944	0.5268	0.000866
8-N	1.204	3.3784	2.4053	9.452	
9-E	1.106	0.22733	29.454	0.2413	0.00132
10-N	4.878	13.688	9.7451	12.42	
11-E	0.968	0.19896	25.779	0.6717	0.00188
12-N	1.604	4.5008	3.2044	12.23	
13-E	1.100	0.22609	29.294	0.4633	0.00113
14-N	1.664	4.6692	3.3243	8.353	
15-E	0.9420	0.19362	25.087	0.2409	0.00280
16-N	4.878	13.688	9.7451	12.52	
17-E	3.270	0.67212	87.084	0.7106	0.00105
18-N	2.730	7.6604	5.4539	7.134	
				Avg.	0.00148 $\pm$ 0.00062

Table B-3. CdO irradiated using fission neutrons

Sample Number	Weight (mg)	Atoms 110 $\times 10^{-17}$	Atoms 111 $\times 10^{-17}$	A $\times 10^{-4}$ (.150 Mev)	A $\times 10^{-4}$ (.247 Mev)	$\frac{n,n'}{n,\gamma}$ (.150 Mev)	$\frac{n,n'}{n,\gamma}$ (.247 Mev)
1-E	0.614	0.18352	28.111	---	41.18	---	1.08
2-N	1.53	8.8893	9.1475	---	25.26		
3-E	0.120	0.03587	5.4939	---	7.521	---	1.07
4-N	1.37	7.9597	8.1909	---	21.24		
5-E	0.788	0.23553	36.077	15.80	27.03	1.14	1.10
6-N	0.994	5.7751	5.9429	4.803	8.332		
7-E	0.120	0.03587	5.4939	2.402	4.008	1.14	1.08
8-N	0.944	5.4846	5.6440	4.551	7.788		
9-E	0.738	0.22058	33.788	16.66	28.56	1.06	1.05
10-N	0.230	1.3363	1.3751	1.293	2.220		
11-E	0.120	0.035867	5.4939	2.281	3.818	1.08	1.03
12-N	0.944	5.4846	5.6440	4.430	7.581		
13-E	0.834	0.24928	38.183	16.58	27.92	1.11	1.07
14-N	1.21	7.0301	7.2343	5.866	10.02		
15-E	0.614	0.18352	28.111	12.92	21.34	1.04	1.02
16-N	1.53	8.8893	9.1475	8.076	13.47		
17-E	0.788	0.23553	36.077	15.05	26.04	1.09	1.08
18-N	1.50	8.7150	8.9682	7.034	12.21		
					Avg.	1.09 ± 0.04	1.06 ± 0.03

Table B-4. CdO irradiated using thermal neutrons

Sample Number	Weight (mg)	Atoms 110 $\times 10^{-17}$	Atoms 111 $\times 10^{-17}$	A $\times 10^{-3}$ (.150 Mev)	A $\times 10^{-3}$ (.247 Mev)	$\frac{n,n'}{n,\gamma}$ (.150 Mev)	$\frac{n,n'}{n,\gamma}$ (.247 Mev)
1-E	0.834	0.24928	38.183	1.536	2.667	0.0134	0.0141
2-N	1.49	8.6569	8.9084	17.68	29.71		
3-E	0.614	0.18352	28.111	1.031	1.904	0.0146	0.0155
4-N	1.37	7.9597	8.1909	14.02	24.92		
5-E	0.120	0.035867	5.4939	---	0.365	---	0.0155
6-N	0.944	5.4846	5.6440	---	16.84		
7-E	0.788	0.23553	36.077	1.687	2.691	0.0147	0.0122
8-N	0.994	5.7751	5.9429	12.93	23.32		
9-E	0.738	0.22058	33.788	1.585	3.065	0.0111	0.0143
10-N	0.236	1.3712	1.4110	3.682	6.044		
					Avg.	0.0134 ± 0.0017	0.0143 ± 0.0014

Table B-5. $Ba(NO_3)_2$ irradiated using fission neutrons

Sample Number	Weight (mg)	Atoms 136 $\times 10^{-17}$	Atoms 137 $\times 10^{-17}$	A $\times 10^{-4}$ (.662 Mev)	$\frac{n,n'}{n,\gamma}$ (.662 Mev)
1-E	0.282	0.037734	5.8294	1.199	3.82
2-N	2.23	3.9960	5.7919	1.404	
3-E	1.80	0.24086	37.2090	7.585	3.77
4-N	2.16	3.8706	5.6101	1.350	
5-E	0.780	0.10437	16.1239	4.287	3.92
6-N	4.57	8.1892	11.8696	3.704	
7-E	0.916	0.12257	18.9352	4.127	3.86
8-N	3.35	6.0030	8.7009	2.231	
9-E	1.16	0.15522	23.9791	4.402	3.82
10-N	1.74	3.1180	4.5193	0.9781	
				Avg.	3.84 ± 0.06

Table B-6. $Ba(NO_3)_2$ irradiated using thermal neutrons

Sample Number	Weight (mg)	Atoms 136 $\times 10^{-17}$	Atoms 137 $\times 10^{-17}$	A $\times 10^{-2}$ (.662 Mev)	$\frac{n,n'}{n,\gamma}$ (.662 Mev)
1-E	1.16	0.15522	23.979	1.90	0.0592
2-N	4.57	8.1892	11.870	10.74	
3-E	0.916	0.12257	18.935	1.44	0.0508
4-N	1.74	3.1180	4.5193	4.44	
5-E	0.780	0.10437	16.124	1.10	0.0495
6-N	2.16	3.8706	5.6101	5.05	
7-E	0.780	0.10437	16.124	1.62	0.0625
8-N	4.57	8.1892	11.870	13.03	
9-E	1.80	0.24086	37.209	3.86	0.0571
10-N	2.16	3.8706	5.6101	6.85	
11-E	0.916	0.12257	18.935	2.39	0.0649
12-N	3.35	6.0030	8.7009	11.64	
				Avg.	0.0573 ± 0.0062

Table B-7. HfO_2 irradiated using fission neutrons

Sam. No.	Weight (mg)	Atoms 179 $\times 10^{-17}$	Atoms 180 $\times 10^{-17}$	A $\times 10^{-4}$ (.215 Mev)	A $\times 10^{-4}$ (.333 Mev)	A $\times 10^{-4}$ (.444 Mev)	$\frac{n,n'}{n,\gamma}$ (.215 Mev)	$\frac{n,n'}{n,\gamma}$ (.333 Mev)	$\frac{n,n'}{n,\gamma}$ (.444 Mev)
1-E	0.368	0.27830	9.8231	0.2314	0.1465	0.0837	0.0193	0.0203	0.0203
2-N	1.90	7.4747	19.146	3.881	2.410	1.377			
3-E	0.456	0.34485	12.172	0.1434	0.0902	0.0515	0.0193	0.0203	0.0190
4-N	2.08	8.1828	20.960	2.124	1.311	0.7580			
5-E	0.188	0.14217	5.0183	0.1182	0.0747	0.0428	0.0193	0.0200	0.0197
6-N	2.82	11.094	28.417	5.760	3.592	2.069			
7-E	0.296	0.22385	7.9012	0.0931	0.0579	0.0335	0.0186	0.0193	0.0187
8-N	2.16	8.4975	21.766	2.206	1.387	0.8209			
9-E	0.272	0.20570	7.2605	0.1710	0.1082	0.0618	0.0195	0.0190	0.0196
10-N	3.34	13.155	33.697	6.800	4.309	2.454			
						Avg.	0.0192 ± 0.0003	0.0198 ± 0.0006	0.0195 ± 0.0006

Table B-8. HfO_2 irradiated using thermal neutrons

Sam. No.	Weight (mg)	Atoms 179 $\times 10^{-17}$	Atoms 180 $\times 10^{-17}$	A $\times 10^{-4}$ (.215 Mev)	A $\times 10^{-4}$ (.333 Mev)	A $\times 10^{-4}$ (.444 Mev)	$\frac{n,n'}{n,\gamma}$ (.215 Mev)	$\frac{n,n'}{n,\gamma}$ (.333 Mev)	$\frac{n,n'}{n,\gamma}$ (.444 Mev)
1-E	0.236	0.17850	6.2996	0.3512	0.2169	0.1245	0.0154	0.0149	0.0166
2-N	2.76	10.858	27.812	14.40	8.983	4.979			
3-E	0.088	0.066559	2.3490	0.1349	0.0805	0.0474	0.0159	0.0147	0.0156
4-N	1.45	5.6965	14.591	7.701	4.713	2.725			
5-E	0.196	0.14824	5.2319	0.2109	0.1786	0.1091	0.0158	0.0145	0.0169
6-N	0.488	1.9198	4.9175	1.8239	1.588	0.9245			
						Avg.	0.0157 ± 0.0003	0.0147 ± 0.0002	0.0164 ± 0.0007

Table B-9. Os irradiated using fission neutrons

Sample Number	Weight (mg)	Atoms 189 $\times 10^{-17}$	Atoms 190 $\times 10^{-17}$	A $\times 10^{-3}$ (.361 Mev)	$\frac{n,n'}{n,\gamma}$ (.361 Mev)
1-E	0.690	.30837	20.878	4.213	1.80
2-N	1.00	5.0944	8.3536	2.238	
3-E	0.244	0.10905	7.3829	1.566	1.92
4-N	1.27	6.4699	10.609	2.944	
5-E	0.874	0.39061	26.445	5.249	1.94
6-N	1.47	7.4888	12.280	3.180	
7-E	0.688	0.30748	20.817	4.286	1.96
8-N	0.980	4.9926	8.1865	2.194	
9-E	0.244	1.0905	7.3829	1.387	1.88
10-N	1.00	5.0944	8.3536	2.063	
				Avg.	1.90 ± 0.06

Table B-10. Os irradiated using thermal neutrons

Sample Number	Weight (mg)	Atoms 189 $\times 10^{-17}$	Atoms 190 $\times 10^{-17}$	A $\times 10^{-3}$ (.361 Mev)	$\frac{n,n'}{n,\gamma}$ (.361 Mev)
1-E	0.852	0.38078	25.780	0.495	0.0917
2-N	0.812	4.1367	6.7831	0.859	
3-E	0.400	0.17877	12.103	0.362	0.0926
4-N	0.592	3.0159	4.9453	0.968	
5-E	0.444	0.19843	13.434	0.346	0.0980
6-N	1.084	5.5224	9.0553	1.537	
7-E	0.690	0.30837	20.878	0.149	0.0926
8-N	1.266	0.64496	10.576	0.495	
				Avg.	0.0937 ± 0.0029

Table B-11. Pt irradiated using fission neutrons

Sample Number	Weight (mg)	Atoms 194 $\times 10^{-17}$	Atoms 195 $\times 10^{-17}$	A $\times 10^{-3}$ (.099 Mev)	$\frac{n,n'}{n,\gamma}$ (.099 Mev)
1-E	0.838	7.2200	15.507	10.40	0.847
2-N	0.158	1.6067	1.6506	1.534	
3-E	0.984	8.4779	18.209	13.31	0.820
4-N	0.212	2.1558	2.2148	2.259	
5-E	0.316	2.7226	5.8476	3.640	0.840
6-N	0.142	1.4440	1.4835	1.283	
7-E	0.452	3.8943	8.3643	6.042	0.840
8-N	0.178	1.8101	1.8596	1.866	
				Avg.	0.837 ± 0.013

Table B-12. Pt irradiated using thermal neutrons

Sample umber	Weight (mg)	Atoms 194 $\times 10^{-17}$	Atoms 195 $\times 10^{-17}$	A $\times 10^{-2}$ (.099 Mev)	$\frac{n,n'}{n,\gamma}$ (.099 Mev)
1-E	0.452	3.8943	8.3643	7.82	0.100
2-N	0.320	3.2540	8.3431	5.93	
3-E	0.316	2.7226	5.8476	5.47	0.102
4-N	0.392	3.9862	4.0953	7.26	
5-E	0.984	8.4779	18.209	17.02	0.100
6-N	0.388	3.9455	4.0535	7.19	
7-E	0.452	3.8943	8.3643	9.03	0.102
8-N	0.392	3.9862	4.0953	8.38	
				Avg.	0.101 ± 0.001

Table B-13. HgO irradiated using fission neutrons

Sample Number	Weight (mg)	Atoms 198×10^{-17}	Atoms 199×10^{-17}	A $\times 10^{-3}$ (.158 Mev)	A $\times 10^{-3}$ (.375 Mev)	$\frac{n,n'}{n,\gamma}$ (.158 Mev)	$\frac{n,n'}{n,\gamma}$ (.375 Mev)
1-E[a]	0.328	0.21107	7.6584	70.70	6.104	2.24	1.85
2-N[b]	0.610	1.6994	2.8561	32.96	2.965		
3-E	0.356	0.22909	8.3121	81.77	6.940	2.18	1.76
4-N	1.05	2.9252	4.9162	60.81	5.405		
5-E	0.308	0.19820	7.1914	72.71	6.096	2.09	1.71
6-N	0.720	2.0059	3.3711	43.20	3.793		
7-E	0.312	0.20078	7.2848	62.04	6.016	2.16	1.83
8-N	0.396	1.1032	1.8541	19.89	1.998		
9-E	0.328	0.21107	7.6584	77.94	6.487	2.16	1.90
10-N	0.610	1.6994	2.8561	36.61	3.132		
11-E	0.356	0.22909	8.3121	71.02	5.975	2.19	1.73
12-N	1.05	2.9252	4.9162	52.74	4.673		
13-E	0.312	0.20078	7.2848	137.3	10.97	2.05	1.72
14-N	0.396	1.1032	1.8541	44.48	3.696		
15-E	0.726	0.46720	16.951	332.5	26.90	2.10	1.73
16-N	0.562	1.5657	2.6313	65.39	5.525		
17-E	1.16	0.74648	27.084	491.0	43.76	2.06	1.69
18-N	1.00	2.7859	4.6821	108.0	10.07		
					Avg.	2.14 ± 0.06	1.77 ± 0.07

Table B-14. HgO irradiated using thermal neutrons

Sample Number	Weight (mg)	Atoms 198 $\times 10^{-17}$	Atoms 199 $\times 10^{-17}$	A $\times 10^{-3}$ (.158 Mev)	$\frac{n,n'}{n,\gamma}$ (.158 Mev)
1-E	0.356	0.22909	8.3121	1.019	0.0175
2-N	1.05	2.9252	4.9162	8.184	
3-E	0.328	0.21107	7.6584	0.8959	0.0180
4-N	0.418	1.1645	1.9571	3.084	
5-E	0.312	0.20078	7.2848	1.071	0.0197
6-N	0.396	1.1032	1.8541	3.544	
7-E	0.726	0.46720	16.951	2.421	0.0190
8-N	0.562	1.5657	2.6313	4.955	
9-E	0.328	0.21107	7.6584	0.7913	0.0175
10-N	0.610	1.6994	2.8561	4.011	
11-E	0.726	0.46720	16.951	4.033	0.0172
12-N	0.562	1.5657	2.6313	1.898	
				Avg.	0.0182 $\pm$ 0.0010

APPENDIX C. TABLES OF ^{137m}Ba:^{87m}Sr RATIOS FOR FISSION AND THERMAL NEUTRON IRRADIATIONS

Table C-1. 1:1 weight ratio of Ba^{137m}:Sr^{87m} irradiated with fission neutrons

Sample Number	$A_{Sr} \times 10^{-3}$ (0.388 Mev)	$A_{Ba} \times 10^{-3}$ (0.662 Mev)	$\frac{A_{Ba}}{A_{Sr}}$
1	3.66	50.0	13.7
2	2.67	36.9	13.8
3	3.66	50.0	13.7
4	3.26	44.9	13.8
		Avg.	13.8 ± 0.1

Table C-2. 1:1 weight ratio of Ba^{137m}:Sr^{87m} irradiated with thermal neutrons

Sample Number	$A_{Sr} \times 10^{-3}$ (0.388 Mev)	$A_{Ba} \times 10^{-3}$ (0.662 Mev)	$\frac{A_{Ba}}{A_{Sr}}$
1	12.9	2.38	0.184
2	13.5	2.43	0.180
3	12.8	2.32	0.181
4	13.3	2.44	0.183
5	13.0	2.38	0.183
6	13.6	2.46	0.182
7	12.6	2.27	0.180
		Avg.	0.182 ± 0.002

Table C-3. 1:2 weight ratio of Ba^{137m}:Sr^{87m} irradiated with fission neutrons

Sample Number	A_{Sr} x10^{-3} (0.388 Mev)	A_{Br} x10^{-3} (0.662 Mev)	$\frac{A_{Ba}}{A_{Sr}}$
1	3.52	22.0	6.25
2	3.52	22.1	6.28
3	3.53	22.1	6.26
4	3.54	22.2	6.27
		Avg.	6.26 ± 0.01

Table C-4. 1:2 weight ratio of Ba^{137m}:Sr^{87m} irradiated with thermal neutrons

Sample Number	A_{Sr} x10^{-3} (0.388 Mev)	A_{Ba} x10^{-3} (0.662 Mev)	$\frac{A_{Ba}}{A_{Sr}}$
1	13.6	1.17	0.0860
2	12.1	1.04	0.0860
3	13.5	1.33	0.0985
4	13.3	1.31	0.0985
5	13.4	1.24	0.0925
6	14.7	1.41	0.0959
7	14.6	1.26	0.0863
		Avg.	0.0920 ± 0.0058

Table C-5. 2:1 weight ratio of Ba^{137m}:Sr^{87m} irradiated with fission neutrons

Sample Number	A_{Sr} $\times 10^{-3}$ (0.388 Mev)	A_{Ba} $\times 10^{-3}$ (0.662 Mev)	$\frac{A_{Ba}}{A_{Sr}}$
1	1.69	48.2	28.5
2	1.73	47.8	27.6
3	1.70	48.5	28.5
4	1.72	48.0	27.9
5	1.48	40.5	27.4
6	1.48	41.4	27.9
		Avg.	28.0 ± 0.5

Table C-6. 2:1 weight ratio of Ba^{137m}:Sr^{87m} irradiated with thermal neutrons

Sample Number	A_{Sr} $\times 10^{-3}$ (0.388 Mev)	A_{Ba} $\times 10^{-3}$ (0.662 Mev)	$\frac{A_{Ba}}{A_{Sr}}$
1	7.27	2.48	0.341
2	6.48	2.23	0.344
3	6.57	2.26	0.344
4	6.79	2.36	0.348
5	7.55	2.59	0.343
		Avg.	0.344 ± 0.002

Table C-7. 1:10 weight ratio of Ba^{137m}:Sr^{87m} irradiated with fission neutrons

Sample Number	A_{Sr} x10^{-3} (0.388 Mev)	A_{Ba} x10^{-3} (0.662 Mev)	$\frac{A_{Ba}}{A_{Sr}}$
1	3.63	5.02	1.38
2	3.54	4.82	1.36
3	3.41	4.70	1.38
4	3.36	4.60	1.37
		Avg.	1.37 ± 0.01

Table C-8. 1:10 weight ratio of Ba^{137m}:Sr^{87m} irradiated with thermal neutrons

Sample Number	A_{Sr} x10^{-3} (0.388 Mev)	A_{Ba} x10^{-3} (0.662 Mev)	$\frac{A_{Ba}}{A_{Sr}}$
1	12.3	0.240	0.0195
2	13.1	0.253	0.0193
3	13.9	0.296	0.0213
4	14.7	0.289	0.0196
5	13.5	0.293	0.0217
		Avg.	0.0203 ± 0.0011

Table C-9. 10:1 weight ratio of Ba^{137m}:Sr^{87m} irradiated with fission neutrons

Sample Number	A_{Sr} x10^{-3} (0.388 Mev)	A_{Ba} x10^{-3} (0.662 Mev)		$\frac{A_{Ba}}{A_{Sr}}$
1	0.343	48.3		141
2	0.311	43.9		141
3	0.351	49.2		140
4	0.320	44.9		140
			Avg.	140 ± 1

Table C-10. 10:1 weight ratio of Ba^{137m}:Sr^{87m} irradiated with thermal neutrons

Sample Number	A_{Sr} x10^{-3} (0.388 Mev)	A_{Ba} x10^{-3} (0.662 Mev)		$\frac{A_{Ba}}{A_{Sr}}$
1	1.18	2.18		1.85
2	1.36	2.36		1.74
3	1.28	2.32		1.81
4	1.21	2.18		1.80
			Avg.	1.80 ± 0.04

Table C-11. 1:100 weight ratio of Ba^{137m}:Sr^{87} irradiated with fission neutrons

Sample Number	A_{Sr} $\times 10^{-3}$ (0.388 Mev)	A_{Ba} $\times 10^{-3}$ (0.662 Mev)	$\frac{A_{Ba}}{A_{Sr}}$
1	3.46	0.447	0.129
2	3.35	0.425	0.127
3	3.58	0.451	0.126
4	3.38	0.427	0.126
		Avg.	0.127 ± 0.001

Table C-12. 1:100 weight ratio of Ba^{137m}:Sr^{87m} irradiated with thermal neutrons

Sample Number	A_{Sr} $\times 10^{-3}$ (0.388 Mev)	A_{Ba} $\times 10^{-3}$ (0.662 Mev)	$\frac{A_{Ba}}{A_{Sr}}$
1	12.8	0.205	0.0160
2	12.5	0.179	0.0143
3	13.5	0.279	0.0207
4	13.1	0.189	0.0144
5	13.5	0.216	0.0160
6	13.5	0.184	0.0136
		Avg.	0.0158 ± 0.0029

Table C-13. 100:1 weight ratio of Ba^{137m}:Sr^{87m} irradiated with fission neutrons

Sample Number	A_{Sr} $\times 10^{-3}$ (0.388 Mev)	A_{Ba} $\times 10^{-3}$ (0.662 Mev)	$\frac{A_{Ba}}{A_{Sr}}$
1	0.143	45.2	316
2	0.331	47.1	142
3	0.092	43.2	469
4	0.182	44.5	245
5	0.080	46.0	575
6	0.169	43.6	258
7	0.048	45.1	940
8	0.198	43.3	219
9	0.120	43.6	364
10	0.309	46.4	150

Table C-14. 100:1 weight ratio of Ba^{137m}:Sr^{87m} irradiated with thermal neutrons

Sample Number	A_{Sr} $\times 10^{-2}$ (0.388 Mev)	A_{Ba} $\times 10^{-2}$ (0.662 Mev)	$\frac{A_{Ba}}{A_{Sr}}$
1	1.49	24.8	16.6
2	1.04	23.4	22.5
3	1.33	20.5	15.4
4	1.19	21.0	17.7
5	0.980	19.7	20.1
		Avg.	18.5 ± 2.8

APPENDIX D. TABLES OF ^{111m}Cd:^{199m}Hg RATIOS FOR FISSION AND THERMAL NEUTRON IRRADIATIONS

Table D-1. 1:1 weight ratio of Cd^{111m}:Hg^{199m} irradiated with fission neutrons

Sample Number	$A_{Cd} \times 10^{-4}$ (0.150 Mev)	(0.247 Mev)	$A_{Hg} \times 10^{-4}$ (0.158 Mev)	(0.375 Mev)	$\frac{A_{Cd}\ .150}{A_{Hg}\ .158}$	$\frac{A_{Cd}\ .150}{A_{Hg}\ .375}$	$\frac{A_{Cd}\ .247}{A_{Hg}\ .158}$	$\frac{A_{Cd}\ .247}{A_{Hg}\ .375}$
1	8.16	13.5	9.33	0.781	0.875	10.5	1.45	17.3
2	8.76	14.4	10.4	0.859	0.840	10.2	1.38	16.8
3	8.31	14.3	10.0	0.839	0.828	9.91	1.43	17.1
4	16.4	26.7	18.8	1.60	0.872	10.2	1.42	16.7
5	17.0	25.6	18.9	1.54	0.902	11.1	1.36	16.8
6	16.5	25.9	19.4	1.55	0.851	10.7	1.34	16.7
7	15.1	25.2	17.9	1.49	0.844	10.1	1.41	16.9
8	16.7	25.5	18.9	1.52	0.882	11.0	1.35	16.8
9	15.9	26.9	19.7	1.62	0.809	9.83	1.36	16.6
				Avg.	0.856 ± 0.029	10.4 ± 0.5	1.39 ± 0.04	16.9 ± 0.2

Table D-2. 1:1 weight ratio of Cd^{111m}:Hg^{199m} irradiated with thermal neutrons

Sample Number	A_{Cd} $\times 10^{-4}$ (0.150 Mev)	(0.247 Mev)	A_{Hg} $\times 10^{-4}$ (0.158 Mev)	(0.375 Mev)	$\frac{A_{Cd}\ .150}{A_{Hg}\ .158}$	$\frac{A_{Cd}\ .150}{A_{Hg}\ .375}$	$\frac{A_{Cd}\ .247}{A_{Hg}\ .158}$	$\frac{A_{Cd}\ .247}{A_{Hg}\ .375}$
1	7.78	12.2	2.96	0.214	2.63	36.4	4.12	57.0
2	7.52	11.5	3.27	0.228	2.30	33.0	3.52	50.4
3	8.83	13.8	4.33	0.234	2.04	37.7	3.19	59.0
4	7.72	12.5	4.15	0.213	1.86	36.2	3.01	58.7
5	7.92	12.2	3.04	0.232	2.60	34.1	4.01	52.6
6	6.94	10.9	3.11	0.210	2.23	33.0	3.50	51.9
7	7.92	12.5	3.98	0.239	1.99	33.1	3.14	52.3
8	18.0	27.3	10.4	0.523	1.73	34.4	2.62	52.2
				Avg.	2.17 ± 0.33	34.7 ± 1.8	3.39 ± 0.42	54.3 ± 3.4

Table D-3. 1:2 weight ratio of Cd^{111m}:Hg^{199m} irradiated with fission neutrons

Sample Number	A_{Cd} $\times 10^{-4}$ (0.150 Mev)	(0.247 Mev)	A_{Hg} $\times 10^{-4}$ (0.158 Mev)	(0.375 Mev)	$\frac{A_{Cd}\ .150}{A_{Hg}\ .158}$	$\frac{A_{Cd}\ .150}{A_{Hg}\ .375}$	$\frac{A_{Cd}\ .247}{A_{Hg}\ .158}$	$\frac{A_{Cd}\ .247}{A_{Hg}\ .375}$
1	12.0	19.4	26.1	2.25	0.458	5.31	0.742	8.60
2	14.4	23.4	31.6	2.59	0.455	5.56	0.740	9.03
3	14.8	22.6	31.4	2.55	0.470	5.78	0.720	8.85
4	16.9	27.4	38.2	3.04	0.442	5.56	0.717	9.01
5	15.3	25.6	35.7	2.85	0.429	5.37	0.716	8.96
				Avg.	0.451 ± 0.016	5.52 ± 0.18	0.727 ± 0.013	8.89 ± 0.18

Table D-4. 1:2 weight ratio of Cd^{111m}:Hg^{199m} irradiated with thermal neutrons

Sample Number	A_{Cd} $\times 10^{-3}$ (0.150 Mev)	A_{Cd} $\times 10^{-3}$ (0.247 Mev)	A_{Hg} $\times 10^{-3}$ (0.158 Mev)	A_{Hg} $\times 10^{-3}$ (0.375 Mev)	$\frac{A_{Cd}\ .150}{A_{Hg}\ .158}$	$\frac{A_{Cd}\ .150}{A_{Hg}\ .375}$	$\frac{A_{Cd}\ .247}{A_{Hg}\ .158}$	$\frac{A_{Cd}\ .247}{A_{Hg}\ .375}$
1	18.7	46.3	8.95	1.66	2.09	11.2	5.17	27.8
2	19.3	46.8	9.64	1.66	2.00	11.7	4.85	28.2
3	26.7	65.9	10.0	2.23	2.66	11.9	6.57	29.5
4	19.7	49.0	11.8	1.91	1.68	10.3	4.16	25.6
5	26.7	64.9	17.4	2.48	1.54	10.7	3.74	26.1
6	22.0	53.4	13.2	1.74	1.66	12.6	4.03	30.7
7	21.7	56.8	17.3	2.10	1.25	10.3	3.28	27.0
8	22.5	56.0	16.7	2.46	1.35	9.15	3.36	22.8
				Avg.	1.79 ± 0.32	11.0 ± 1.1	4.40 ± 1.10	27.2 ± 2.5

Table D-5. 2:1 weight ratio of Cd^{111m}:Hg^{199m} irradiated with fission neutrons

Sample Number	A_{Cd} $\times 10^{-4}$ (0.150 Mev)	(0.247 Mev)	A_{Hg} $\times 10^{-4}$ (0.158 Mev)	(0.375 Mev)	$\frac{A_{Cd}\ .150}{A_{Hg}\ .158}$	$\frac{A_{Cd}\ .150}{A_{Hg}\ .375}$	$\frac{A_{Cd}\ .247}{A_{Hg}\ .158}$	$\frac{A_{Cd}\ .247}{A_{Hg}\ .375}$
1	12.2	21.0	7.93	0.619	1.54	19.7	2.64	33.9
2	11.4	19.7	7.20	0.575	1.58	19.8	2.74	34.3
3	12.0	20.6	7.30	0.604	1.65	19.9	2.83	34.2
4	12.6	21.5	7.54	0.622	1.67	20.3	1.71	34.6
				Avg.	1.61 ± 0.06	19.9 ± 0.3	2.48 ± 0.52	34.2 ± 0.3

Table D-6. 2:1 weight ratio of Cd^{111m}:Hg^{199m} irradiated with thermal neutrons

Sample Number	A_{Cd} $\times 10^{-3}$ (0.150 Mev)	(0.247 Mev)	A_{Hg} $\times 10^{-3}$ (0.158 Mev)	(0.375 Mev)	$\frac{A_{Cd}\ .150}{A_{Hg}\ .158}$	$\frac{A_{Cd}\ .150}{A_{Hg}\ .375}$	$\frac{A_{Cd}\ .247}{A_{Hg}\ .158}$	$\frac{A_{Cd}\ .247}{A_{Hg}\ .375}$
1	29.7	48.1	6.40	0.347	4.64	85.6	7.52	138
2	28.6	46.6	7.68	0.543	3.72	52.6	6.06	85.7
3	29.2	52.2	8.86	0.378	3.29	77.2	5.90	138
4	31.0	59.1	10.9	0.471	2.84	65.9	5.40	126
				Avg.	3.62 ± 0.77	70.3 ± 14.3	6.22 ± 0.91	122 ± 25

Table D-7. 1:10 weight ratio of Cd^{111m}:Hg^{199m} irradiated with fission neutrons

Sample Number	A_{Cd} $\times 10^{-4}$ (0.150 Mev)	A_{Cd} $\times 10^{-4}$ (0.247 Mev)	A_{Hg} $\times 10^{-4}$ (0.158 Mev)	A_{Hg} $\times 10^{-4}$ (0.375 Mev)	$\frac{A_{Cd}\ .150}{A_{Hg}\ .158}$	$\frac{A_{Cd}\ .150}{A_{Hg}\ .375}$	$\frac{A_{Cd}\ .247}{A_{Hg}\ .158}$	$\frac{A_{Cd}\ .247}{A_{Hg}\ .375}$
1	4.01	5.56	37.5	3.08	0.107	1.30	0.148	1.80
2	3.36	5.32	35.8	3.00	0.094	1.12	0.149	1.78
3	2.37	3.61	23.7	2.15	0.100	1.10	0.152	1.69
4	3.51	4.13	28.3	2.41	0.124	1.46	0.146	1.71
5	3.54	4.87	32.4	2.68	0.109	1.32	0.150	1.82
				Avg.	0.107 ± 0.011	1.26 ± 0.15	0.149 ± 0.002	1.76 ± 0.06

Table D-8. 1:10 weight ratio of Cd^{111m}:Hg^{199m} irradiated with thermal neutrons

Sample Number	A_{Cd} $\times 10^{-4}$ (0.150 Mev)	A_{Cd} $\times 10^{-4}$ (0.247 Mev)	A_{Hg} $\times 10^{-4}$ (0.158 Mev)	A_{Hg} $\times 10^{-4}$ (0.375 Mev)	$\frac{A_{Cd}\ .150}{A_{Hg}\ .158}$	$\frac{A_{Cd}\ .150}{A_{Hg}\ .375}$	$\frac{A_{Cd}\ .247}{A_{Hg}\ .158}$	$\frac{A_{Cd}\ .247}{A_{Hg}\ .375}$
1	1.49	1.90	4.10	0.328	0.362	4.54	0.463	5.80
2	0.997	1.87	3.88	0.345	0.257	2.89	0.482	5.41
3	0.884	1.94	4.26	0.360	0.207	2.45	0.455	5.39
4	0.764	1.77	3.74	0.342	0.204	2.23	0.473	5.18
5	0.470	1.18	2.51	0.208	0.187	2.26	0.469	5.66
6	0.571	1.94	4.07	0.331	0.140	1.72	0.476	5.85
				Avg.	0.226 ± 0.076	2.68 ± 0.99	0.470 ± 0.010	5.55 ± 0.26

Table D-9. 10:1 weight ratio of Cd^{111m}:Hg^{199m} irradiated with fission neutrons

Sample Number	A_{Cd} $\times 10^{-4}$ (0.150 Mev)	A_{Cd} $\times 10^{-4}$ (0.247 Mev)	A_{Hg} $\times 10^{-4}$ (0.158 Mev)	A_{Hg} $\times 10^{-4}$ (0.375 Mev)	$\frac{A_{Cd}\ .150}{A_{Hg}\ .158}$	$\frac{A_{Cd}\ .150}{A_{Hg}\ .375}$	$\frac{A_{Cd}\ .247}{A_{Hg}\ .158}$	$\frac{A_{Cd}\ .247}{A_{Hg}\ .375}$
1	53.0	81.5	1.05	0.441	50.2	120	77.3	185
2	56.3	85.1	1.13	0.465	50.0	121	75.6	183
3	55.4	82.8	1.00	0.461	55.4	120	82.8	180
4	57.9	87.6	1.32	0.481	43.9	120	66.4	182
				Avg.	49.9 ± 4.6	120 ± 1	75.5 ± 6.8	182 ± 2

Table D-10. 10:1 weight ratio of Cd^{111m}:Hg^{199m} irradiated with thermal neutrons

Sample Number	A_{Cd} $\times 10^{-4}$ (0.150 Mev)	A_{Cd} $\times 10^{-4}$ (0.247 Mev)	A_{Hg} $\times 10^{-4}$ (0.158 Mev)	A_{Hg} $\times 10^{-4}$ (0.375 Mev)	$\frac{A_{Cd}\ .150}{A_{Hg}\ .158}$	$\frac{A_{Cd}\ .150}{A_{Hg}\ .375}$	$\frac{A_{Cd}\ .247}{A_{Hg}\ .158}$	$\frac{A_{Cd}\ .247}{A_{Hg}\ .375}$
1	9.20	14.8	1.14	0.213	8.07	432	12.9	692
2	9.82	15.6	1.63	---	6.04	---	9.59	---
3	10.4	16.8	2.54	---	4.09	---	6.62	---
4	66.3	102.	32.4	0.235	2.05	283	3.14	434
5	13.8	21.8	1.30	0.0239	10.7	577	16.8	910
6	27.8	44.4	4.33	0.0660	6.43	422	10.2	672
7	87.2	132.	34.3	0.334	2.54	261	3.84	394
				Avg.	5.70 ± 3.09	395	9.01 ± 4.91	620

Table D-11. 1:100 weight ratio of Cd^{111m}:Hg^{199m} irradiated with fission neutrons

Sample Number	A_{Cd} $\times 10^{-4}$ (0.150 Mev)	A_{Cd} $\times 10^{-4}$ (0.247 Mev)	A_{Hg} $\times 10^{-4}$ (0.158 Mev)	A_{Hg} $\times 10^{-4}$ (0.375 Mev)	$\frac{A_{Cd}\ .150}{A_{Hg}\ .158}$	$\frac{A_{Cd}\ .150}{A_{Hg}\ .375}$	$\frac{A_{Cd}\ .247}{A_{Hg}\ .158}$	$\frac{A_{Cd}\ .247}{A_{Hg}\ .375}$
1	----	0.454	30.8	2.66	---	---	0.0147	0.170
2	----	0.452	34.7	2.65	---	---	0.0130	0.170
3	----	0.314	21.5	1.82	---	---	0.0146	0.172
4	----	0.514	36.0	2.98	---	---	0.0143	0.173
				Avg.	---	---	0.0142 ± 0.0008	0.171 ± 0.002

Table D-12. 1:100 weight ratio of Cd^{111m}:Hg^{199m} irradiated with thermal neutrons

Sample Number	A_{Cd} $\times 10^{-4}$ (0.150 Mev)	A_{Cd} $\times 10^{-4}$ (0.247 Mev)	A_{Hg} $\times 10^{-4}$ (0.158 Mev)	A_{Hg} $\times 10^{-4}$ (0.375 Mev)	$\frac{A_{Cd}\ .150}{A_{Hg}\ .158}$	$\frac{A_{Cd}\ .150}{A_{Hg}\ .375}$	$\frac{A_{Cd}\ .247}{A_{Hg}\ .158}$	$\frac{A_{Cd}\ .247}{A_{Hg}\ .375}$
1	----	1.41	33.2	3.17	---	---	0.0425	0.446
2	----	1.74	38.9	3.56	---	---	0.0447	0.490
3	----	1.52	31.2	2.83	---	---	0.0487	0.536
4	----	1.85	36.4	3.42	---	---	0.0508	0.540
				Avg.	---	---	0.0467 ± 0.0038	0.503 ± 0.044

Table D-13. 100:1 weight ratio of Cd^{111m}:Hg^{199m} irradiated with fission neutrons

Sample Number	A_{Cd} $\times 10^{-4}$ (0.150 Mev)	A_{Cd} $\times 10^{-4}$ (0.247 Mev)	A_{Hg} $\times 10^{-4}$ (0.158 Mev)	A_{Hg} $\times 10^{-4}$ (0.375 Mev)	$\frac{A_{Cd}\ .150}{A_{Hg}\ .158}$	$\frac{A_{Cd}\ .150}{A_{Hg}\ .375}$	$\frac{A_{Cd}\ .247}{A_{Hg}\ .158}$	$\frac{A_{Cd}\ .247}{A_{Hg}\ .375}$
1	27.29	46.17	---	0.1667	---	164	---	277
2	26.50	46.11	---	0.2208	---	120	---	209
3	26.45	46.28	---	0.1869	---	142	---	248
4	25.65	44.84	---	0.1900	---	135	---	236
5	22.85	43.59	---	0.1868	---	122	---	233
				Avg.	---	137 ± 18	---	241 ± 25

Table D-14. 100:1 weight ratio of Cd^{111m}:Hg^{199m} irradiated with thermal neutrons

Sample Number	A_{Cd} $\times 10^{-3}$ (0.150 Mev)	A_{Cd} $\times 10^{-3}$ (0.247 Mev)	A_{Hg} $\times 10^{-3}$ (0.158 Mev)	A_{Hg} $\times 10^{-3}$ (0.375 Mev)	$\frac{A_{Cd}\ .150}{A_{Hg}\ .158}$	$\frac{A_{Cd}\ .150}{A_{Hg}\ .375}$	$\frac{A_{Cd}\ .247}{A_{Hg}\ .158}$	$\frac{A_{Cd}\ .247}{A_{Hg}\ .375}$
1	78.01	146.0	3.831	0.598	20.4	38.1	130	244
2	85.13	157.1	2.862	0.681	29.7	54.9	125	231
3	86.90	155.1	---	0.654	---	---	133	237
4	89.49	154.7	---	0.664	---	---	135	233
				Avg.	---	---	131 ± 4	236 ± 6

APPENDIX E. SPECTRA OF NORMALLY ABUNDANT AND ENRICHED ISOTOPES IRRADIATED WITH FISSION AND THERMAL NEUTRONS

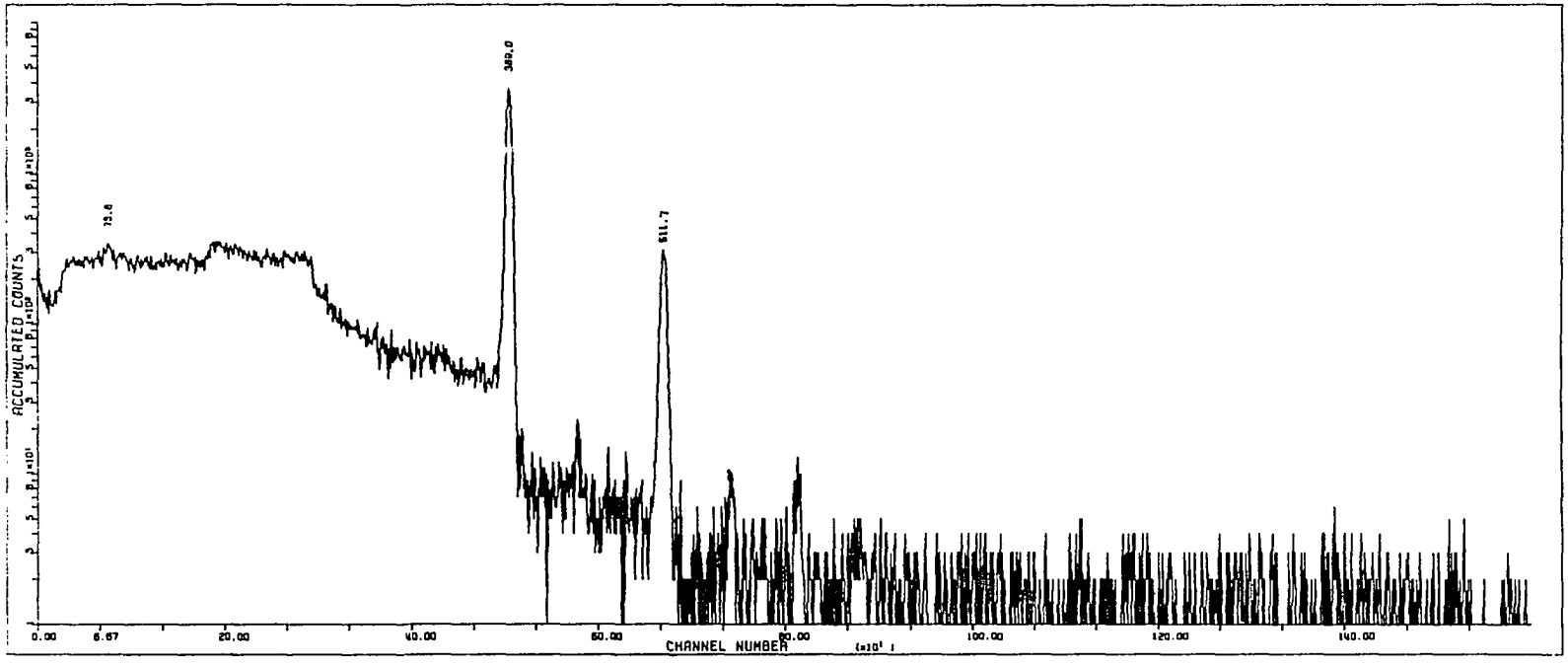

Figure E-1. $Sr(NO_3)_2$, 93% enriched in ^{87}Sr, irradiated with fission neutrons

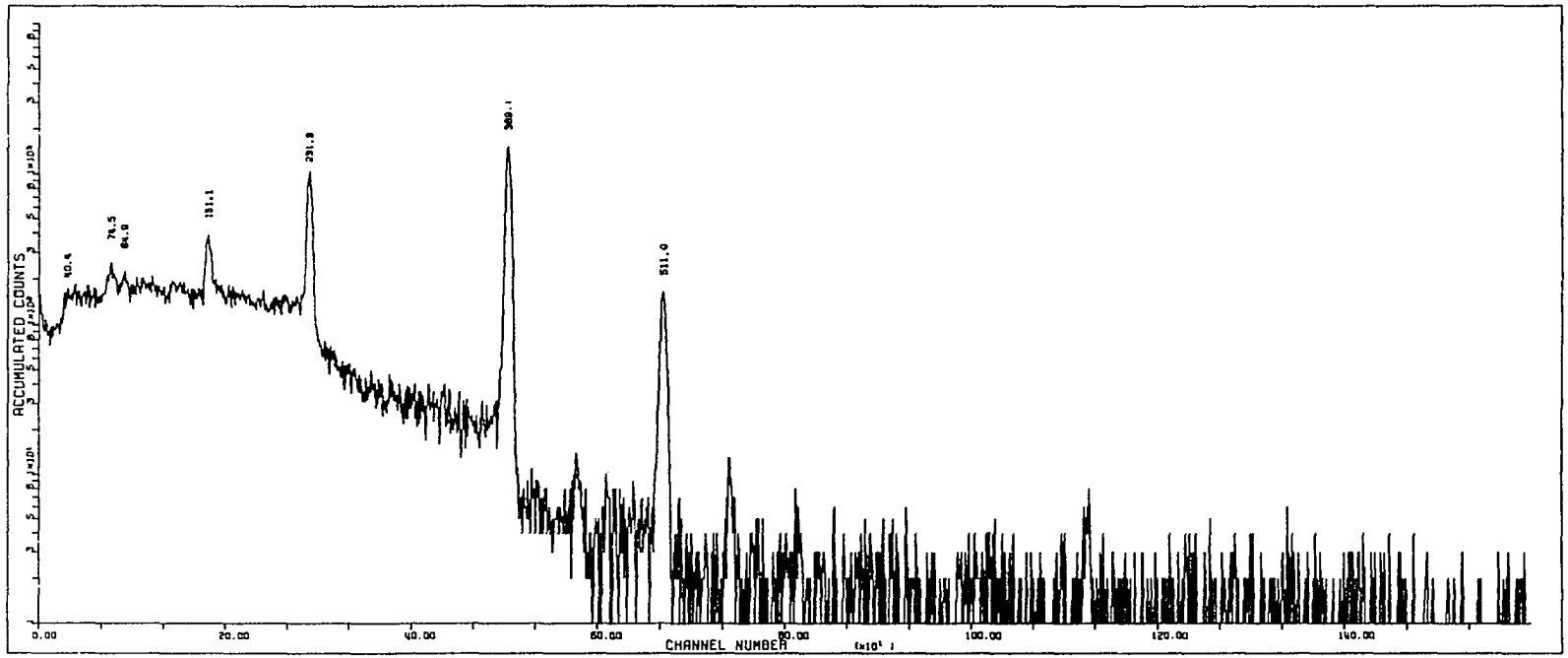

Figure E-2. $Sr(NO_3)_2$, normally abundant, irradiated with fission neutrons

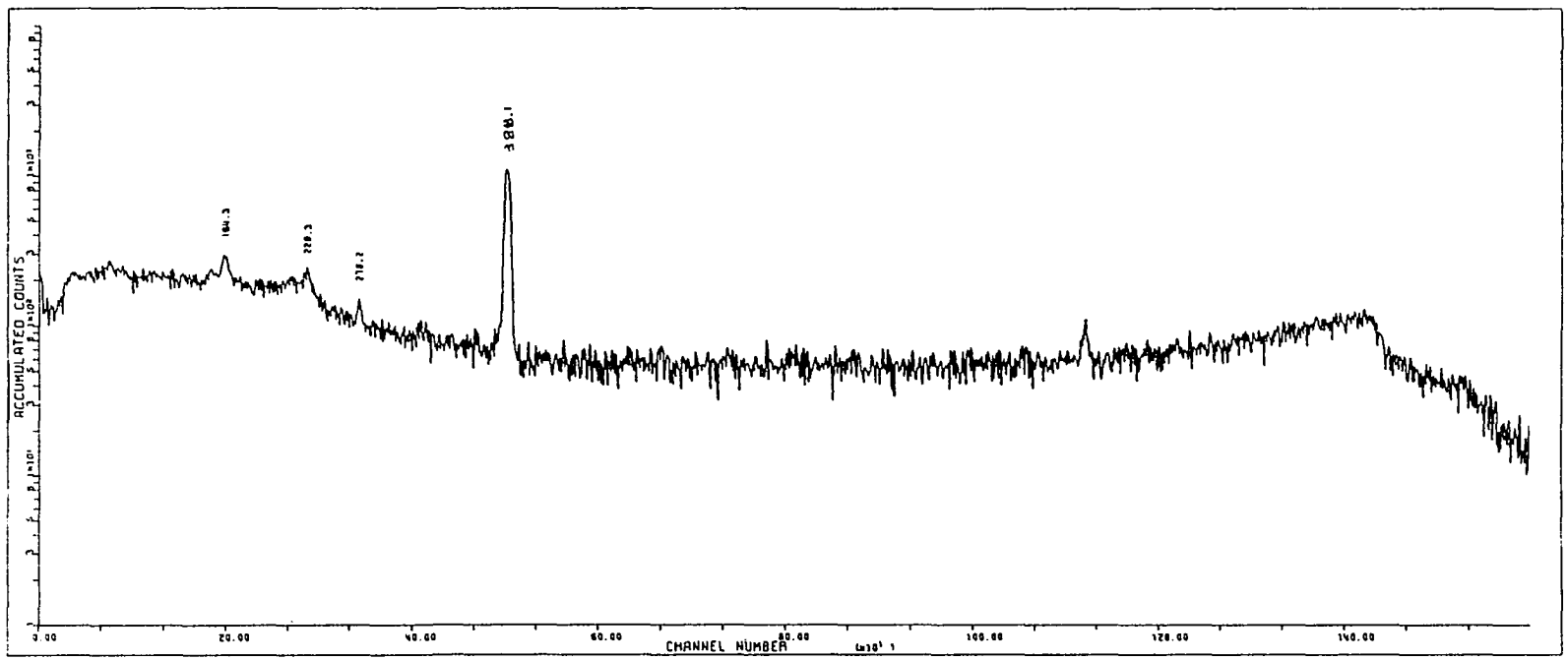

Figure E-3. $Sr(NO_3)_2$, 93% enriched in ^{87}Sr, irradiated with thermal neutrons

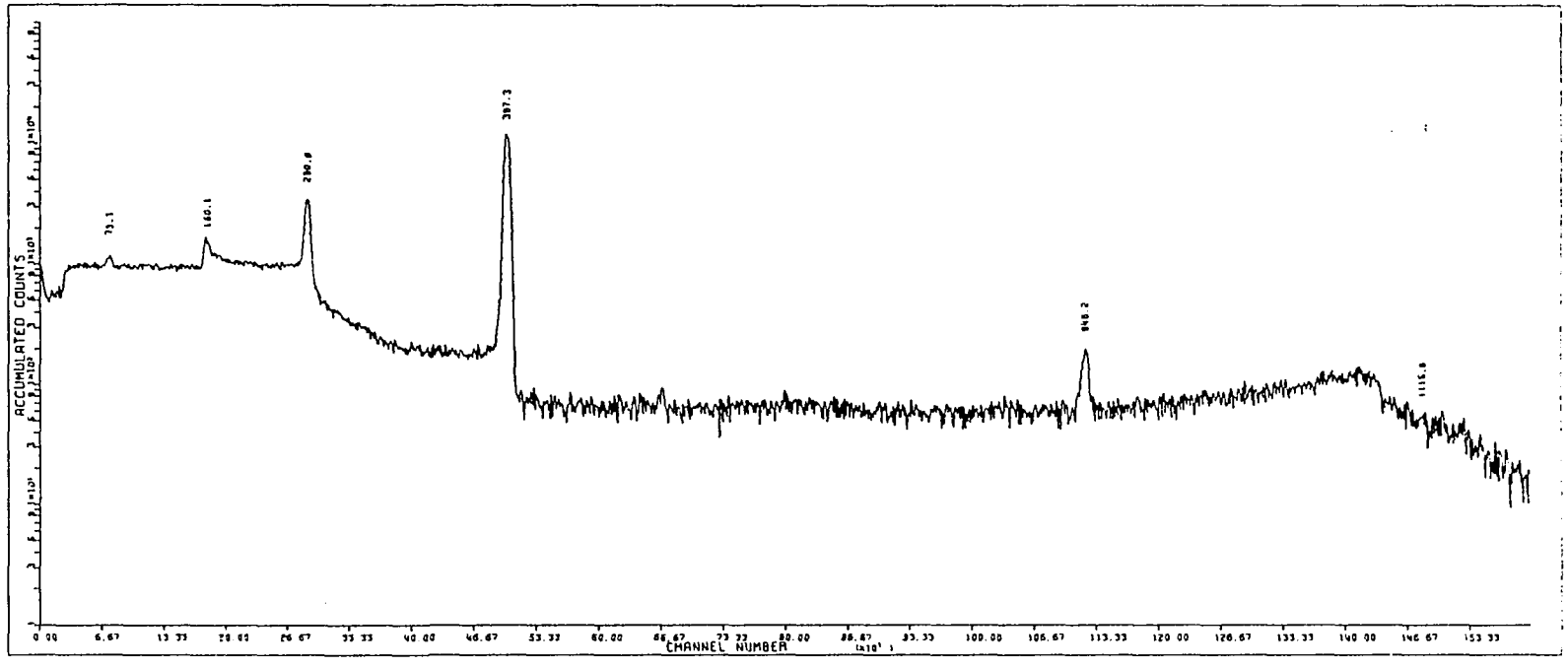

Figure E-4. $Sr(NO_3)_2$, normally abundant, irradiated with thermal neutrons

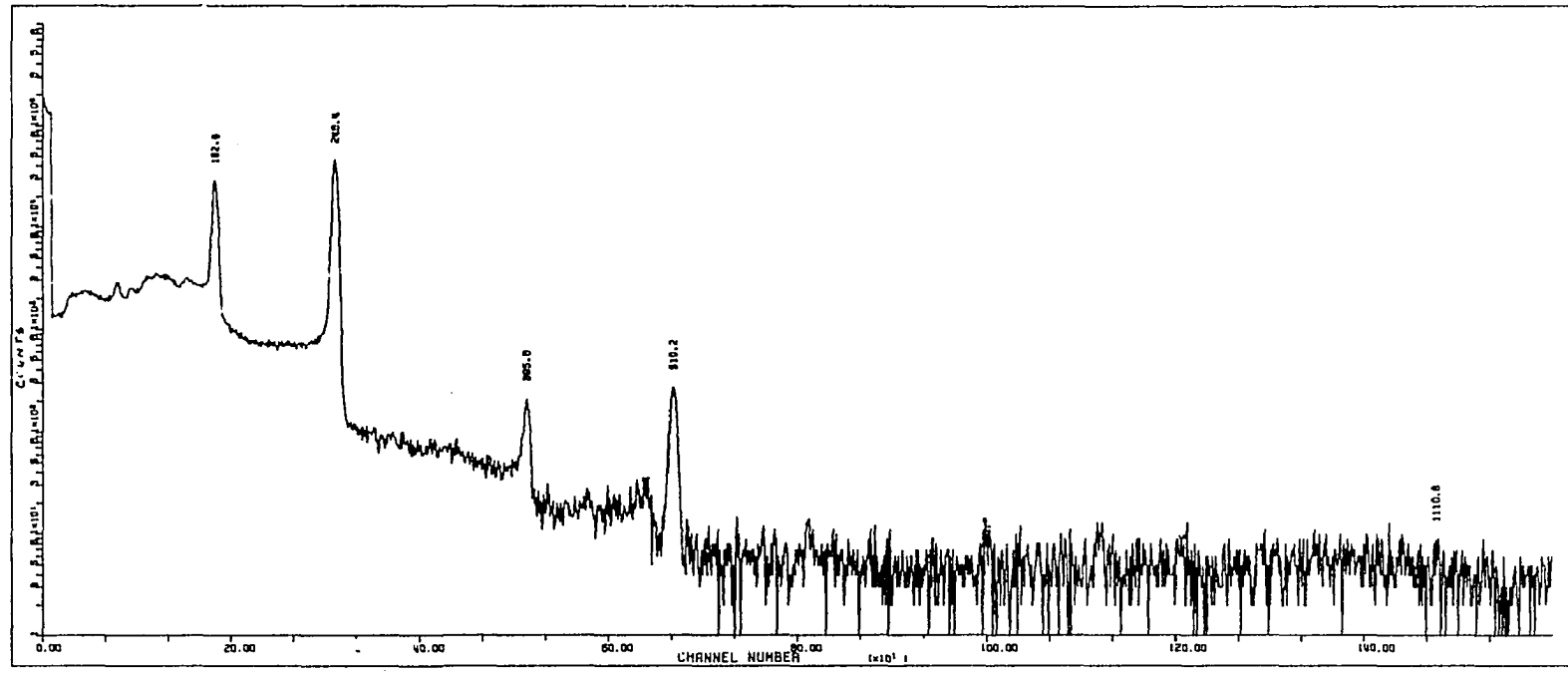

Figure E-5. CdO, 96% enriched in ^{111}Cd, irradiated with fission neutrons

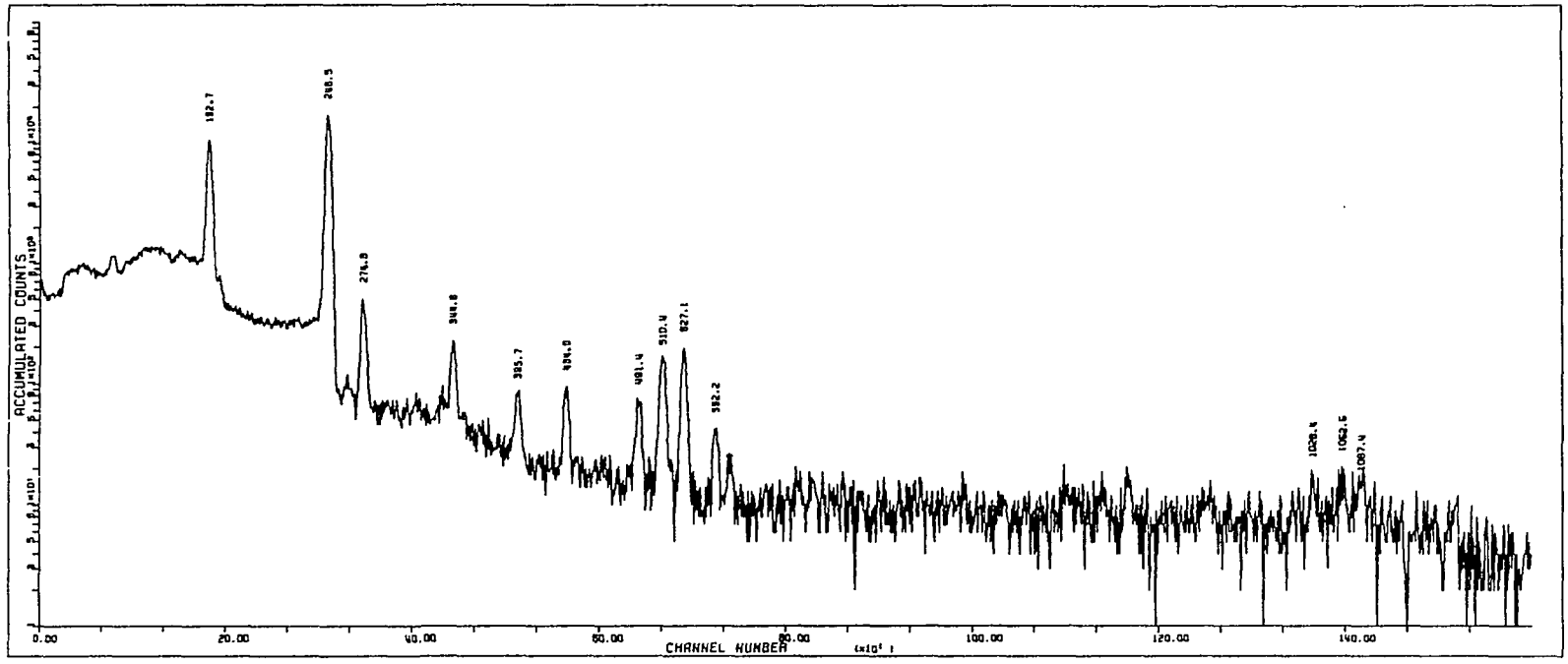

Figure E-6. CdO, normally abundant, irradiated with fission neutrons

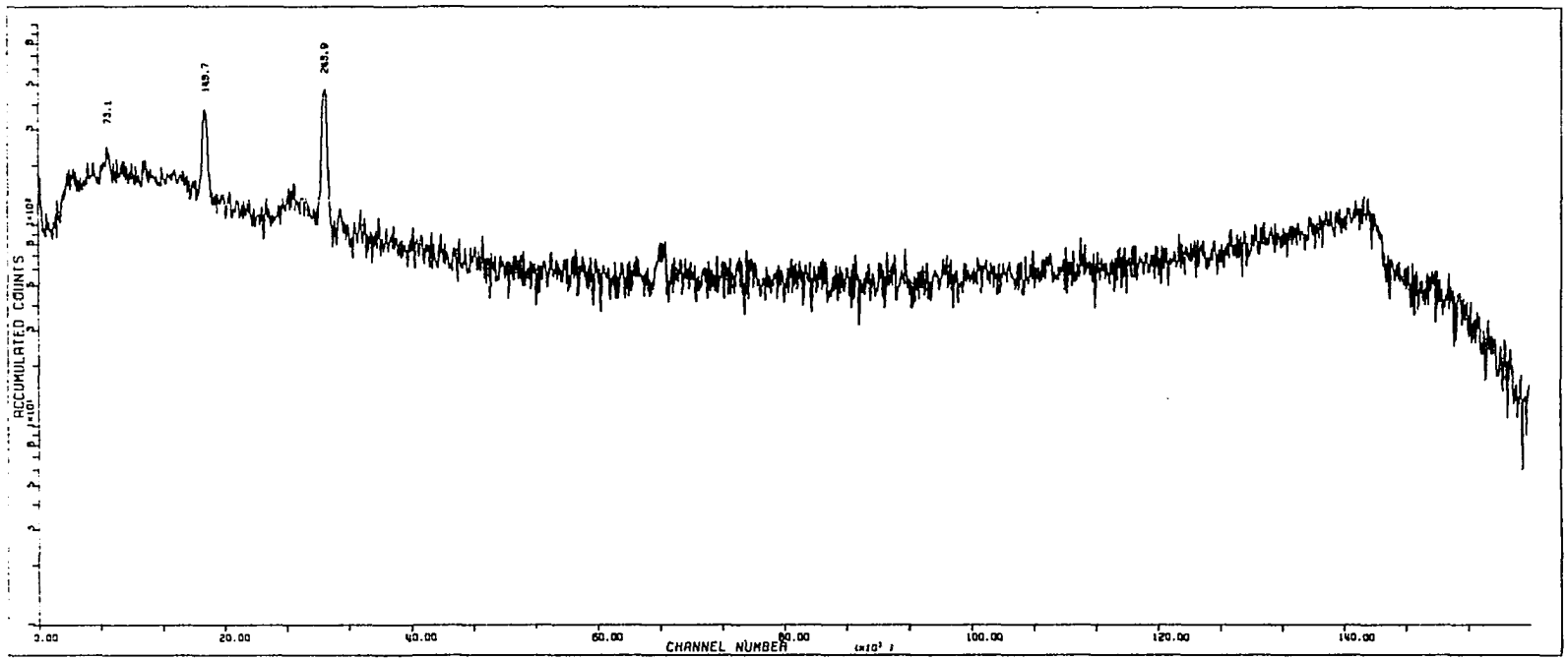

Figure E-7. CdO, 96% enriched in ^{111}Cd, irradiated with thermal neutrons

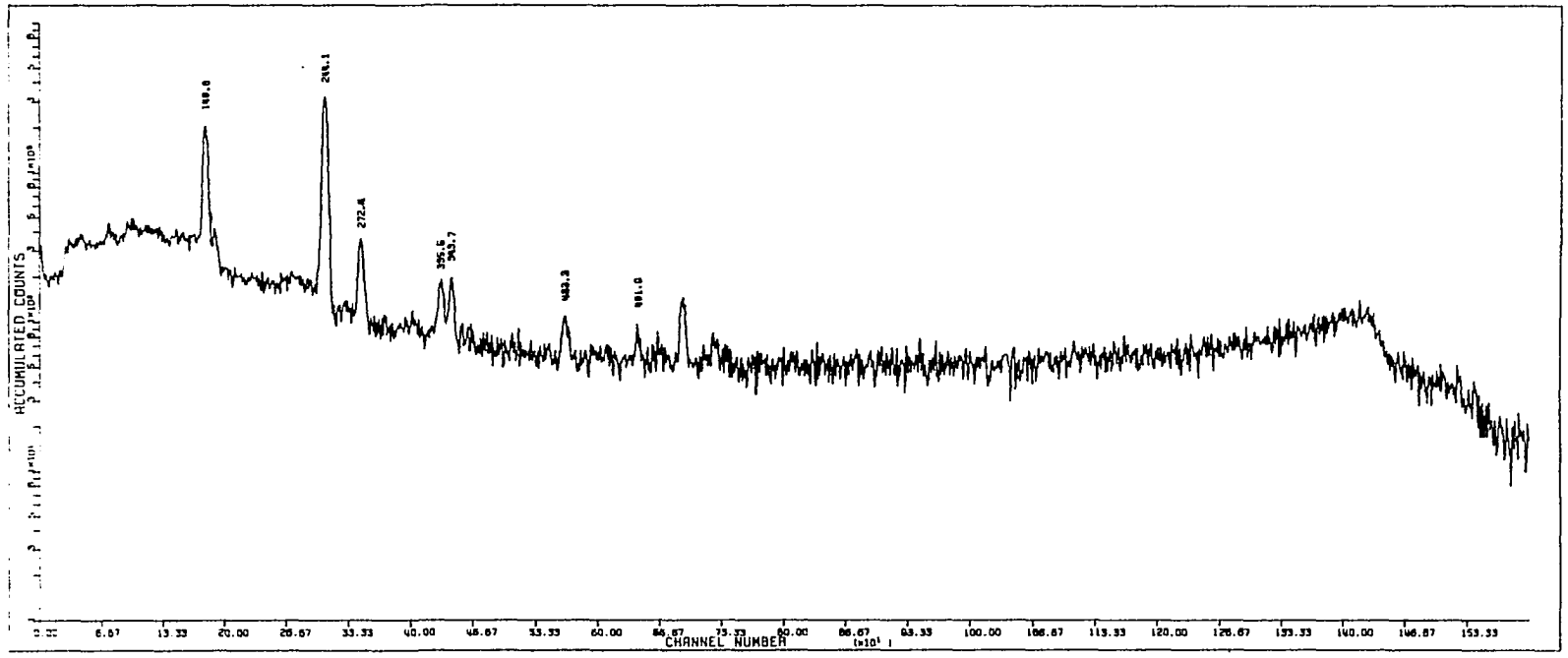

Figure E-8. CdO, normally abundant, irradiated with thermal neutrons

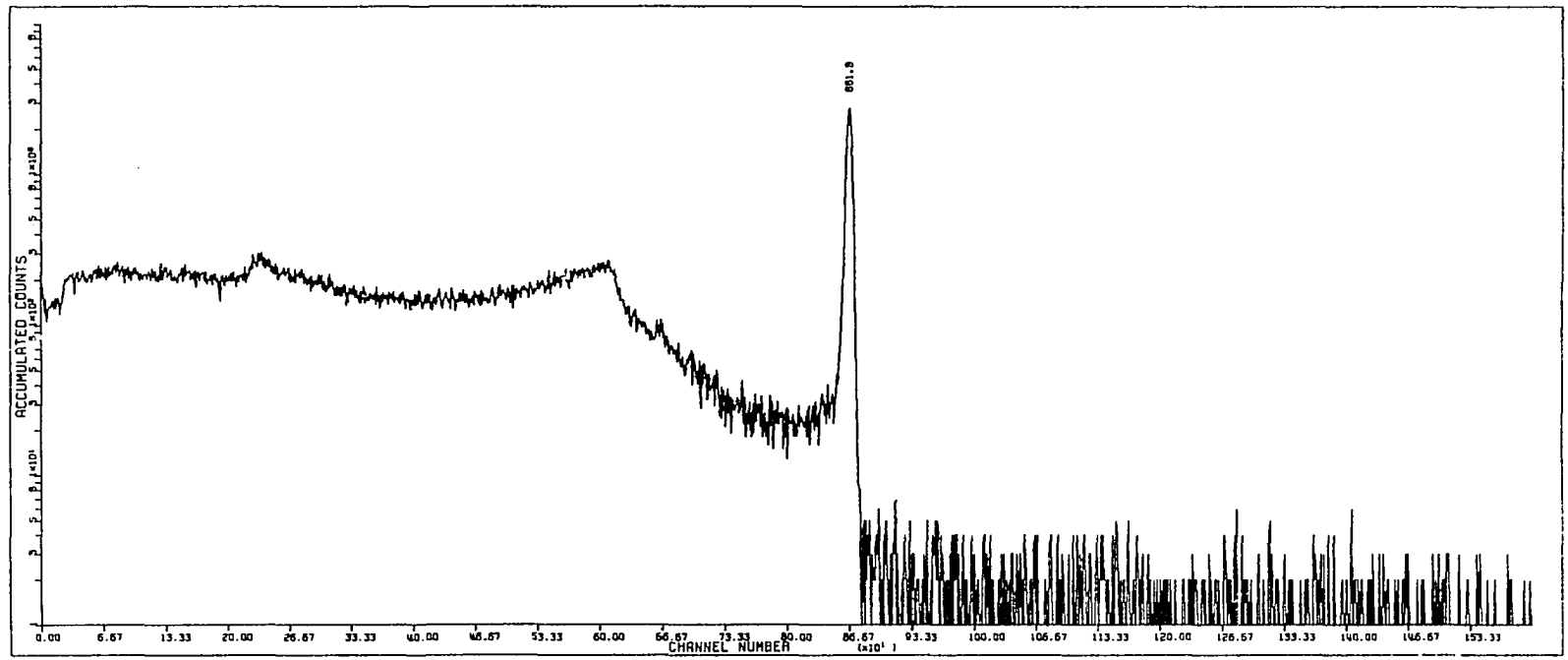

Figure E-9. $Ba(NO_3)_2$, 90% enriched in ^{137}Ba, irradiated with fission neutrons

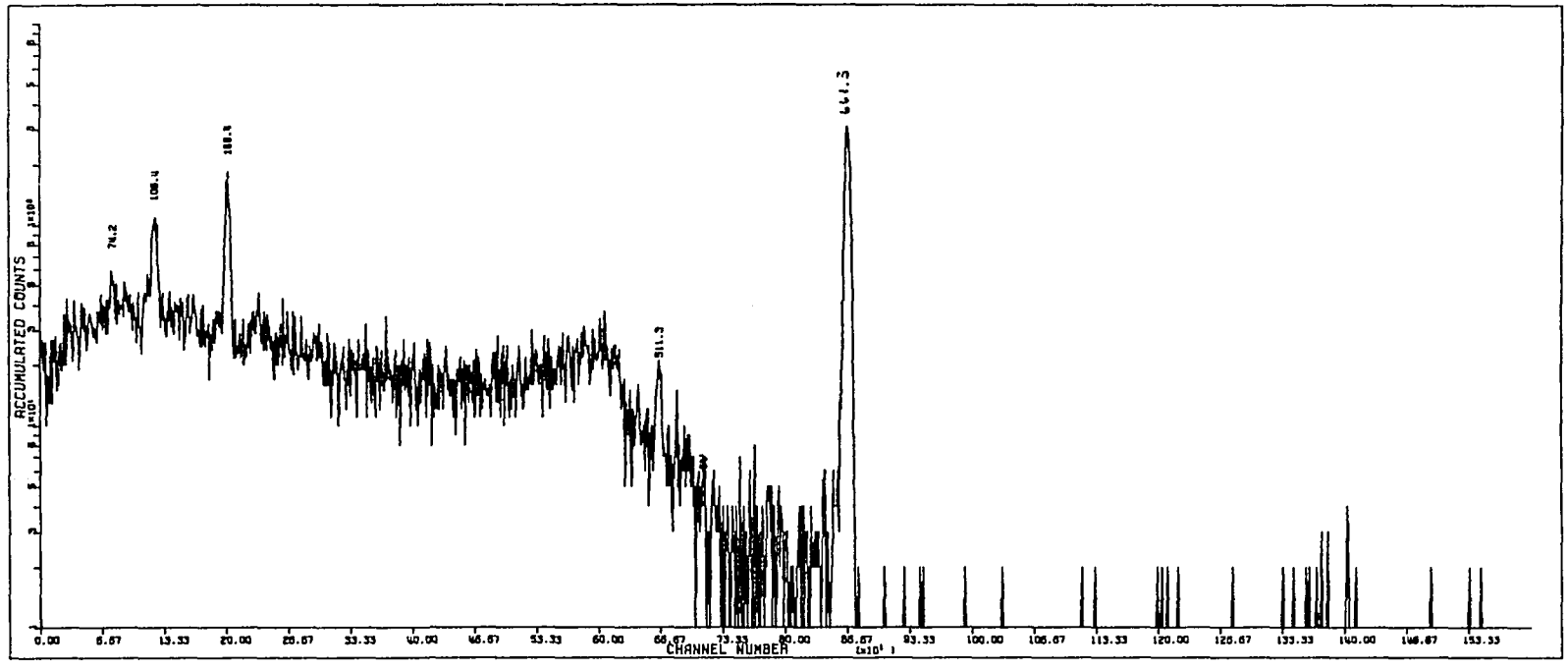

Figure E-10. $Ba(NO_3)_2$, normally abundant, irradiated with fission neutrons

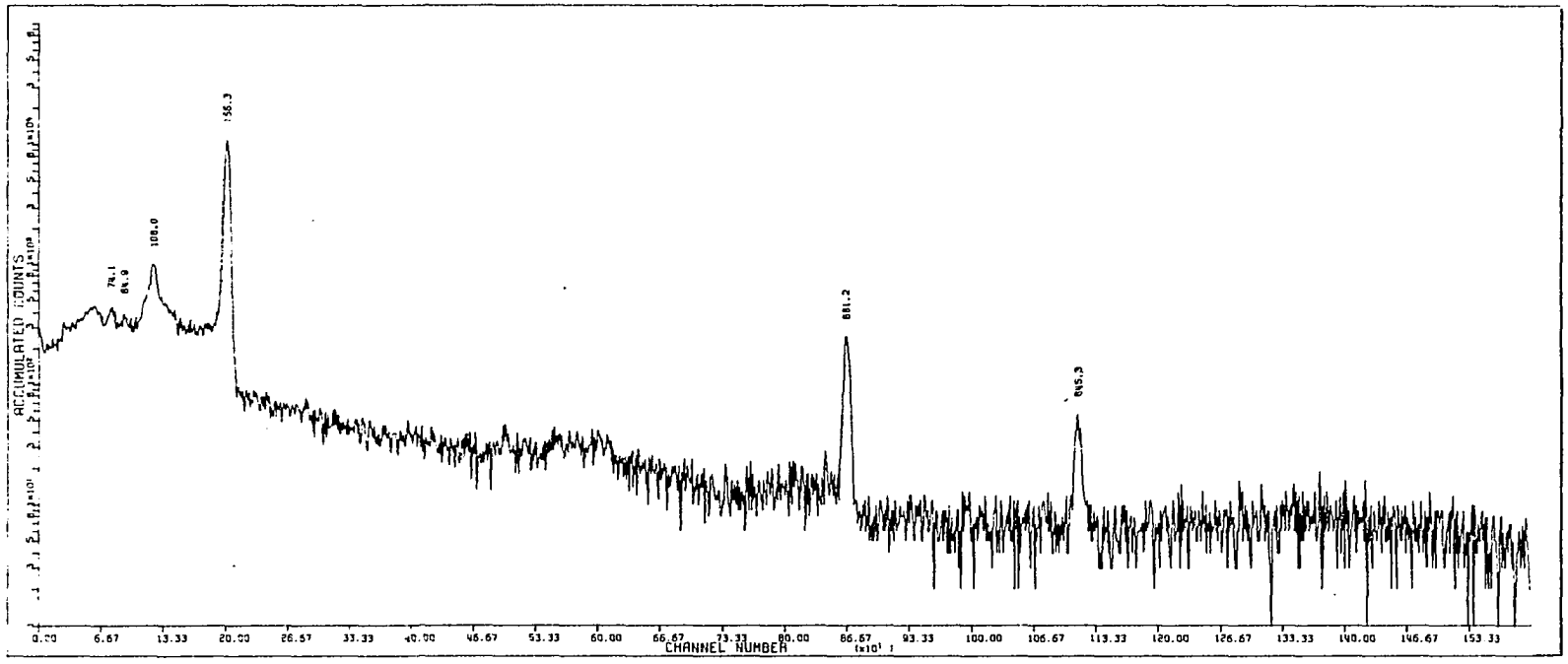

Figure E-11. $Ba(NO_3)_2$, 90% enriched in ^{137}Ba, irradiated with thermal neutrons

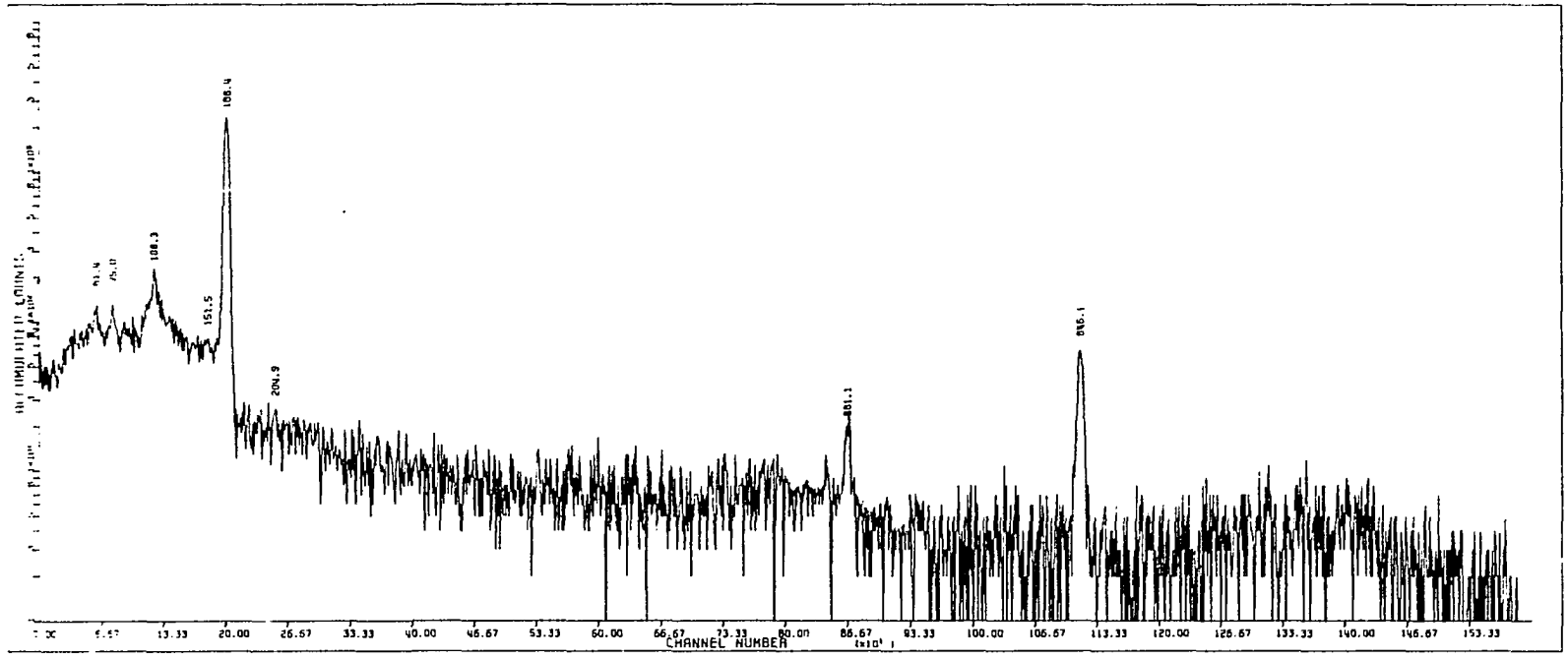

Figure E-12. $Ba(NO_3)_2$, normally abundant, irradiated with thermal neutrons

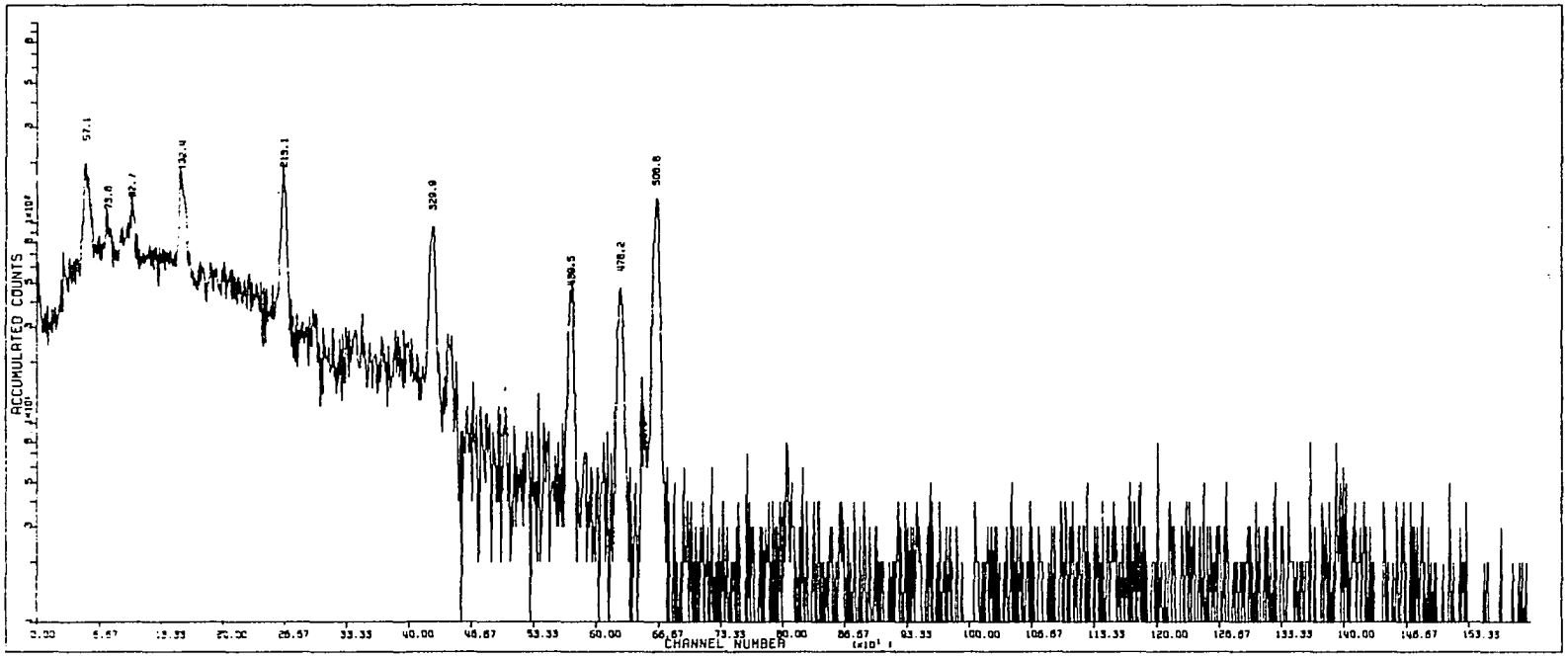

Figure E-13. HfO_2, 94% enriched in ^{180}Hf, irradiated with fission neutrons

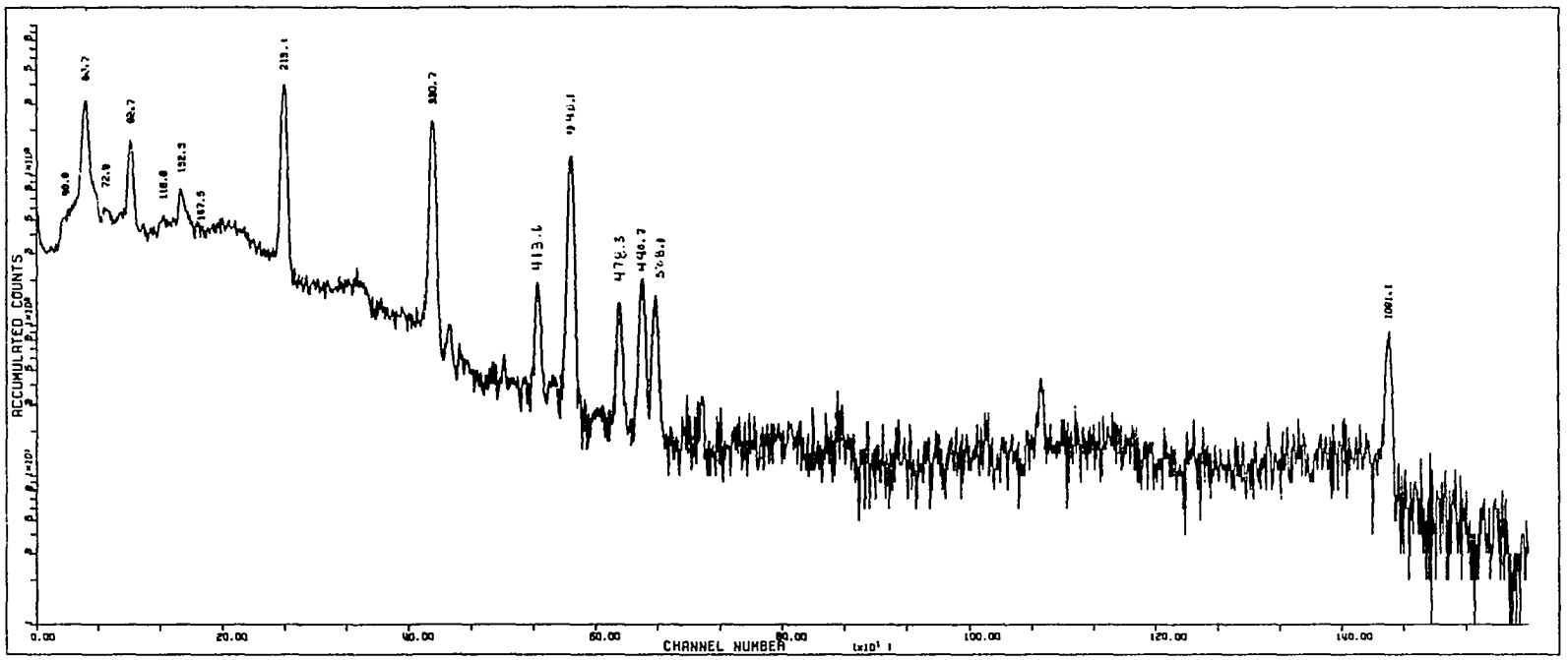

Figure E-14. HfO_2, normally abundant, irradiated with fission neutrons

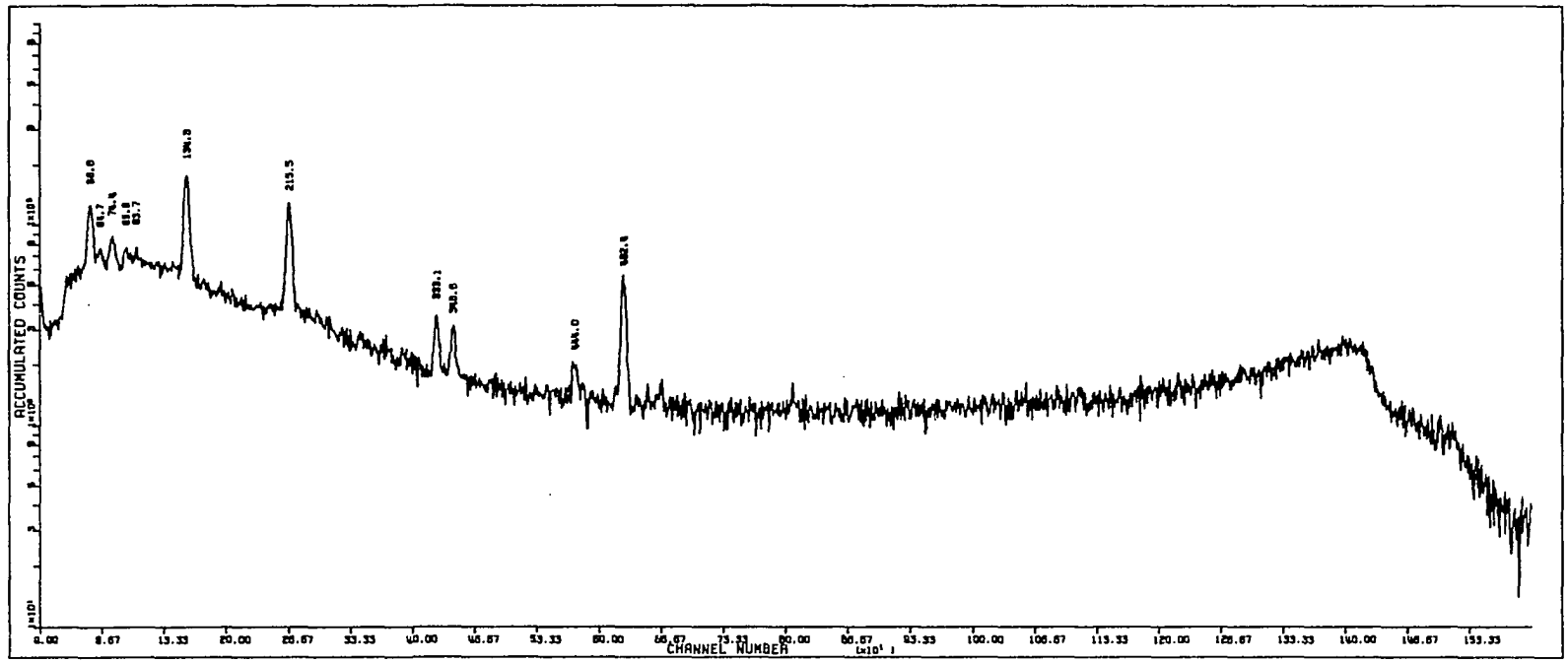

Figure E-15. HfO_2, 94% enriched in ^{180}Hf, irradiated with thermal neutrons

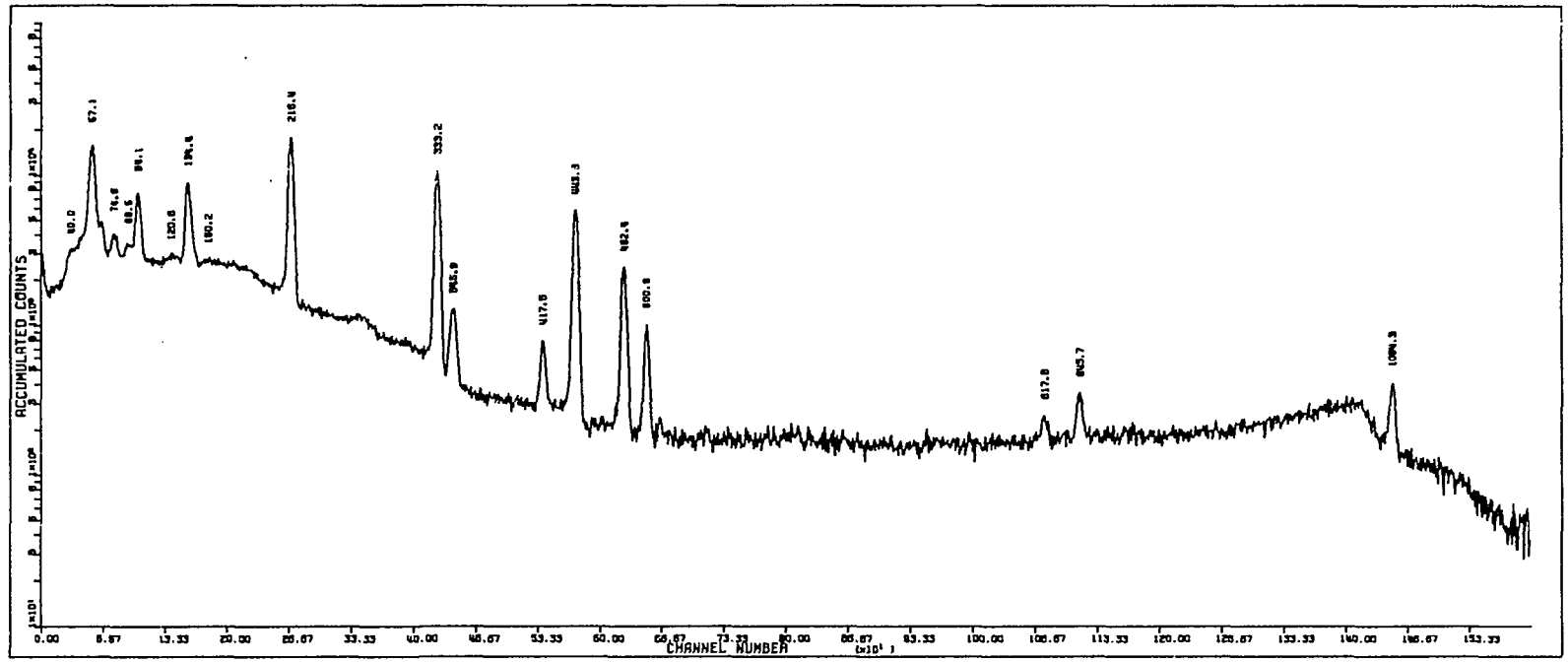

Figure E-16. HfO_2, normally abundant, irradiated with thermal neutrons

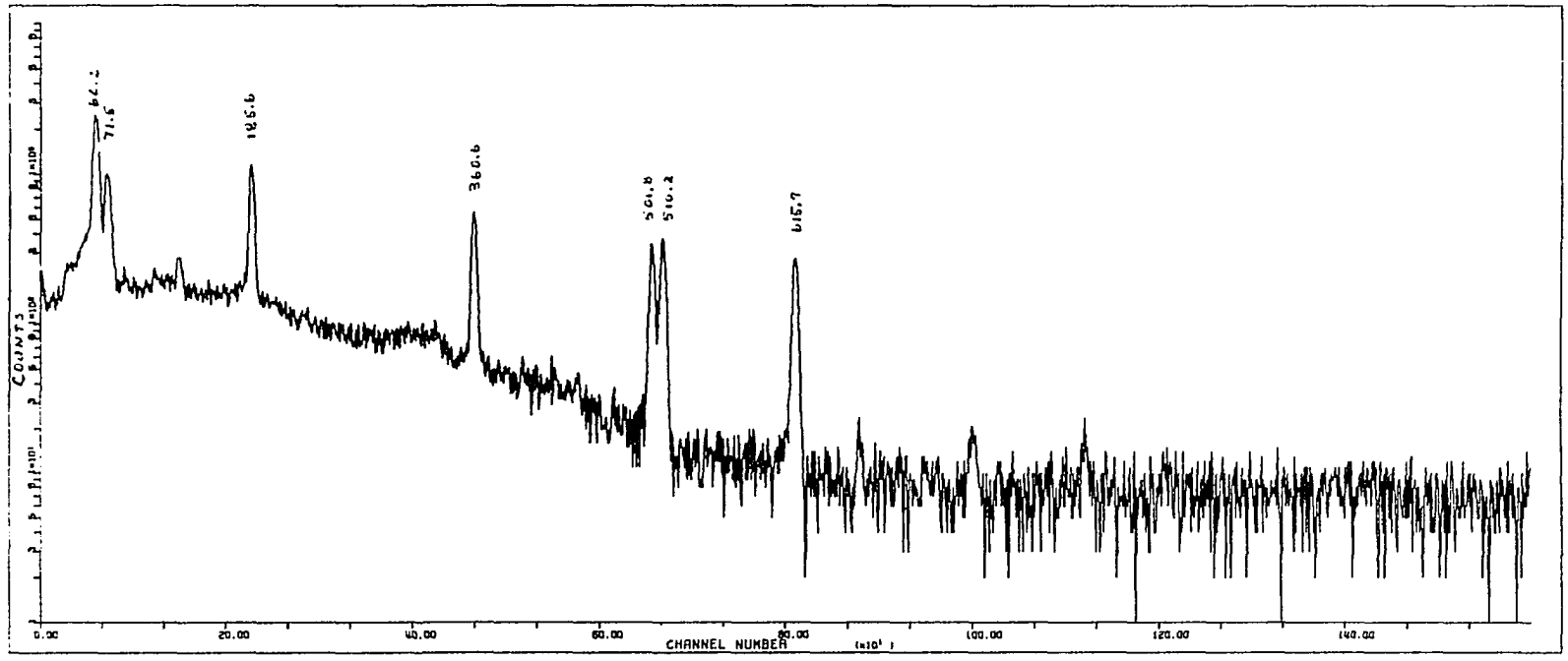

Figure E-17. Os, 95% enriched in ^{190}Os, irradiated with fission neutrons

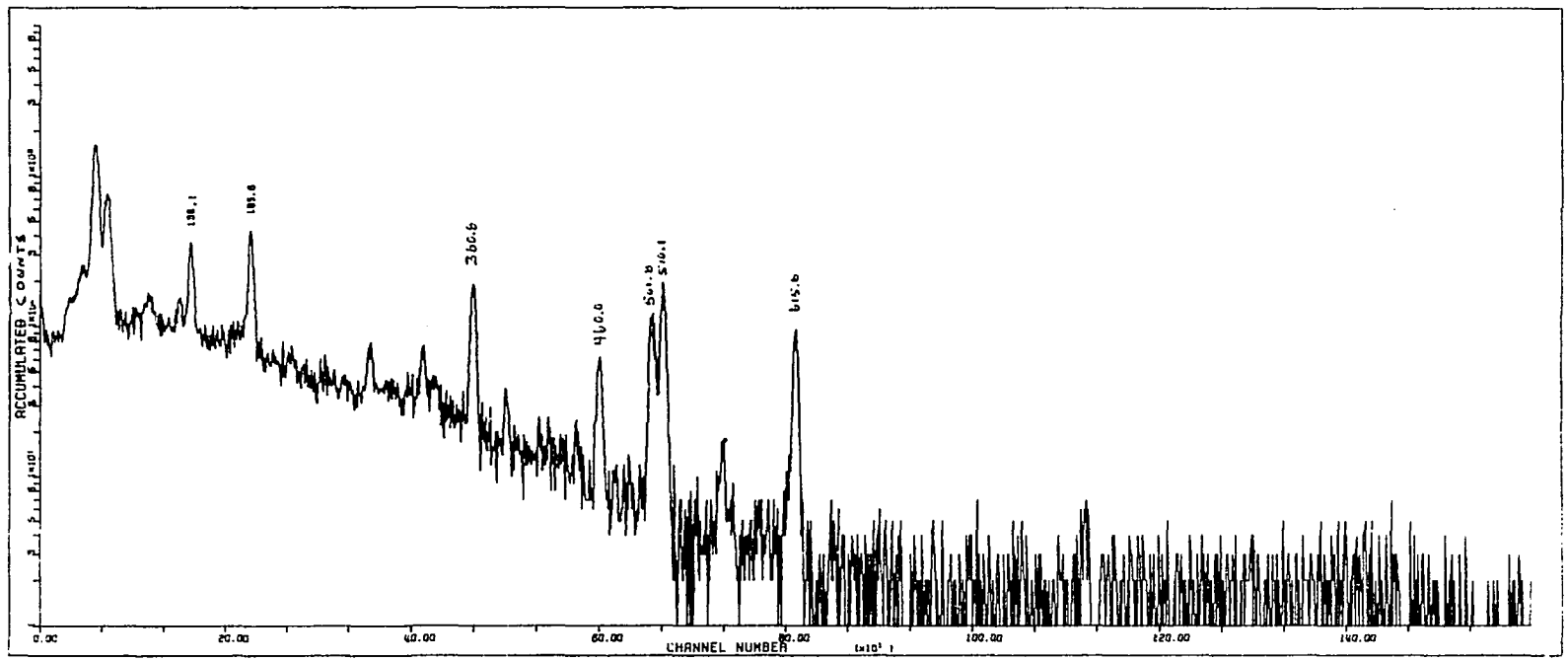

Figure E-18. Os, normally abundant, irradiated with fission neutrons

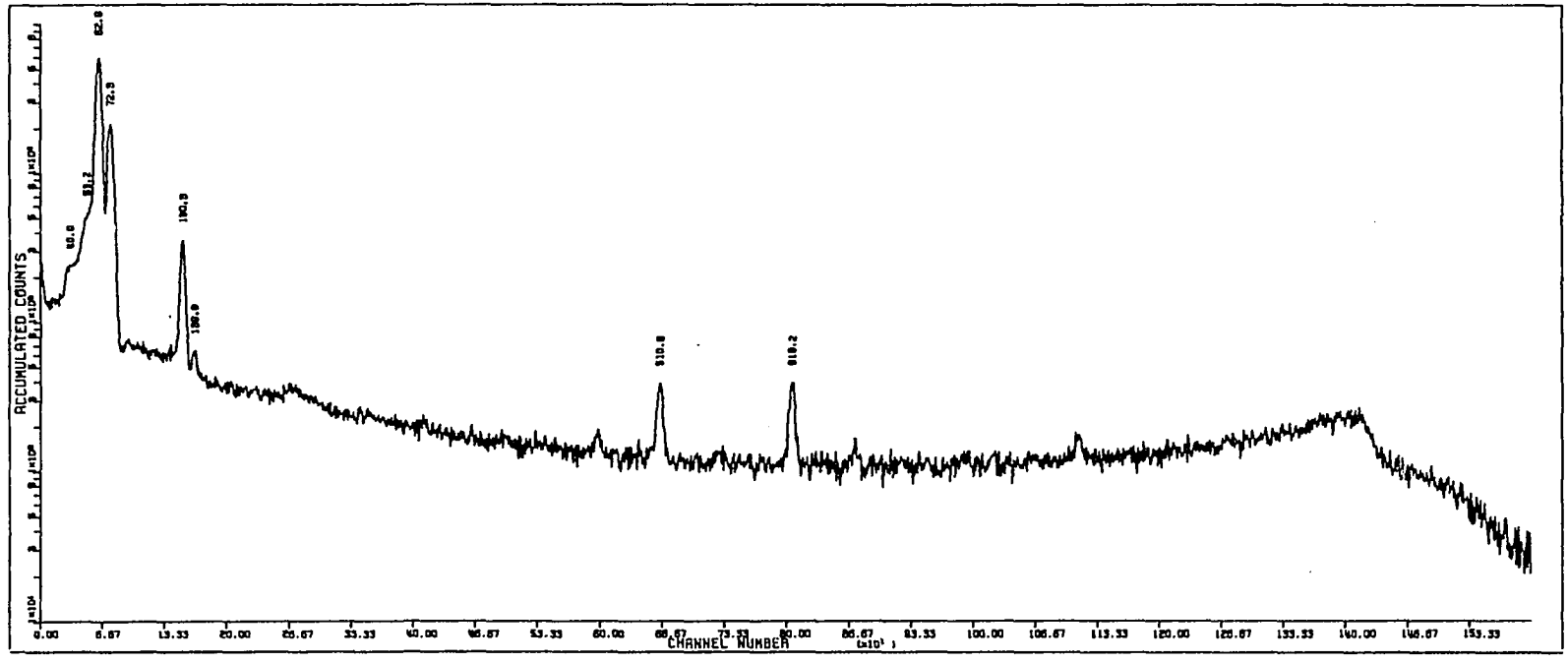

Figure E-19. Os, 95% enriched in ^{190}Os, irradiated with thermal neutrons

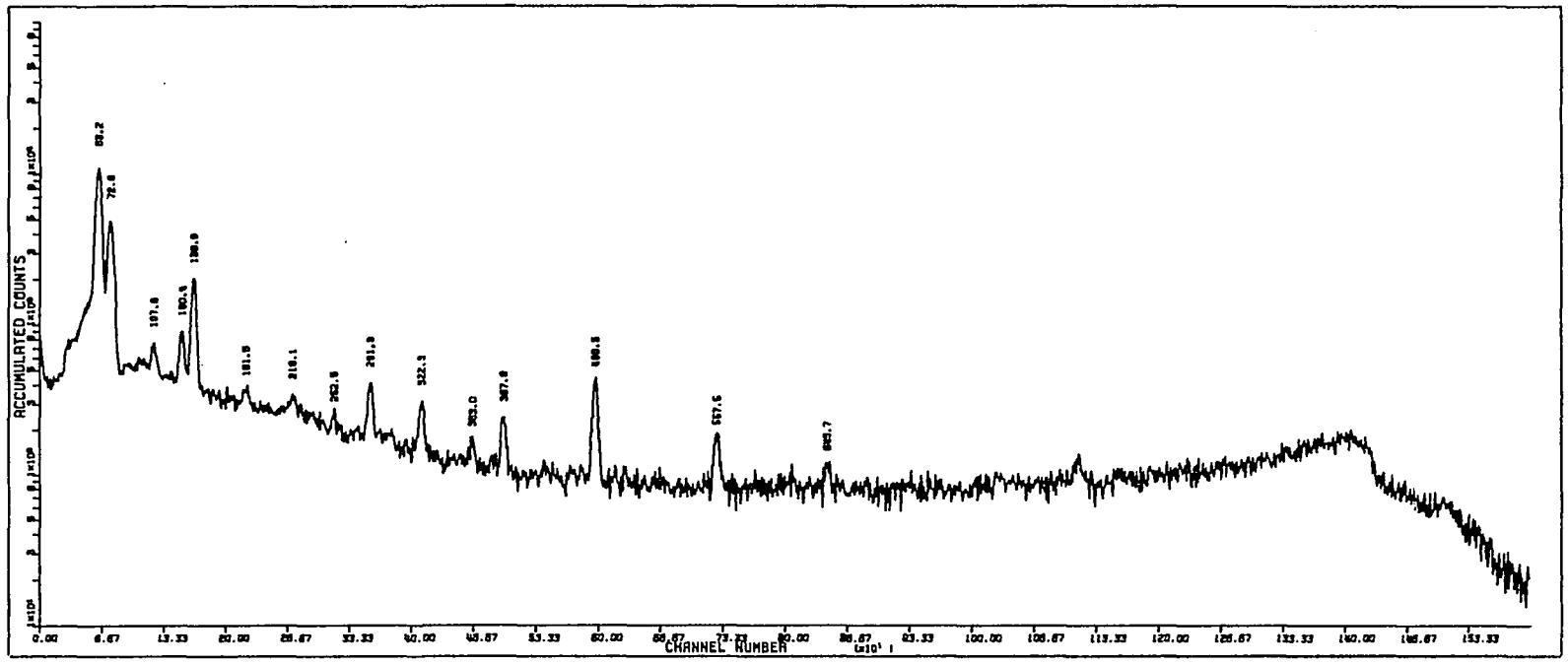

Figure E-20. Os, normally abundant, irradiated with thermal neutrons

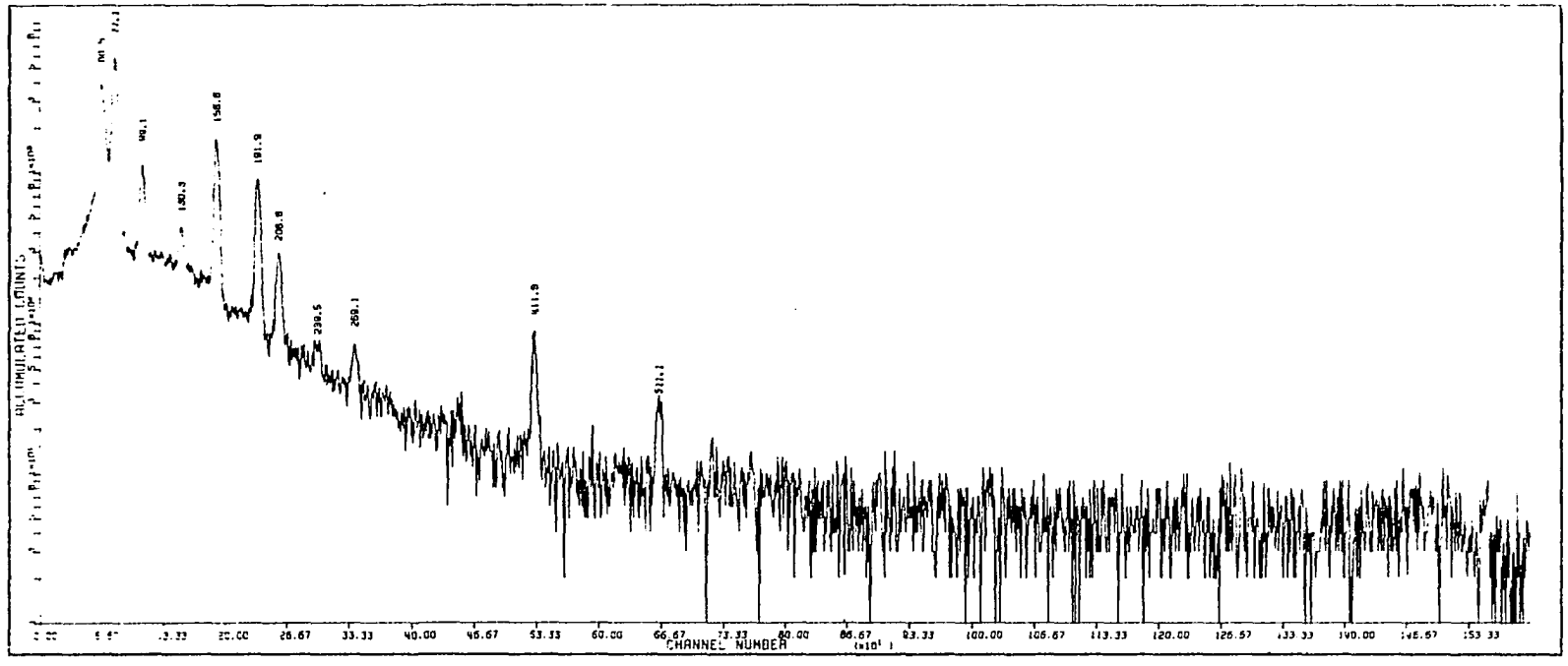

Figure E-21. Pt, 60% enriched in ^{195}Pt, irradiated with fission neutrons

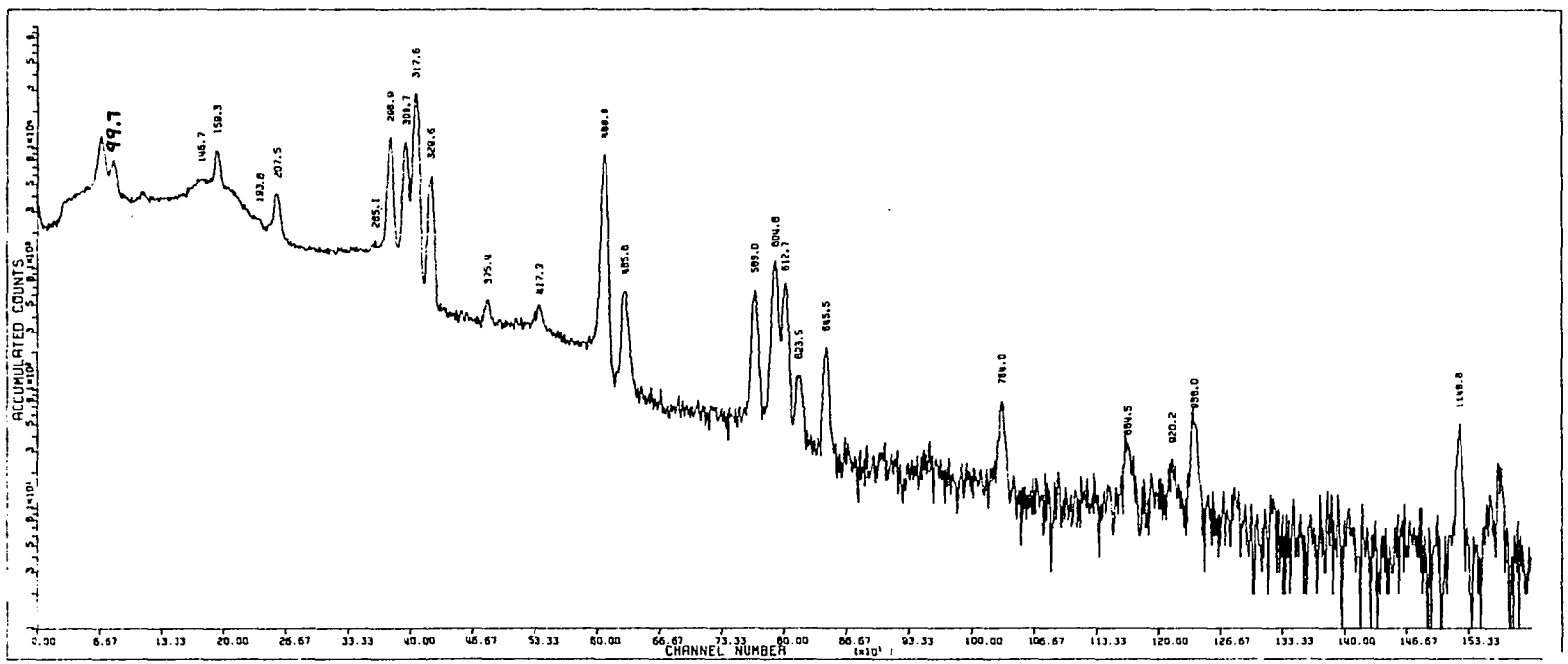

Figure E-22. Pt, normally abundant, irradiated with fission neutrons

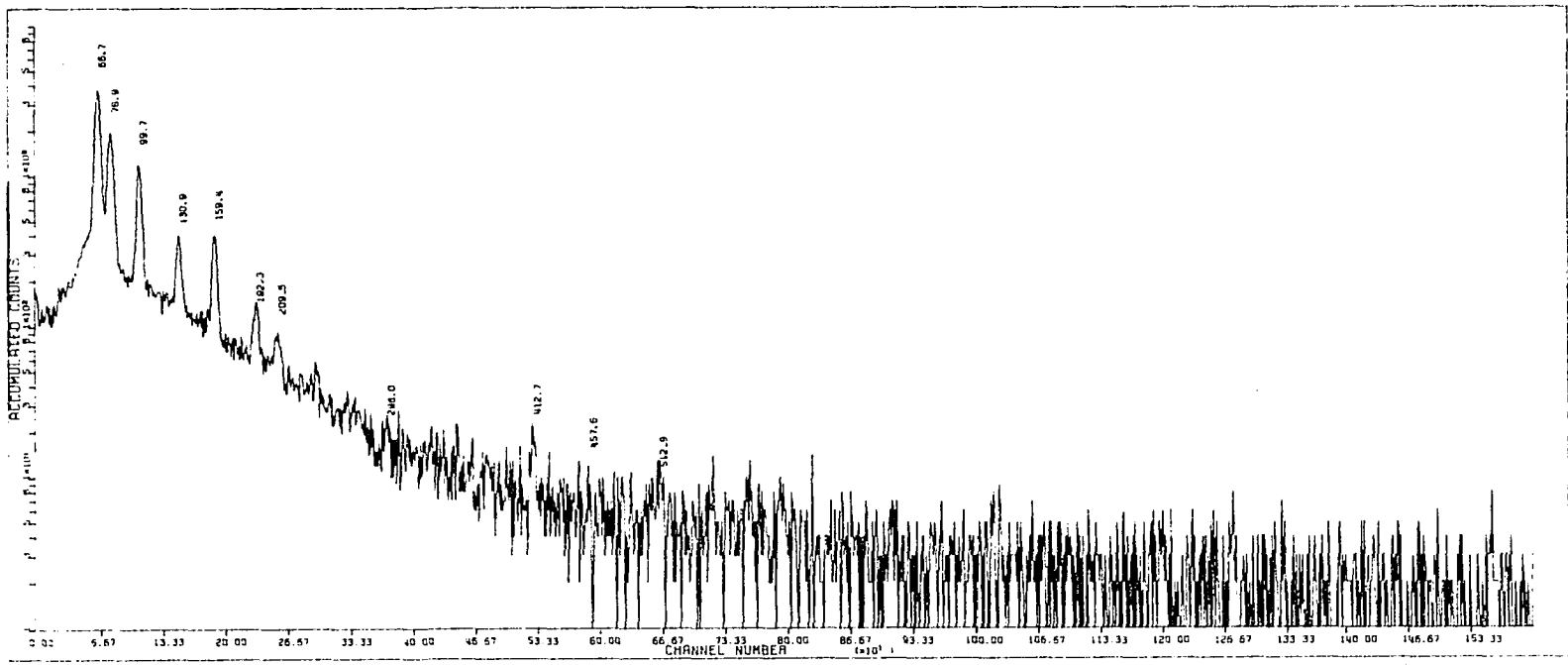

Figure E-23. Pt, 60% enriched in ^{195}Pt, irradiated with thermal neutrons

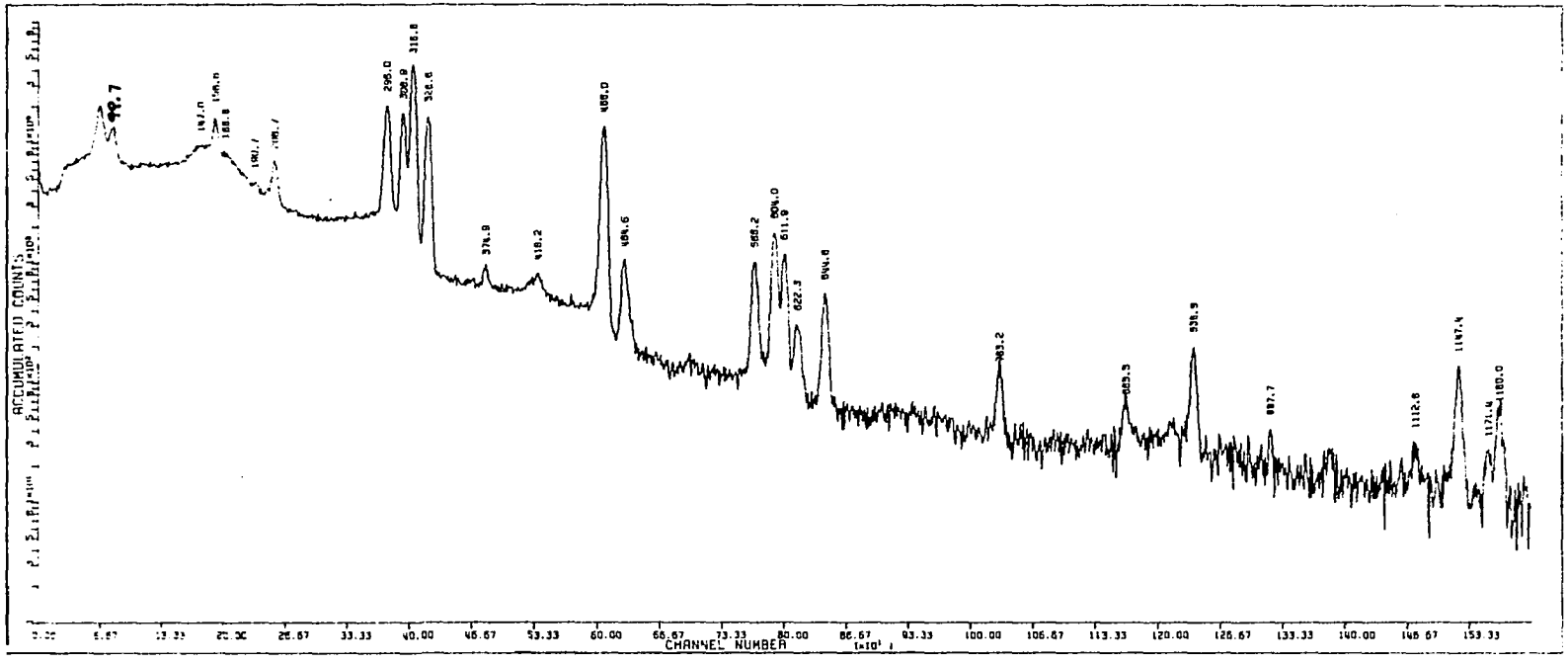

Figure E-24. Pt, normally abundant, irradiated with thermal neutrons

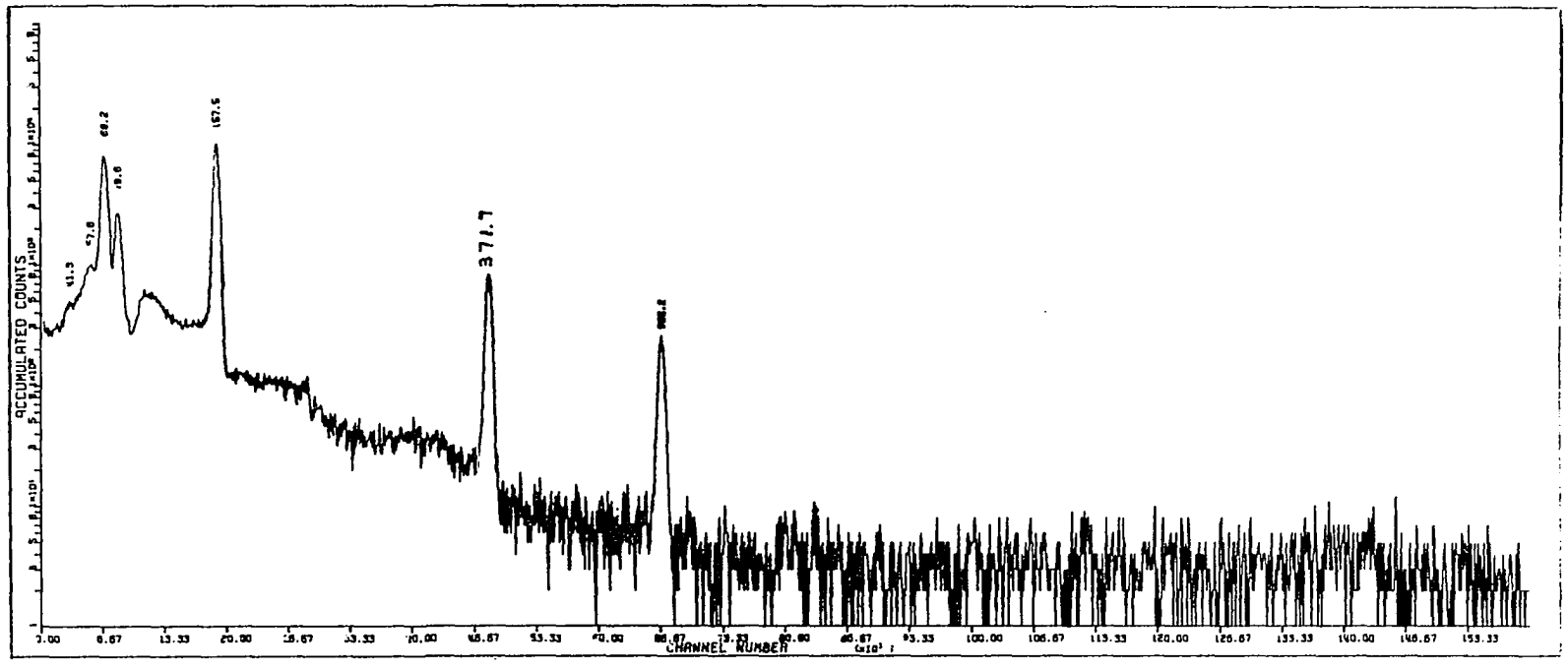

Figure E-25. HgO, 83% enriched in ^{199}Hg, irradiated with fission neutrons

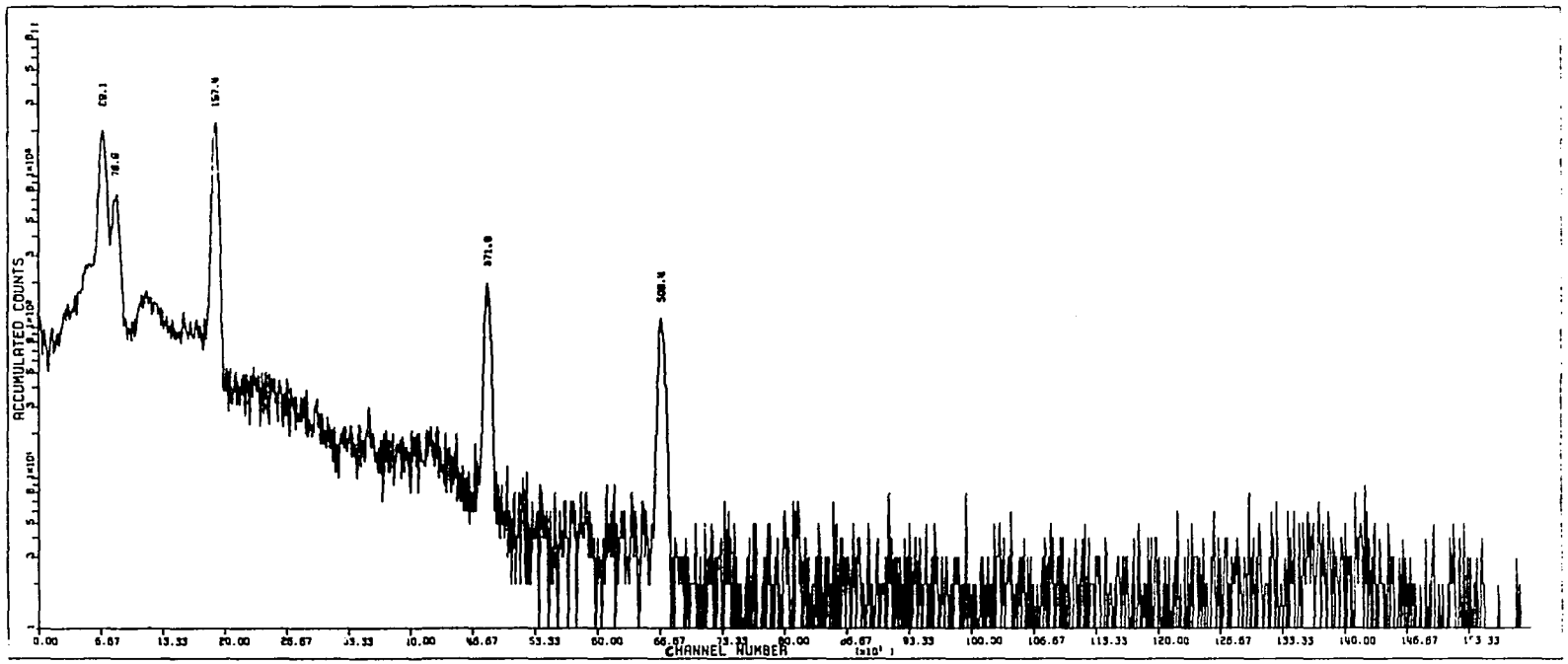

Figure E-26. HgO, normally abundant, irradiated with fission neutrons

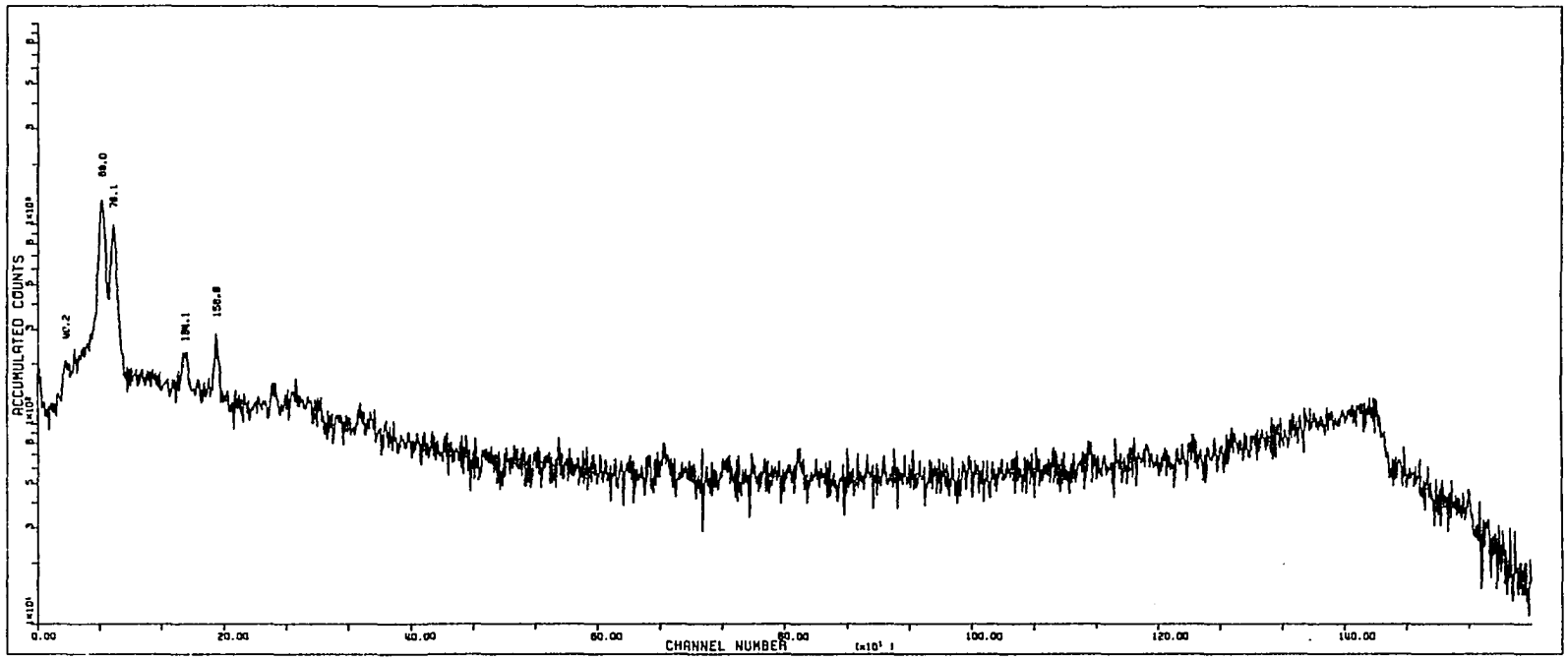

Figure E-27. HgO, 83% enriched in ^{199}Hg, irradiated with thermal neutrons

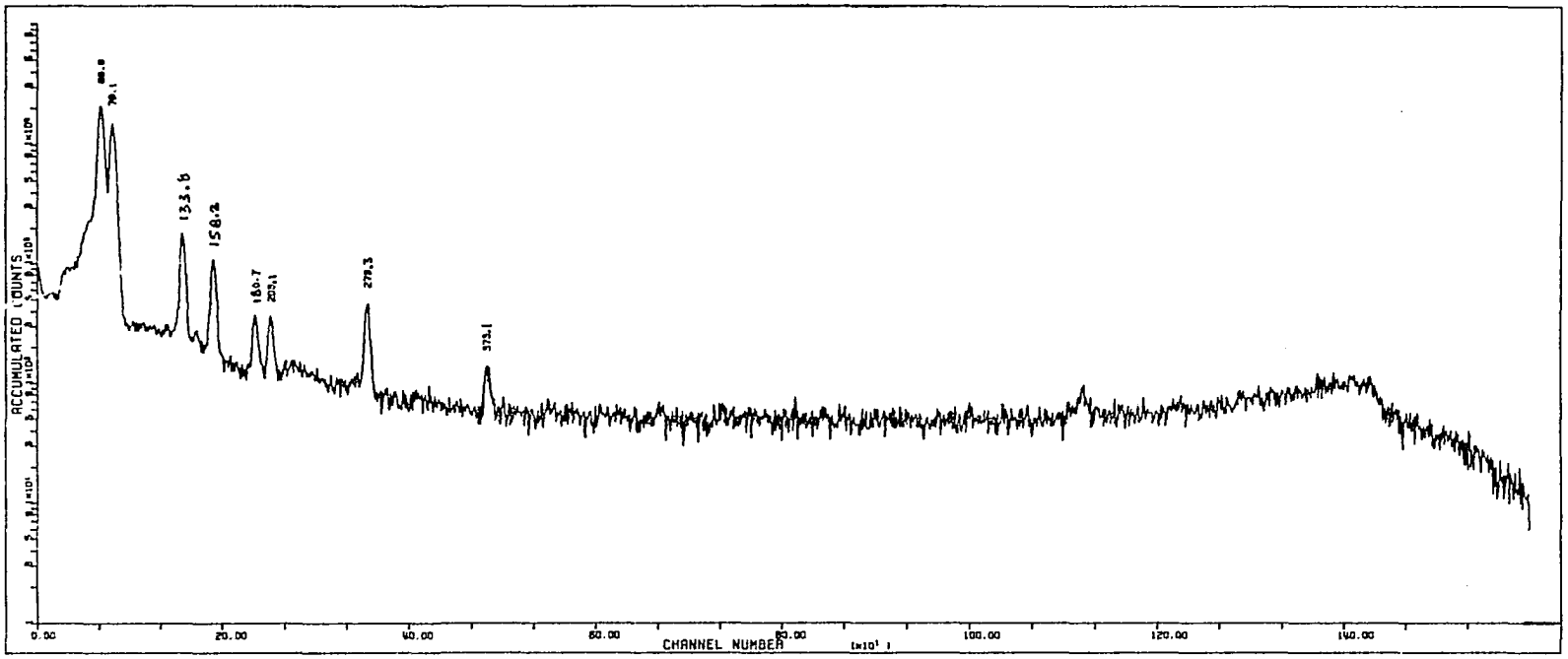

Figure E-28. HgO, normally abundant, irradiated with thermal neutrons

APPENDIX F. SPECTRA OF BARIUM AND STRONTIUM MIXTURES IRRADIATED WITH FISSION AND THERMAL NEUTRONS

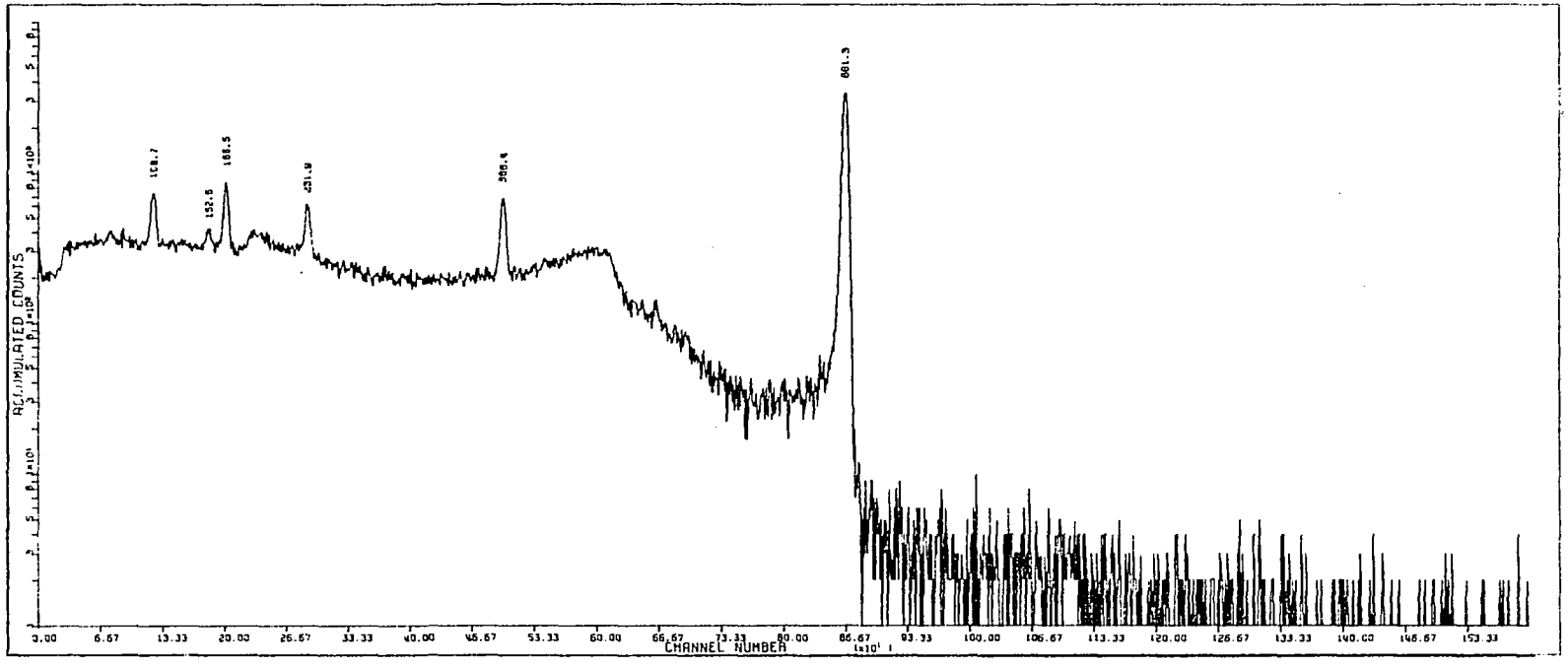

Figure F-1. Spectrum of a 1:1 weight ratio of Ba:Sr irradiated with fission neutrons

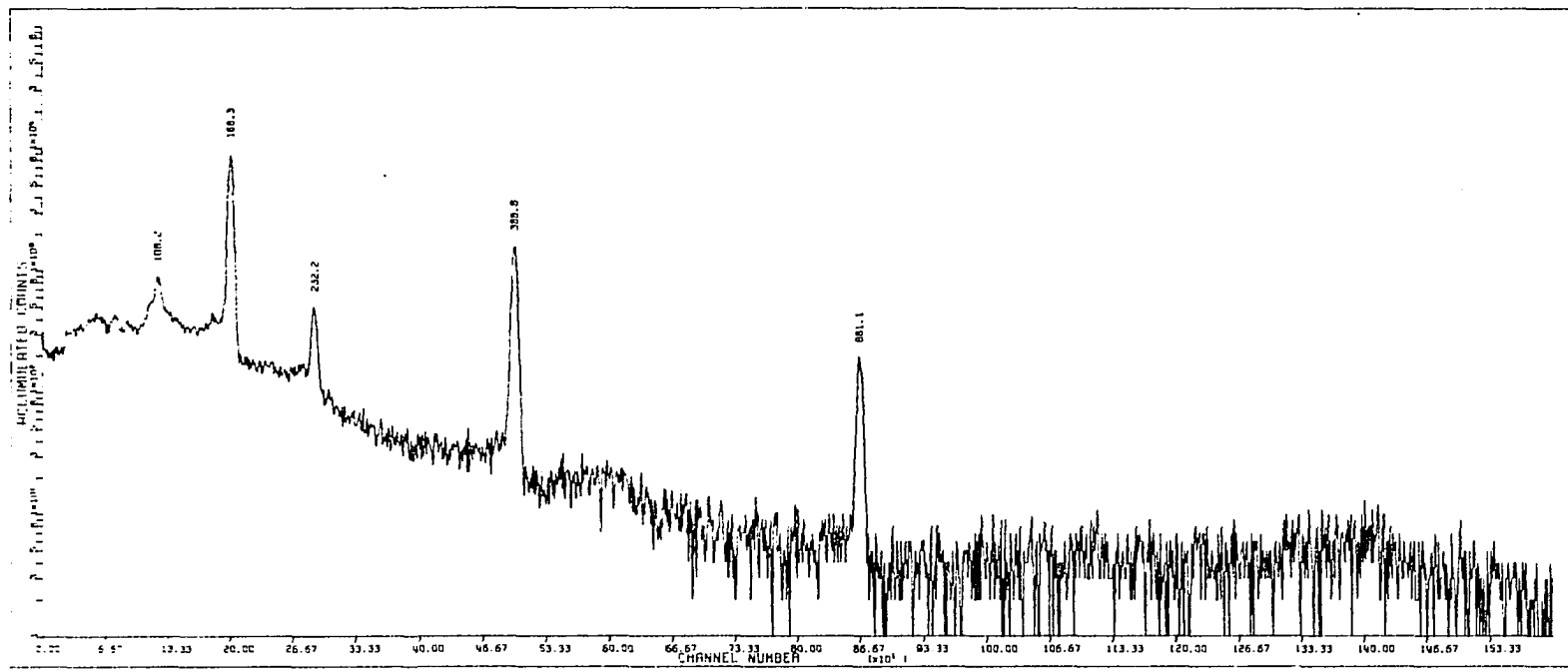

Figure F-2. Spectrum of a 1:1 weight ratio of Ba:Sr irradiated with thermal neutrons

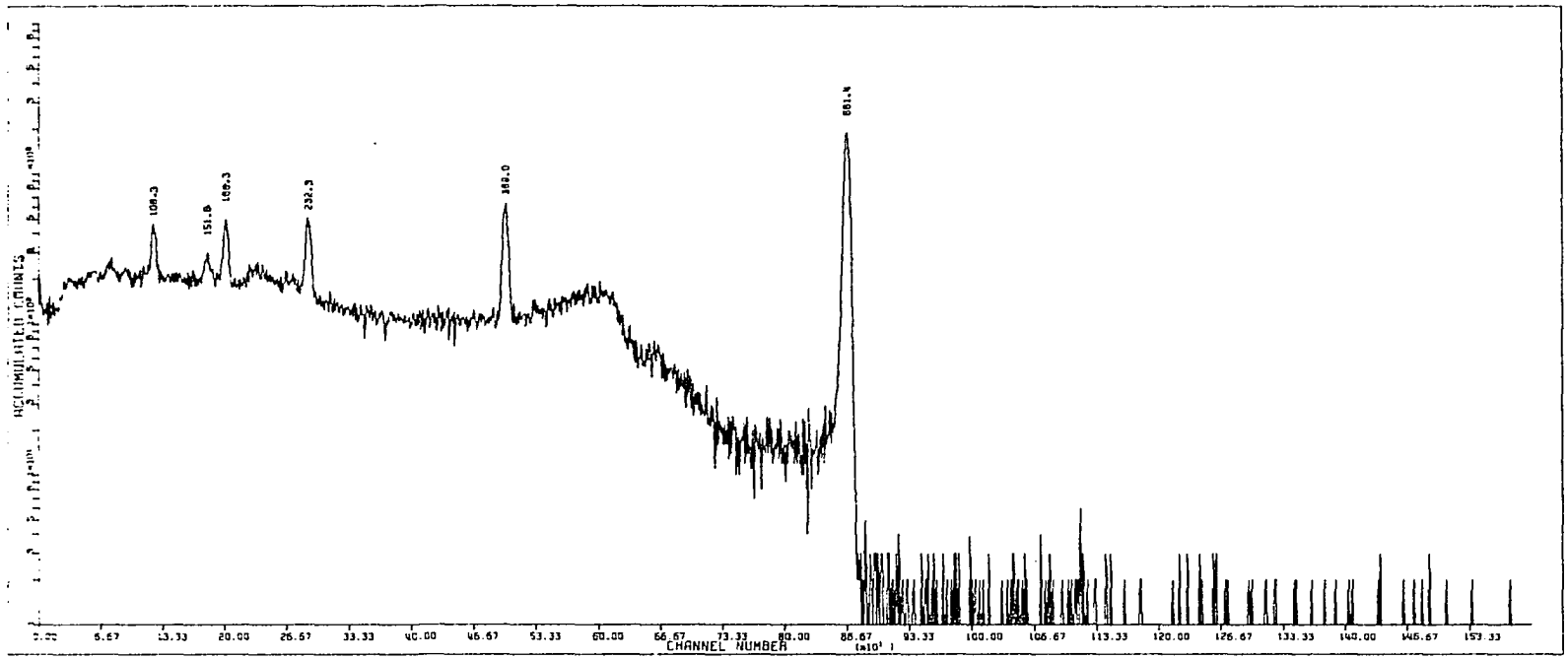

Figure F-3. Spectrum of a 1:2 weight ratio of Ba:Sr irradiated with fission neutrons

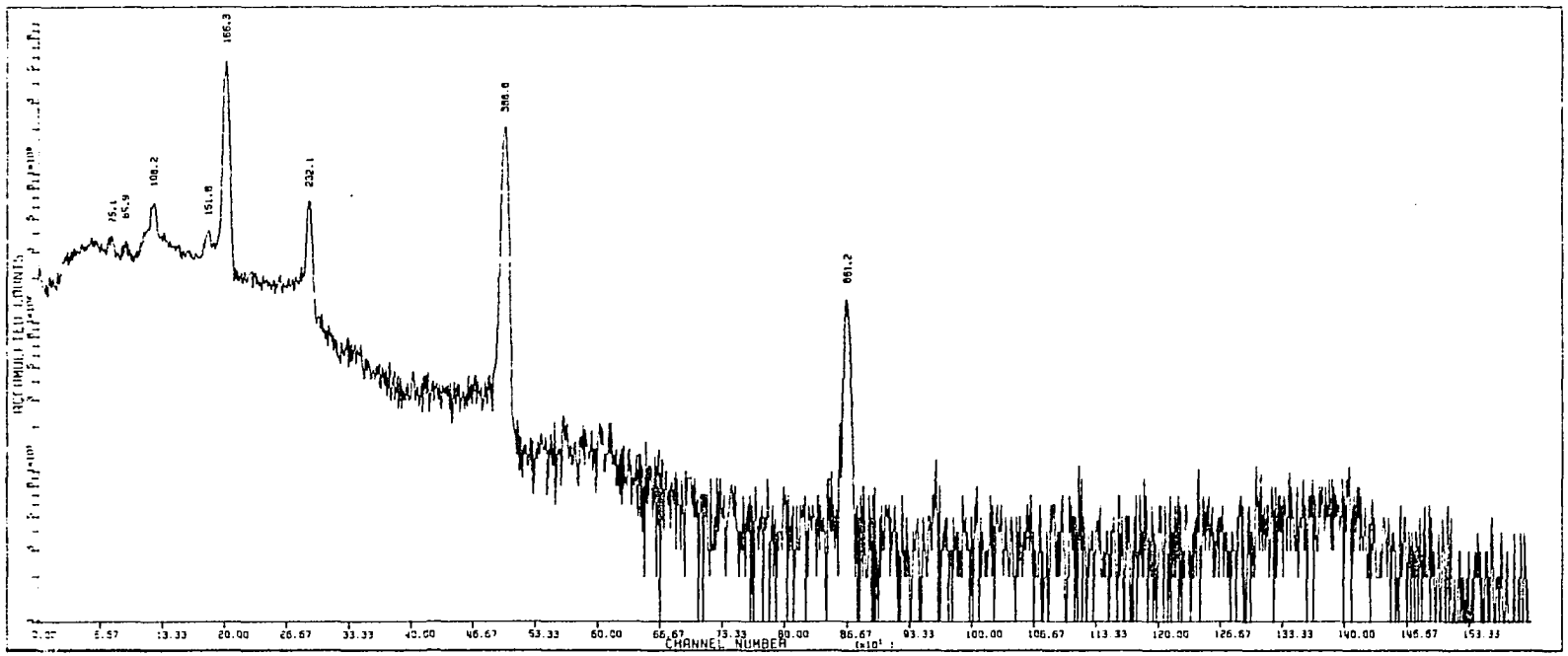

Figure F-4. Spectrum of a 1:2 weight ratio of Ba:Sr irradiated with thermal neutrons

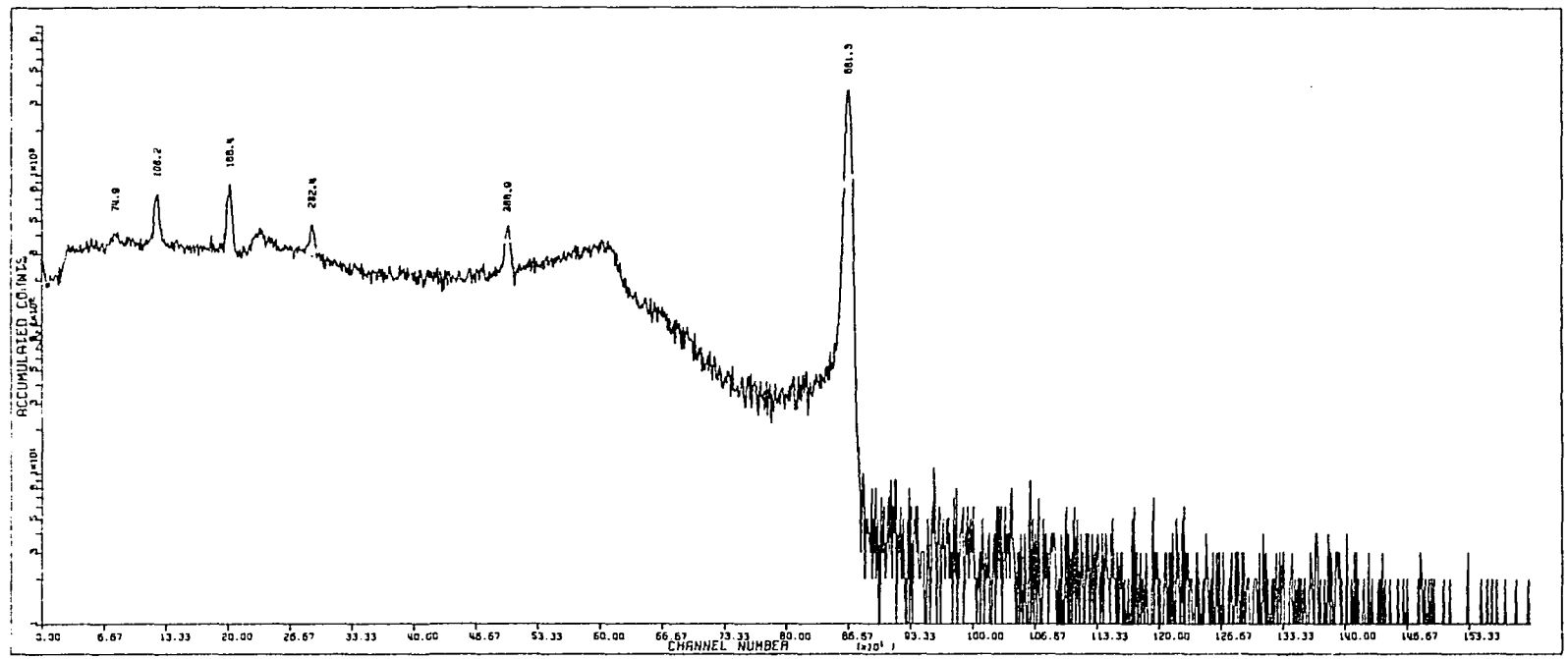

Figure F-5. Spectrum of a 2:1 weight ratio of Ba:Sr irradiated with fission neutrons

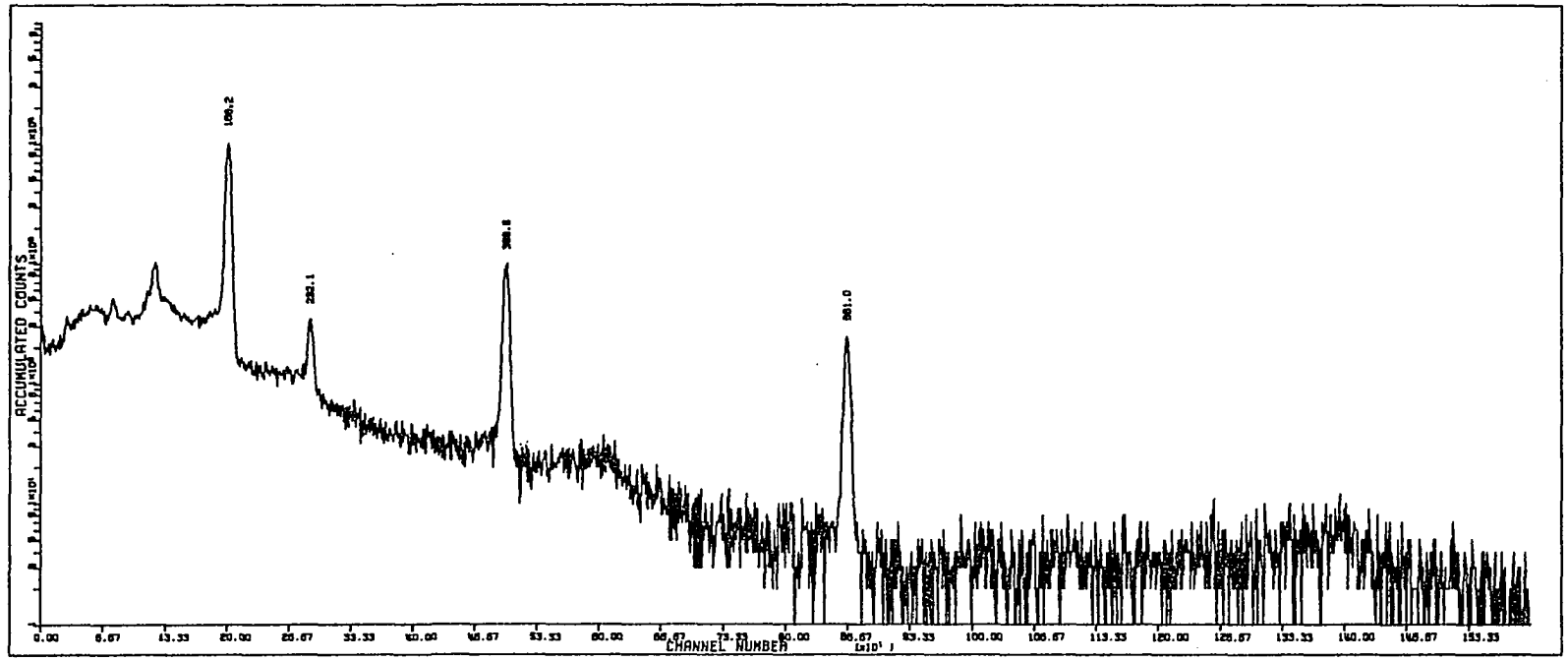

Figure F-6. Spectrum of a 2:1 weight ratio of Ba:Sr irradiated with thermal neutrons

APPENDIX G. SPECTRA OF CADMIUM AND MERCURY MIXTURES IRRADIATED WITH FISSION AND THERMAL NEUTRONS

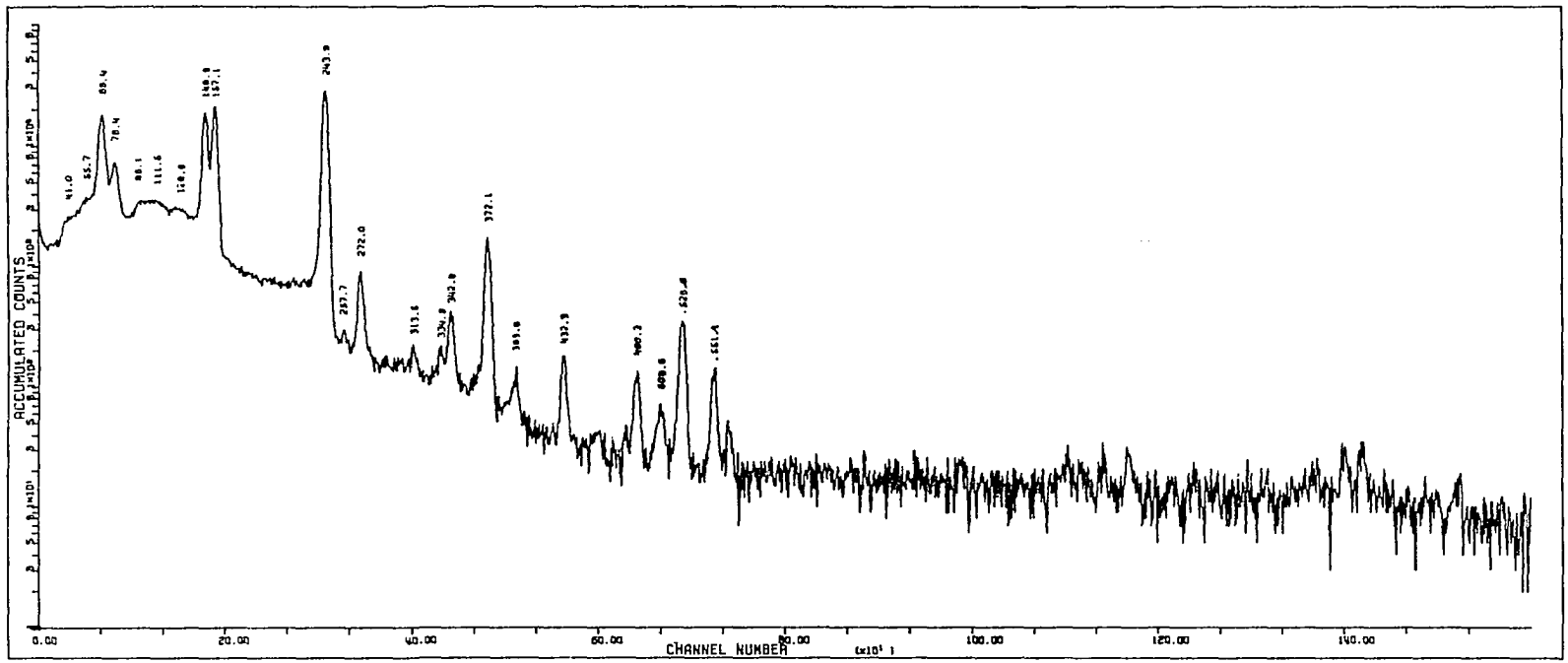

Figure G-1. Spectrum of a 1:1 weight ratio of Cd:Hg irradiated with fission neutrons

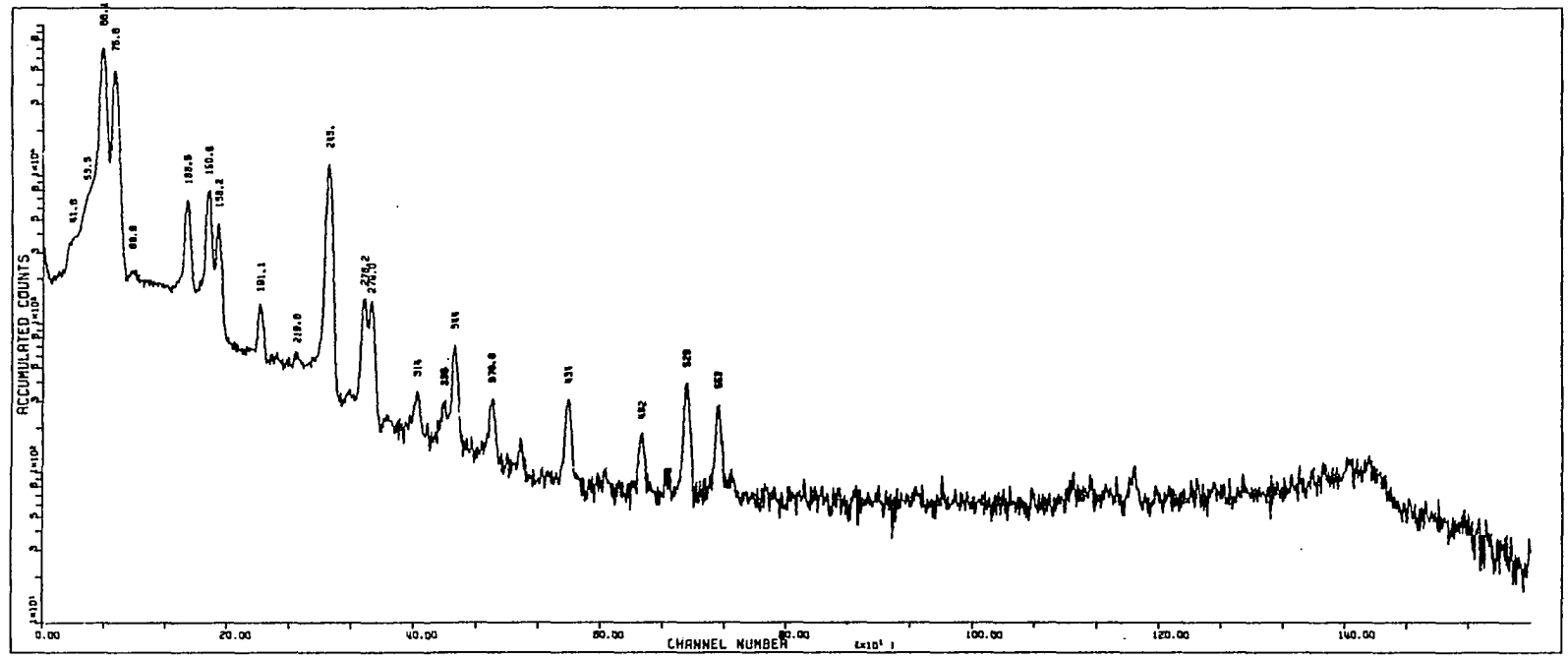

Figure G-2. Spectrum of a 1:1 weight ratio of Cd:Hg irradiated with thermal neutrons

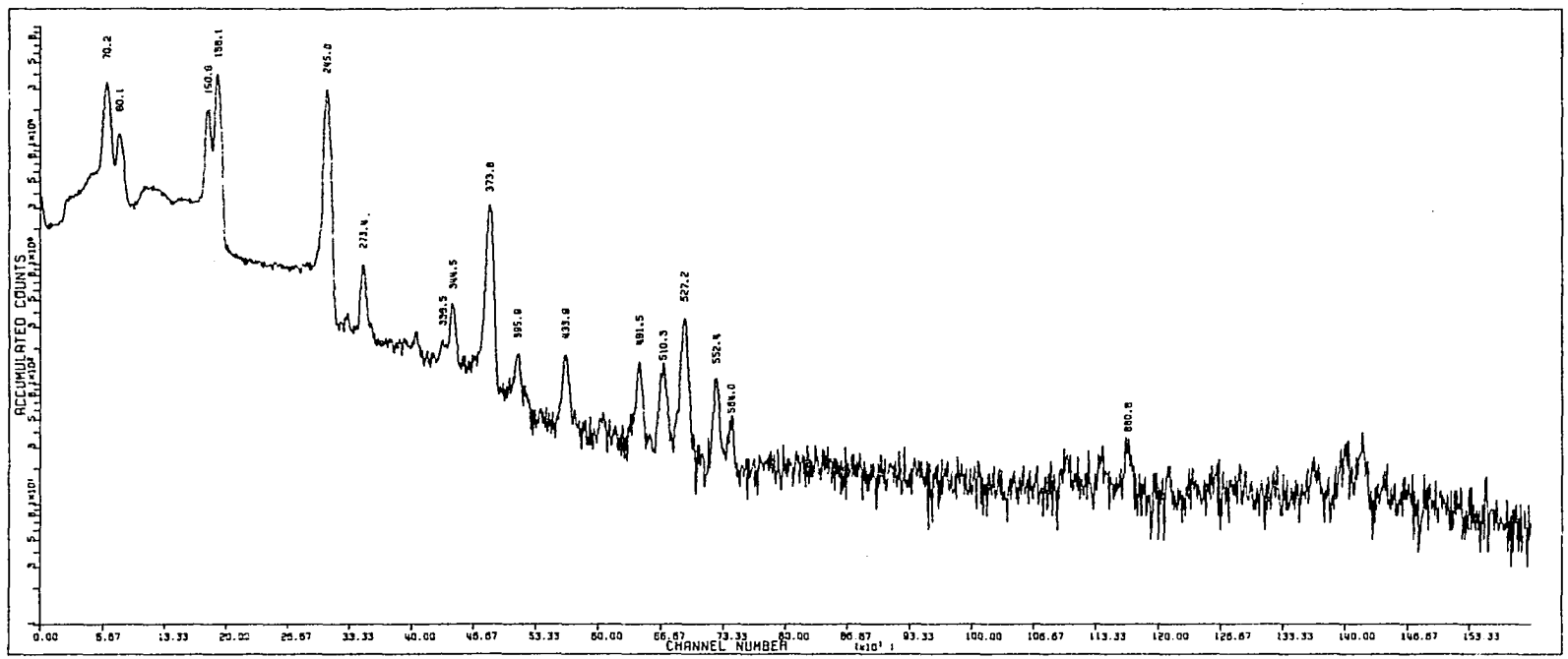

Figure G-3. Spectrum of a 1:2 weight ratio of Cd:Hg irradiated with fission neutrons

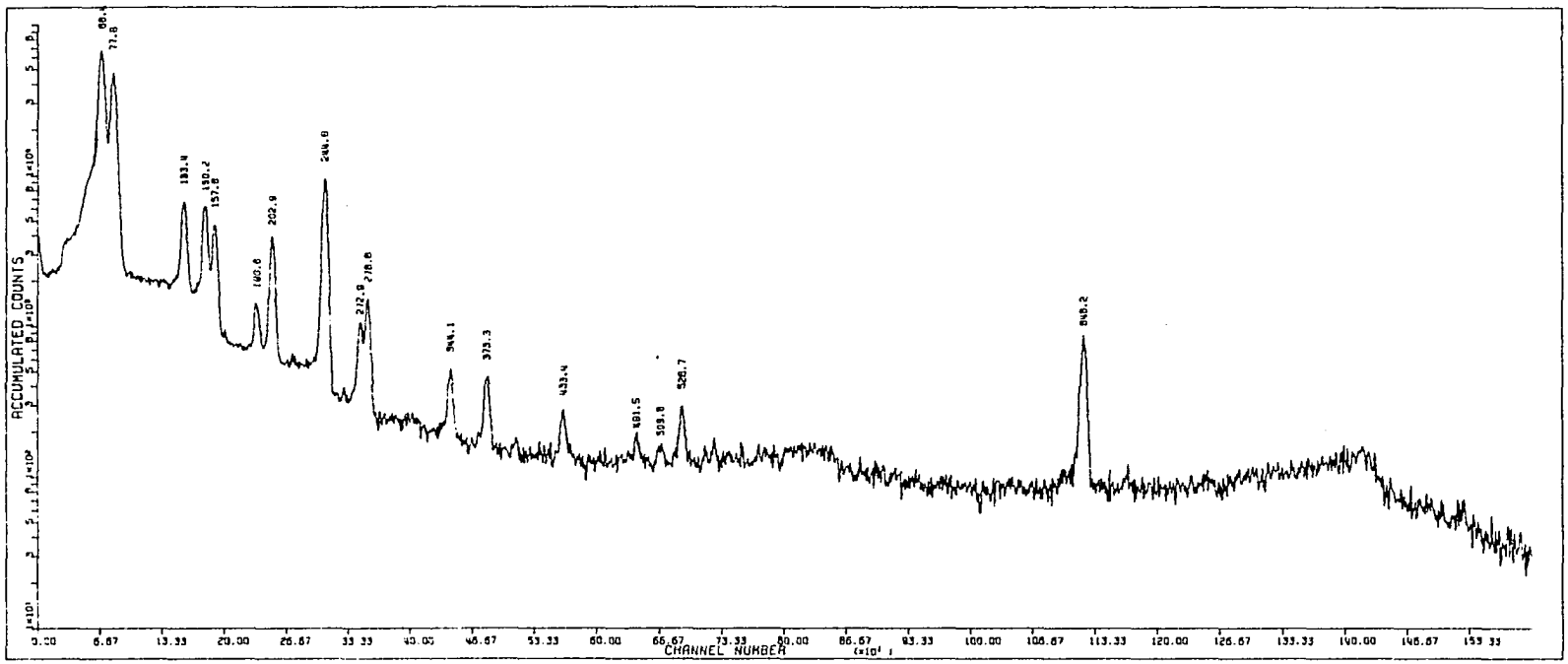

Figure G-4. Spectrum of a 1:2 weight ratio of Cd:Hg irradiated with thermal neutrons

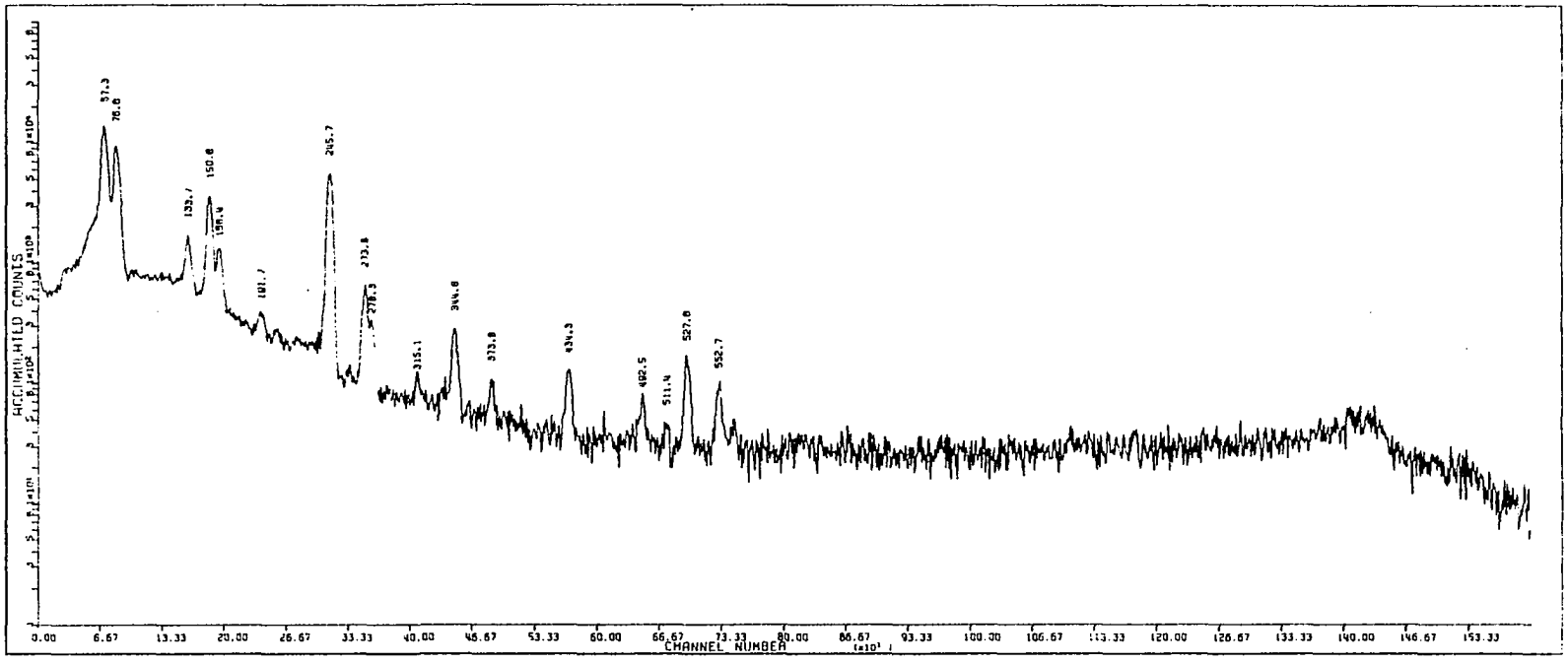

Figure G-5. Spectrum of a 2:1 weight ratio of Cd:Hg irradiated with fission neutrons

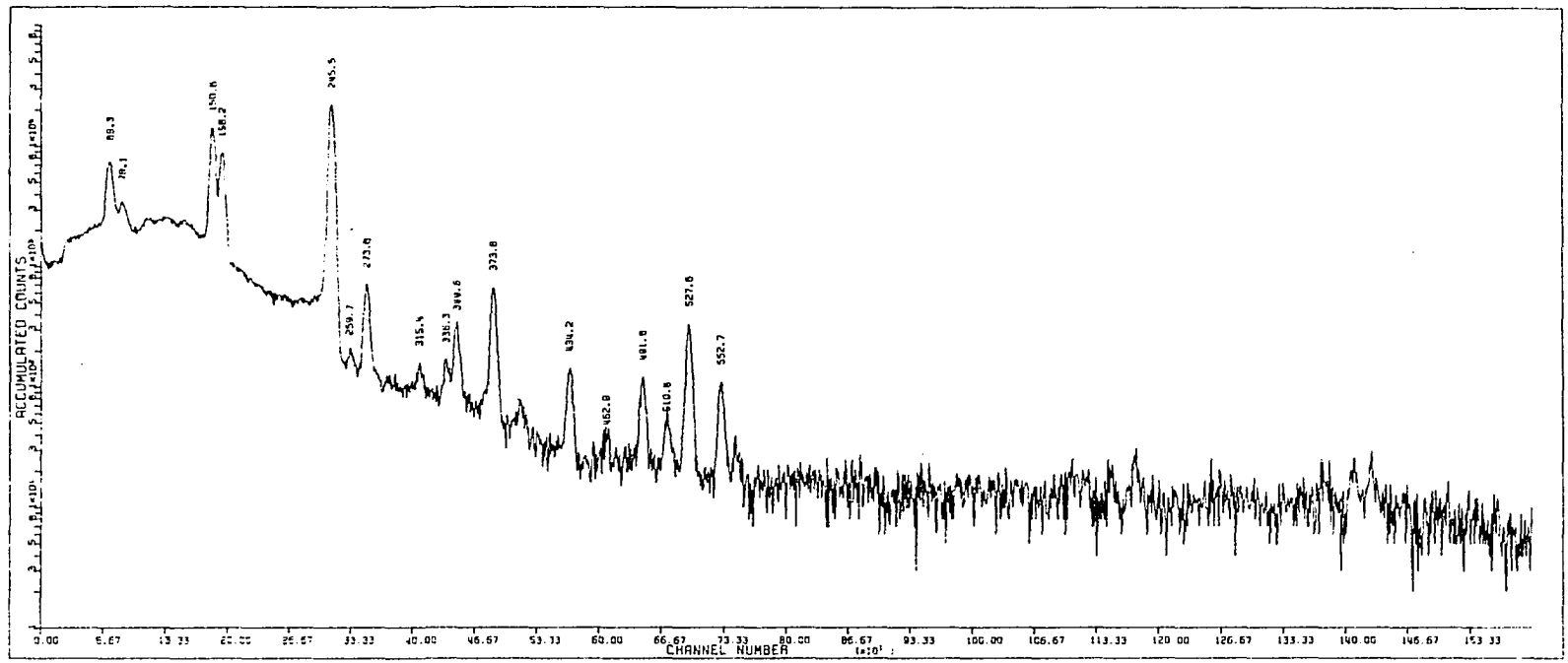

Figure G-6. Spectrum of a 2:1 weight ratio of Cd:Hg irradiated with thermal neutrons